

# NOTE TO USERS

This reproduction is the best copy available.

**UMI**®



# **FLEXURAL STRENGTHENING OF REINFORCED CONCRETE BEAMS WITH MECHANICALLY BONDED STEEL PLATES**

By

**Syed Ali Kashif**

B.E. Civil, M. Ed. University of Engineering and Technology, Pakistan, 1998

A thesis

presented to Ryerson University

in partial fulfillment of the  
requirement for the degree of  
Master of Applied Science  
(Civil Engineering)

Toronto, Ontario, Canada, 2004

© Syed Ali Kashif, 2004

RYERSON

UMI Number: EC52937

## INFORMATION TO USERS

The quality of this reproduction is dependent upon the quality of the copy submitted. Broken or indistinct print, colored or poor quality illustrations and photographs, print bleed-through, substandard margins, and improper alignment can adversely affect reproduction.

In the unlikely event that the author did not send a complete manuscript and there are missing pages, these will be noted. Also, if unauthorized copyright material had to be removed, a note will indicate the deletion.

**UMI**<sup>®</sup>

---

UMI Microform EC52937

Copyright 2008 by ProQuest LLC.

All rights reserved. This microform edition is protected against unauthorized copying under Title 17, United States Code.

ProQuest LLC  
789 E. Eisenhower Parkway  
PO Box 1346  
Ann Arbor, MI 48106-1346

## BORROWER'S PAGE

Borrowers undertake to give proper credit for any use made of the thesis. Ryerson University requires the signatures of all persons using or photocopying this thesis.

Please sign below and give address and date.

[illegible]

# **FLEXURAL STRENGTHENING OF REINFORCED CONCRETE BEAMS WITH MECHANICALLY BONDED STEEL PLATES**

*Syed Ali Kashif*

Master of Applied Science, Department of Civil Engineering  
RYERSON UNIVERSITY, Canada, 2004

## **ABSTRACT**

Steel plate bonding technology is widely accepted for the strengthening of reinforced concrete structures. Researches in the past showed that epoxy bonded steel plated composite beams are highly prone to variation in temperature and environmental conditions. This research study introduces a novel approach to steel plate composite beam in which bond between the concrete and the steel plate is provided by welding the steel plate to the legs of the uniformly spaced stirrups. Experimental investigation showed that the parameters such as interface connections, geometric dimensions, stirrups spacing and thickness of steel plate have a great influence on the strength, deformation and failure characteristics of such composite beams. A finite element model has been developed using commercial software, *ABAQUS*, to predict the strength of such composite beams and its performance is validated through experimental results. The direct finite element simulation of proposed composite beams with developed finite element model gives an average of experimental to predicted strength ratio of 0.99, which confirms the accuracy of prediction. The finite element model is then used to simulate a large number of numerical beams with varying geometric and material properties to formulate design guidelines. Design charts are developed and their performance is validated through test results with experimental to design chart predictions giving an average value of 0.94. Design procedures for such beams are illustrated with calculated design examples. Such simple design procedures can be adopted in the actual design of proposed composite beams in practical applications.

## PREFACE

This thesis is mainly based on the work done from January 2003 - to - July 2004, at the Division of Structural Engineering, Department of Civil Engineering at Ryerson University, Canada. The thesis is performed to give a reference material in strengthening technology using mechanical bonded steel plate for upgrading civil engineering structures with emphasize on the need of quick and accurate solutions.

I would like to express my deepest gratitude to my supervisors, Dr. Mohamed Lachemi and Dr. K.M. Anwar Hossain, for their guidance, support and patience during the development of this thesis. A special thank to Dr. K.M. Anwar Hossain who for the past two years, has always given me the encouragement, support and wisdom to grow and excel in all my endeavors, I am indebted to him.

Furthermore, I would to thank my fellow classmates Garry, Bijal, Atashi and Mehmud for boosting my enthusiasm to complete this endless journey. Finally, I want to thank, the people in our computer and administration department specially Des Rogan to support me during trouble shooting with *ABAQUS* and related computer issues.

Finally, special gratitude goes to my family. Without their constant love, support and sacrifices my successes would not be possible.

## DEDICATION

*To my parents*



# TABLE OF CONTENTS

<b>AUTHOR'S DECLARATION .....</b>	<b>ii</b>
<b>BORROWER'S PAGE.....</b>	<b>iii</b>
<b>ABSTRACT.....</b>	<b>iv</b>
<b>PREFACE.....</b>	<b>v</b>
<b>DEDICATION.....</b>	<b>vi</b>
<b>TABLE OF CONTENTS .....</b>	<b>vii</b>
<b>LIST OF TABLES .....</b>	<b>x</b>
<b>LIST OF FIGURES .....</b>	<b>xi</b>
<b>NOTATION AND ABBREVIATIONS .....</b>	<b>xvi</b>
<b>Chapter 1 Introduction .....</b>	<b>1</b>
1.1. Need for Strengthening Structures.....	1
1.2. Identification of Problems and Prediction of Solution .....	4
1.3. Introduction of New Technique.....	5
1.4. Research Objectives.....	7
1.5. Plan of Investigations.....	8
1.6. Organization of the Thesis.....	9
<b>Chapter 2 Literature Review.....</b>	<b>11</b>
2.1. Need for Strengthening Structures.....	11
2.2. Strengthening of Reinforced Concrete Beams with Adhesively Bonded Steel Plates.....	11
2.2.1. Debonding of Steel Plates Due to Flexural and Shear Peeling Stresses.....	12
2.2.2. Strengthening of Reinforced Concrete Beams with Mechanically Bonded Steel Plates.....	21
2.2.3. New Approach to Steel Plate Bonding .....	26
<b>Chapter 3 A New Approach to Steel Plate Bonding Technique: Review of         Experimental Investigations .....</b>	<b>30</b>
3.1. Introduction.....	30
3.2. Introduction of New Approach .....	30
3.3. Characteristics of Proposed Technique.....	31

3.4. Field Application Procedure .....	33
3.5. Experimental Studies .....	34
3.5.1. Beam Geometric Properties .....	35
3.5.2. Fabrication, Casting, Curing and Material Properties .....	36
3.5.3. Instrumentation and Test Setup .....	39
3.5.4. Failure Modes of Tested Beams .....	40
3.5.4.1. Beams with 0.4-mm Thick Plate.....	40
3.5.4.2. Beams with 3mm Thick Plate .....	43
3.5.4.3. Effect of Variable Parameters on Failure Modes of Pilot Beams .....	44
3.5.5. Load -Deflection Responses of Beams .....	46
3.5.5.1. Beams with 0.4mm Thick Plate .....	46
3.5.5.2. Beams with 3-mm Thick Plate.....	48
3.5.5.3. Effect of Variable Parameters on Ultimate Load-Deflection Response. ....	49
<b>Chapter 4 Development of Finite Element Model.....</b>	<b>56</b>
4.1. Introduction.....	56
4.2. Development of a Finite Element Model.....	56
4.2.1. Beam Geometry, Loading and Boundary Conditions.....	57
4.2.2. Modeling the Non-Linear Behavior of Concrete.....	58
4.2.2.1. Cracking Behavior of Concrete .....	58
4.2.2.2. Tensile Behavior of Concrete .....	61
4.2.2.3. Compressive Behavior of Concrete .....	62
4.2.2.4. Modeling of Shear Retention in Concrete .....	64
4.2.3. Modeling the Behavior of Longitudinal Steel Reinforcement.....	65
4.2.4. Non-Linear Solution .....	67
4.2.5. Load Steps and Response of Finite Element Model .....	69
4.2.6. Finite Element Analysis with Various Interface Models.....	70
4.2.6.1. Use of 2D Shell Element.....	70
4.2.6.2. Combined Use of 3D Solid and 2D Shell Elements .....	76
4.2.6.3. Shear-Stud Model .....	85
4.3. Comparative Study on Finite Element Models.....	94

<b>Chapter 5 Development of Design Guidelines and Performance Validation.....</b>	<b>96</b>
5.1. Introduction.....	96
5.2. Development of Design Guidelines .....	96
5.3. Development of Design Charts by Finite Element Predictions .....	97
5.4. Influence of Various Parameters on Ultimate Moment Capacity .....	99
5.4.1. Effect of the Compressive Strength of Concrete ( $f'_c$ ) on the Ultimate Moment Capacity.....	100
5.4.2. Effect of Yield Strength of Steel Reinforcement on Ultimate Moment Capacity .....	101
5.4.3. Effect of Longitudinal Reinforcement Ratio ( $\rho$ ) on the Ultimate Moment Capacity .....	102
5.4.4. Effect of Stirrups Spacing “S” on the Ultimate Moment Capacity .....	103
5.4.5. Effect of the Beam Width on the Ultimate Moment Capacity.....	104
5.4.6. Effect of the Beam Depth on the Ultimate Moment Capacity.....	105
5.4.7. Effect of Length-to-Depth ratio on Ultimate Moment Capacity of Finite Element Models. ....	106
5.4.8. Effect of the Plate Thickness on the Ultimate Moment.....	107
5.5. Design Charts.....	108
5.6. Performance Validation of Design Chart.....	109
5.7. Applicability of Design Charts for Beams with Different Strengthening Systems .....	121
5.8. Use of Proposed Design Charts – Design Example.....	128
<b>Chapter 6 Conclusions and Recommendations .....</b>	<b>133</b>
6.1. Summary of Research Effort .....	133
6.2. Conclusions.....	134
6.3. Suggestion for Further Research.....	135
<b>REFERENCES.....</b>	<b>136</b>
<b>Appendix – A (Input File) .....</b>	<b>143</b>
<b>Appendix – B (Prediction of Moment Capacity Based on Codes).....</b>	<b>149</b>
<b>Appendix – C (Proposed Design Charts).....</b>	<b>168</b>

## LIST OF TABLES

Table 3.1	Description of geometrical properties of test series.....	36
Table 3.2	Material properties of experimental reinforced concrete beams.....	38
Table 3.3	Response of pilot beams during experiments (Hossain 2001).....	46
Table 4.1	Prediction of ultimate load and central deflection using different FE models .....	95
Table 4.2	Comparative study on finite element models.....	95
Table 5.1	Parameters of numerically simulated computer beams .....	98
Table 5.2	Properties of beam tested by Jim (1999) and Nupiri (2000).....	110
Table 5.3	Comparative study with different methods of prediction .....	119
Table 5.4	Predicted strength for epoxy bonded steel plated beams with design charts .....	123

## LIST OF FIGURES

Fig. 1.1 General durability design procedure (Siemes 1996).....	2
Fig. 1.2 Schematic showing application of concepts of durability and damage tolerance (Kabahari et al. 2003) .....	3
Fig. 1.3 Detail of mechanically bonded connection.....	6
Fig. 1.4 Application of mechanically bonded steel plate on exiting structures .....	7
Fig. 2.1 Types of application of steel plate bonding according to infrastructure statistics (Bonaci and Maalej 2000).....	12
Fig. 2.2 Representation of flexural peeling mechanism (Oehlers and Moran 1990). ....	12
Fig. 2.3 Interaction between shear and flexure peeling (Oehlers 1992). ....	15
Fig. 2.4 Ultimate forces acting on a plated beam section (Hussain et al. 1994) .....	16
Fig. 2.5 Shear peeling mechanism (Ali et al. 2001).....	19
Fig. 2.6 Forces in cracked steel plated beams (Ali et al. 2001). ....	19
Fig. 2.7 Typical cross section of conventional tube tunnel (Naraynan et al. 1987).....	22
Fig. 2.8 Typical cross section of double skin composite beam (Oduyemi and Wright 1989) .....	23
Fig. 2.9 System components of mechanically bonded/welded strengthening system .....	27
Fig. 3.1 Mechanically plate bonding technique with different plate arrangement.....	33
Fig. 3.2 Cross-section details of pilot beams. ....	35
Fig. 3.3 Assembly of test specimens during casting (Hossain 2001).....	37
Fig. 3.4 Tensile test specimen (Hossain 2001).....	37
Fig. 3.5 Assembly of test setup (Hossain 1999, Hossain 2001).....	39
Fig. 3.6 Schematic of test set-up and instrumentation (Hossain 1999).....	40
Fig. 3.7 Failure modes of Series 1 beams (Hossain 2001).....	41
Fig. 3.8 Failure modes of Series 2 beams (Hossain 1999).....	42
Fig. 3.9 Strain development in Series 1 and Series 2 beams (Hossain 2001) .....	42
Fig. 3.10 Failure modes of series 1 beams with 3mm thick steel plate.....	43
Fig. 3.11 Load deflection response of series 1 beams.....	47
Fig. 3.12 Load deflection response of series 2 beams.....	47
Fig. 3.13 Load-deflection response of series 1 beams .....	48
Fig. 3.14 Load deflection response of series 2 beams.....	49

Fig. 3.15	Effect of internal tensile reinforcement on ultimate load capacity of beam with 0.4-mm thick steel plate.....	50
Fig. 3.16	Effect of internal tensile reinforcement on ultimate load capacity of beams with 3-mm thick steel plate .....	50
Fig. 3.17	Effect of internal tensile reinforcement on central deflection of beams with 0.4-mm thick steel plate .....	51
Fig. 3.18	Effect of internal tensile reinforcement on central deflection of beams with 3-mm thick steel plate .....	51
Fig. 3.19	Effect of plate thickness on ultimate load of Series 1 beams .....	52
Fig. 3.20	Effect of plate thickness on ultimate load of series 2 beams .....	53
Fig. 3.21	Effect of plate thickness on central deflection of series 1 beams .....	54
Fig. 3.22	Effect of plate thickness on central deflection of series 2 beams .....	54
Fig. 4.1	Schematic of general reinforced concrete beam .....	57
Fig. 4.2	Typical beam dimension (not to scale), loading and boundary conditions.....	58
Fig. 4.3	Typical strength concrete under uni-axial tension and compression (Abaqus User's Manula Volume II 2004). .....	58
Fig. 4.4	Multi-axial state of stress in concrete (Abaqus User's Manula Volume II 2004)..	59
Fig. 4.5	Tension stiffening model for concrete (Abaqus User's Manula Volume II 2004)..	61
Fig. 4.6	Adapted model of uni-axial curve for concrete in compression.....	64
Fig. 4.7	Shear retention model (Abaqus User's Manula Volume II 2004). .....	65
Fig. 4.8	General stress-strain relation for steel reinforcement. ....	67
Fig. 4.9	Proportional loading with unstable response (Abaqus User's Manula Volume II 2004). .....	67
Fig. 4.10	Newton-Raphson iterative solution for 2 load increments (Abaqus User's Manula Volume II 2004).....	69
Fig. 4.11	Connection of hypothetical rebar with steel plate using connector element .....	71
Fig. 4.12	Typical finite element descritization with 4-node shell elements.....	73
Fig. 4.13	Optimization of element type using various shell elements for S <sub>2</sub> B <sub>100</sub> .....	75
Fig. 4.14	Load Vs central deflection response of numerical beam for selection of element type.....	75
Fig. 4.15	Effect of mesh size on ultimate load versus central deflection.....	76

Fig. 4.16	Typical Finite Element discretization of the beam with mixed solid and shell elements .....	77
Fig. 4.17	Effect of mesh size on load-deflection response of FEA-S <sub>2</sub> B <sub>100</sub> beam .....	78
Fig. 4.18	Comparative study on various mesh size used with mixed model .....	79
Fig. 4.19	Effect of different types of solid elements on load-deflection response.....	80
Fig. 4.20	Error obtained with different solid element.....	80
Fig. 4.21	Effect of shell element types on load-deflection response.....	81
Fig. 4.22	Optimization of element type for steel plate.....	82
Fig. 4.23	Load vs. central deflection response for S <sub>2</sub> B <sub>50</sub> and S <sub>1</sub> B <sub>50</sub> Beams.....	83
Fig. 4.24	Load vs. central deflection response for S <sub>1</sub> B <sub>100</sub> and S <sub>2</sub> B <sub>100</sub> Beams .....	83
Fig. 4.25	Load vs. central deflection for S <sub>1</sub> B <sub>150</sub> and S <sub>2</sub> B <sub>150</sub> Beams.....	84
Fig. 4.26	Load vs. Central Deflection for S <sub>1</sub> B <sub>180</sub> and S <sub>2</sub> B <sub>180</sub> Beams.....	84
Fig. 4.27	Tensile stress contours in typical S <sub>2</sub> B <sub>100</sub> beam .....	85
Fig. 4.28	Cross-section of beam with Shear - Stud Model .....	86
Fig. 4.29	Schematic of interface connection in shear-stud model. ....	87
Fig. 4.30	Properties of Spot-welded plates in Lap-Shear Test (Hossain 2001) .....	87
Fig. 4.31	Optimization of element type for Shear -Stud Model.....	88
Fig. 4.32	Optimization of solid element types to model the concrete part in S <sub>2</sub> B <sub>100</sub> beam .	89
Fig. 4.33	Optimization of element type to model the steel plate in the shear stud model ...	90
Fig. 4.34	Load vs. central deflection response of S <sub>2</sub> B <sub>50</sub> and S <sub>1</sub> B <sub>50</sub> beam using Shear-Stud Model .....	91
Fig. 4.35	Load vs. central deflection response of S <sub>2</sub> B <sub>100</sub> and S <sub>1</sub> B <sub>100</sub> beam using Shear-Stud Model .....	91
Fig. 4.36	Load vs. central deflection response of S <sub>2</sub> B <sub>150</sub> and S <sub>1</sub> B <sub>150</sub> beam using Shear-Stud Model .....	92
Fig. 4.37	Load vs. central deflection response on S <sub>2</sub> B <sub>180</sub> and S <sub>1</sub> B <sub>180</sub> beam using Shear-Stud Model .....	92
Fig. 4.38	Typical stress contour corresponding to the beam longitudinal direction .....	93
Fig. 4.39	Punching failure of concrete node into steel plate nodes in numerical beams. ....	94
Fig. 5.1	Effect of compressive strength of concrete ( $f'_c$ ) on ultimate moment capacity .....	100

Fig. 5.2	Effect of yield strength of steel rebars ( $f_{ys}$ ) and steel plate ( $f_{yp}$ ) on ultimate moment capacity .....	101
Fig. 5.3	Effect of internal reinforcement ratio ( $\rho$ ) on ultimate moment capacity .....	102
Fig. 5.4	Effect of stirrups spacing ( $S$ ) on ultimate moment capacity .....	103
Fig. 5.5	Effect of width of beam on ultimate moment capacity .....	104
Fig. 5.6	Effect of beam depth ( $h$ ) on ultimate moment capacity .....	105
Fig. 5.7	Effect of length-to-depth ratio ( $L/h$ ) on ultimate moment capacity .....	106
Fig. 5.8	Effect steel plate thickness ( $t_p$ ) on ultimate moment capacity .....	107
Fig. 5.9	Typical design chart showing prediction of moment capacity .....	108
Fig. 5.10	Chart and F.E prediction of $S_1B_{50}$ -0.4 mm Beam .....	111
Fig. 5.11	Chart and F.E prediction of $S_1B_{50}$ - 3 mm Beam .....	111
Fig. 5.12	Chart and F.E prediction of $S_1B_{100}$ - 0.4 mm Beam .....	112
Fig. 5.13	Chart and F.E prediction of $S_1B_{100}$ - 3 mm Beam .....	112
Fig. 5.14	Chart and F.E prediction of $S_1B_{150}$ - 0.4 mm Beam .....	113
Fig. 5.15	Chart and F.E prediction of $S_1B_{150}$ - 3 mm Beam .....	113
Fig. 5.16	Chart and F.E prediction of $S_1B_{180}$ - 0.4 mm Beam .....	114
Fig. 5.17	Chart and F.E prediction of $S_1B_{180}$ - 3 mm Beam .....	114
Fig. 5.18	Chart and F.E prediction of $S_2B_{50}$ - 0.4 mm Beam .....	115
Fig. 5.19	Chart and F.E prediction of $S_2B_{50}$ - 3 mm Beam .....	115
Fig. 5.20	Chart and F.E prediction of $S_2B_{100}$ - 0.4 mm Beam .....	116
Fig. 5.21	Chart and F.E prediction of $S_2B_{100}$ - 3 mm Beam .....	116
Fig. 5.22	Chart and F.E prediction of $S_2B_{150}$ - 0.4 mm Beam .....	117
Fig. 5.23	Chart and F.E prediction of $S_2B_{150}$ - 3 mm Beam .....	117
Fig. 5.24	Chart and F.E prediction of $S_2B_{180}$ - 0.4 mm Beam .....	118
Fig. 5.25	Chart and F.E prediction of Beam $S_2B_{180}$ - 3 mm Beam .....	118
Fig. 5.26	Chart and experimental prediction for S23 beam (Byung et al. 2003) .....	124
Fig. 5.27	Chart and experimental prediction for S43S1 beam (Byung et al. 2003) .....	124
Fig. 5.28	Chart and experimental prediction for 2/2/S beam (Oehlers 1992) .....	125
Fig. 5.29	Chart and experimental prediction for 2/4/S beam (Oehler 1992) .....	125
Fig. 5.30	Chart and experimental prediction for beam (Aprile et al. 2001) .....	126
Fig. 5.31	Chart and experimental prediction for FBR2 beam (Hussain et al. 1995) .....	126



Fig. 5.32	Chart and experimental prediction for FBR3 beam (Hussain et al. 1995).....	127
Fig. 5.33	Chart and experimental prediction for O beam (Ritchie et al. 1991).....	127
Fig. 5.34	Details of example beam.....	129
Fig. 5.35	Typical chart selected for design example.....	131
Fig. 5.36	Schematic of strengthened example beam.....	132

## NOTATION AND ABBREVIATIONS

$a$ = Depth of rectangular compressive stress block	C3D8R = 3-dimentional 8-nodes continuum/solid element with reduced integration
$A_p$ = Area of external steel plate	CFRP = Carbon fiber reinforced polymer
$A_s$ = Area of internal longitudinal steel reinforcement	$d'$ = Distance from extreme compression fiber of concrete to centroid of compression reinforcement.
$A_s'$ = Area of top longitudinal reinforcement	$d_p$ = Depth of steel plate
$A_v/S$ = Ratio of total area of steel stirrups -to- spacing of stirrups	$E_c$ = Modulus of elasticity of concrete
$b$ = Width of concrete beam	$E_s$ = Modulus of Elasticity of steel
$b_p$ = Width of steel plate	$f$ = Concrete compressive stress
$c$ = Depth of neutral axis	$f'_c = 0.8 f'_c$
$C$ = Compressive force of concrete	$f'_c$ = Ultimate cylindrical compressive strength of concrete
C3D20H = 3-dimentional 20-nodes continuum/solid hybrid element	$f_r$ = Modulus of rupture of reinforced concrete or flexural tensile strength of concrete
C3D20R = 3-dimentional 20-nodes continuum/solid element with reduced integration	FRP = Fiber reinforced polymer
C3D20RH = 3-dimentional 20-nodes continuum/solid hybrid element with reduced integration	$f_s$ = Stress at bottom longitudinal reinforcement
C3D8 = 3-dimentional 8-nodes continuum/solid element	$f_s'$ = Stress at top longitudinal reinforcement
C3D8H = 3-dimentional 8-nodes continuum/solid hybrid element	$f_t$ = Direct tensile strength of concrete
C3D8I = 3-dimentional 8-nodes continuum/solid incompatible element	$f_{yp}$ = Yield strength of external steel plate
	$f_{ys}$ = Yield strength of internal longitudinal steel reinforcement

$G_{\text{applied}}$  = Applied strain energy release rate

$G_{\text{cr}}$  = Critical strain energy release rate

$h$  = Total depth of reinforced concrete member

$L/h$  = Length -to- depth ratio of reinforced concrete member

$l_{\text{period}}$  = Total arc length factor

$L_s$  = Shear span of beam

$M$  = Applied moment applied

$m$  = Modular ratio

$M_{\text{aret.}}$  = Moment of member required after retrofitting.

$M_{\text{exp.}}$  = Experimental moment capacity of concrete member

$M_{\text{max.}}$  = Maximum Applied Moment

$M_p$  = Moment at the end of plate when peeling occurred

$M_p$  = Moment at the end of plate when peeling occurred

MPC's = Multipoint constraints

$M_r$  = Moment of resisting of concrete member

$M_{\text{re}}$  = Existing moment of resisting of concrete member

$M_u$  = Moment at ultimate stage

$M_{\text{up}}$  = Ultimate peeling moment at the end of plate when shear force ( $V$ ) is zero

$P$  = Applied load

$P_{\text{(total)}}$  = Total magnitude of applied loading

$P_{\text{(total)}}$  = Total magnitude of applied loading

$P_{\text{applied}}$  = Applied load

$P_{\text{cr}}$  = Critical load

$P_o$  = Load at first increment

$P_{\text{ref}}$  = Reference load vector

$R(t)$  = Resistance as function of time

$S(t)$  = Load as function of time

$S$  = Spacing of Stirrups

$S4$  = 4- nodes shell element

$S4R$  = 4- nodes shell element with reduced integration

$S8$  = 8-nodes shell element

$S8R$  = 8 - nodes shell element with reduced integration

$t_p$  = Force developed in steel plate

$T_s$  = Force developed in longitudinal steel reinforcement

$V_{\text{cr}}$  = Applied shear force required to developed diagonal cracks.

$V_p$  = Shear load at the end of peeling when peeling occurred.

$V_{\text{uc}}$  = Shear strength of reinforced concrete beam without stirrups

$x$  = Horizontal projection of diagonal crack

$\beta$  = Shape factor for Whitney's rectangular compressive block

$\Delta l_{\text{in}}$  = Initial load proportionality factor

$\Delta l_{\text{in}(i)}$  = Initial increment of arc length

$\lambda$  = Load proportionality factor

$\lambda_c$  = Factor accounts for low tensile strength for concrete (1 = for normal density concrete; 0.85 = for semi- low density of concrete; 0.75 = low density of concrete)

$\xi_c$  = Compressive strain of concrete at extreme compressive fiber

$\xi_{c(max)}$  = Maximum compressive strain at concrete extreme compressive fiber

$\xi_{cu}$  = Ultimate compressive strain at concrete extreme compressive fiber

$\rho$  = Shear Retention factor

$\rho_b$  = Balanced steel ratio

$\rho_s$  = Reinforcement ratio

$\Phi$  = Factor of safety for moment and shear

# Chapter 1 Introduction

## 1.1. Need for Strengthening Structures

A large number of reinforced concrete infrastructures in the U.S. and Canada are structurally deficient by today's standards and are currently deteriorating much faster than they are being rehabilitated or replaced. The main contributing factors are changes in their use, an increase in load requirements, or deterioration due to exposure to an aggressive environment. In order to preserve those infrastructures, rehabilitation is often considered essential to maintain their capability and to increase public safety. Busel and Barno (1996) stated that the estimated size of U.S concrete construction market was \$8 billion/year, of which 70% is for repairs and remediation services, whereas only 30% (2.4 billion) is for new construction. In Canada, the infrastructure deficit - the gap between needed and actual infrastructure investment - is estimated to be \$74 billion (ISIS Canada 1997; Neale 2001).

In Alberta, more than 5000 bridges require retrofitting in the next 10-20 years due to increase of 30% of truckloads with less design requirement at the time, when these bridges were built. Another emerging problem parallel to bridge rehabilitation is the deterioration of parking garages (Bonaci and Maalej 2000; Ali and Oehlers 2003).

Strengthening of a structural member is required when the strength of the existing member is insufficient. Repair or retrofitting, refers to the member strengthening in

instances where the capacity has been reduced by environmental effects, manmade hazards, or human error, such as a tall vehicle striking the girders beneath a bridge etc.

If load resisting strength of a structure is taken as a function of time and taking into consideration other factors, which are causing reduction in the strength of structure, it can be observed that strength of structures is decreasing with time while the load for which the structure was designed is increasing (Mirza et al. 2003). Fig. 1.1, represents general durability design procedure for structure having load " $S(t)$ " and resistance " $R(t)$ " as function of time (Siemes 1996). Fig. 1.1 indicates the time when the structures require maintenance and rehabilitation.

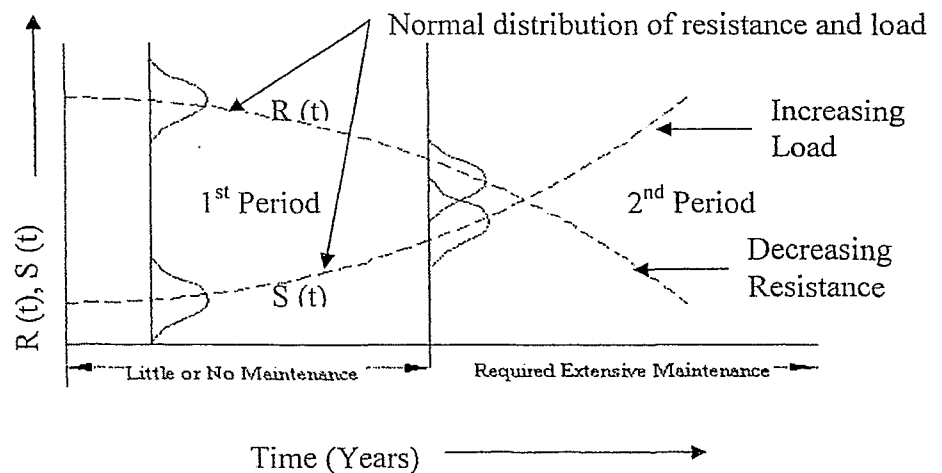


Fig. 1.1 General durability design procedure (Siemes 1996)

The durability of a structure is expressed, as the time period in which structure requires little or no maintenance so as to attain a desired service life. However, the structure's desired life still remains a question among all the designers, practitioners and researchers. This concept is realized in design through the application of sound design principles and

the principles of damage tolerance, whereby levels of performance are guaranteed through relationships between performance levels and damage/degradation occurred over specified periods of time. In this sense, damage tolerance is defined as the ability of a material or structure to resist failure and continue performing at prescribed levels of performance in the presence of flaws, cracks, or other forms of damage/degradation for a specified period of time under specified environmental conditions. The overall concept is shown schematically in Fig. 1.2 (Kabahari et al. 2003).

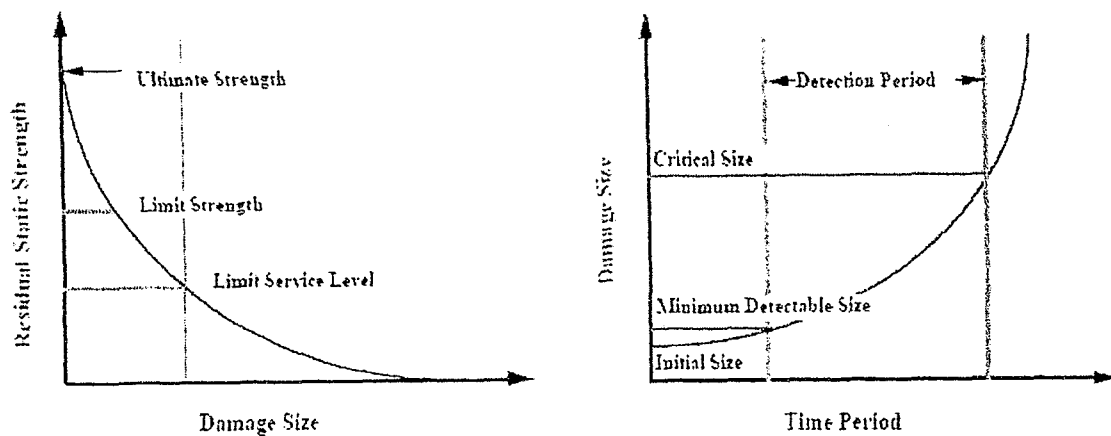


Fig. 1.2 Schematic showing application of concepts of durability and damage tolerance (Kabahari et al. 2003)

Hence strengthening of structures is required in parallel as the age of structure increases with reduction in strength due to deterioration and manmade errors.

This research deals with the 2<sup>nd</sup> period presented in Fig. 1.1 and concentrates on the residual life of a structure in which effort has been made to strengthen the structural performance and to increase the residual life rather than demolish the whole structure and built a new one, depending on severity of deterioration and financial conditions.

## 1.2. Identification of Problems and Prediction of Solution

Columns and beams are frequently wrapped with steel or fiber reinforced polymer (FRP) laminates to increase the capacity and to make them behave in a ductile manner. A common strengthening method currently in use is to use adhesive bond strips or “thin plates” of steel or FRP laminates bonded to the surface of concrete beams or slabs to strengthen in shear or flexure depending upon the distress mechanism.

The bond between concrete and composite plates, using epoxy is highly prone to the temperature and environment (Tadeu and Branco 2000). In addition, the method of construction such as surface preparation, drying time and maintaining appropriate thickness of adhesive layers is found to have a great influence on overall strength of structural components (Chajes et al. 1996; Tureyen and Frosch 2002). Hence, it is desirable to develop new, innovative, optimized strengthening techniques, which are simple as well as cost effective. Advanced composites such as Carbon Fiber Reinforced Polymer (CFRP) and Glass Fiber Reinforced Polymer (GFRP) are not easily available on the market and strengthening reinforced concrete structures using these composites require high cost as compared to conventional composites such as steel plate. This situation reflects the attention of researchers towards the commonly available and low cost material, steel.

Typical reinforced concrete flexural members are designed such that the tensile steel reinforcement yields well before the concrete fails in compression. This design methodology results in a ductile member, which undergoes large deflection when the load approaches the ultimate capacity. The use of larger amount of tensile steel



reinforcement which lead to an over reinforced member is not desirable because of the prospect of a concrete crushing failure associated with lower ductility.

Strengthening of reinforced concrete flexural members by using external steel strips began in the late 1960s. These early methods consisted of bonding a steel strip to the tension side of an existing flexural member with an epoxy. The concrete surface has to be made smooth, which required careful grinding, sandblasting, and priming. Typically, anchor bolts at the ends of the steel strip are used, mainly to prevent the steel strip from falling if the integrity of the adhesive is destroyed by fire (Garden and Hollaway 1998).

The adhesive layer between concrete and FRP strip can cause problems and can govern the behavior of the strengthened member. Peeling stresses are induced at the ends of the FRP or steel strip, which tend to pull the strip away from the concrete. If these peeling stresses are larger than the strength of the adhesive, the strip will peel away from the beam suddenly, resulting in the loss of strength, and may cause a sudden and undesirable failure. The strip can also detach if the vertical displacement of two sides of cracks occurs on tension face of strengthened member that contact the adhesive layer, resulting sudden failure without warning (Marco and Nanni 1997).

### **1.3. Introduction of New Technique**

In this study, a method of strengthening reinforced concrete beams with thin gauge steel plate or steel strip mechanically bonded to the bottom surface of beam by means of welded stirrup-plate assembly proposed by Hossain (1999, 2001) as shown in Fig. 1.3 has been investigated.

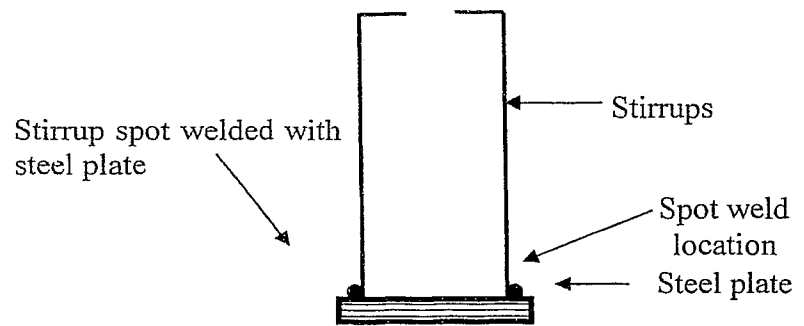


Fig. 1.3 Detail of mechanically bonded connection

In adhesively bonded steel plate strengthening procedure, steel strips are attached on the tension surface when strengthening is needed in flexure and on the web, when required for shear. However, using this technique, reinforced concrete members can be strengthened in both shear and flexure at the same time.

As bond between the steel plate and the concrete will be secured by steel plate-stirrup (embedded in concrete) welded connection, there will be no peeling stress as well as temperature effects compared with epoxy-bonded laminates. A schematic representation in possible field application is presented in Fig. 1.4.

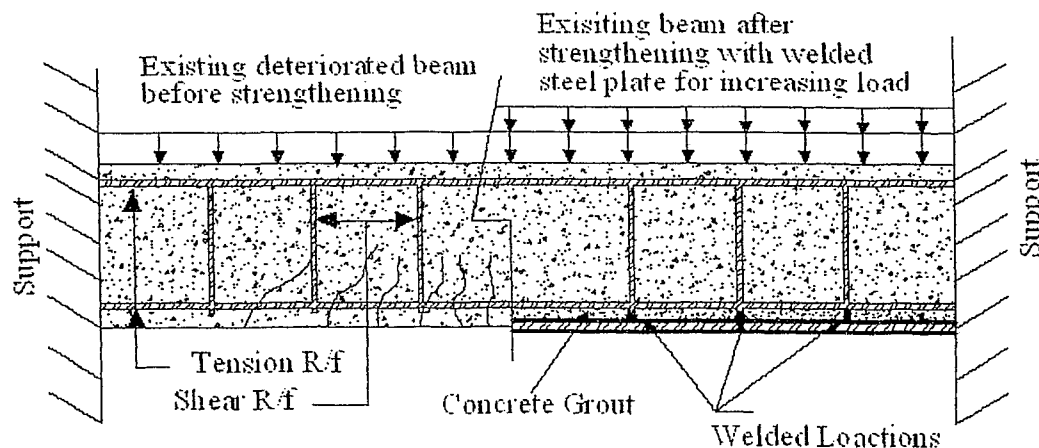


Fig. 1.4 Application of mechanically bonded steel plate on existing structures

#### 1.4. Research Objectives

The main objective of this research is to understand the behavior of beams with the proposed mechanically bonded steel plate and develop design aids for professional designers and practitioners based on comprehensive experimental, numerical and design oriented analyses. Within the main objective, sub objectives are:

- To study various finite element models developed by previous researchers to model mechanical connections e.g. shear stud connections systems using nonlinear behavior of reinforced concrete and steel (Basker 2002).
- To analyze various modes of failure of proposed beams observed during experimental tests conducted by Hossain (2001) and to identify factors affecting the ultimate strength of beams and mechanical connections.
- To develop numerical models for the prediction of strength and failure modes of beams strengthened by the proposed technique based on experimental results.

- To explore the problems encountered in the numerical modeling of the proposed strengthening system using the finite element software, *ABAQUS*.
- To explore the performance of different types of compatible connections available in *ABAQUS* to simulate the behavior of experimental beams.
- To develop design aids in the form of charts for the prediction of strength of beams with proposed mechanically bonded steel plates.
- To validate the performance of proposed design charts through experimental, various Code based procedures and other design-oriented analyses.

### **1.5. Plan of Investigations**

To conduct the research efficiently, a plan of investigation has been developed so that each part of the research can contribute in a meaningful way to the overall research. First, an experimental data is collected from previous research projects (Nupiri 2000, Jim 1999, Hossain 2001). Heavily instrumented test specimens provided information on load deflection response, stress-strain characteristics, failure modes and overall behavior of reinforced concrete beams with proposed mechanically bonded steel plate technique.

In terms of numerical analysis, the results of experimental studies are used to develop finite element models to simulate the behavior with the proposed strengthening technique using the finite element software, *ABAQUS*. Extensive parametric studies are conducted to optimize various numerical parameters associated with concrete/steel material properties, interface connections using various interface elements, element/mesh characteristics, non-linear solution schemes and convergence criteria.

In the final stage, using the developed finite element model, a large number of beams with various geometric and material properties are simulated to develop design aids that can be used for the design of members with the proposed technique. The performance of design charts are validated through Code based design procedures, other design oriented analysis and further experimental results. Other aspects such as construction of such novel form of beams, cost effectiveness and aspects of durability are also discussed to shed light on the significance of this approach.

#### **1.6. Organization of the Thesis**

This thesis is organized into six main chapters, each chapter having a main topic. Chapter 1 is the introduction, which provides a brief introduction about the need of strengthening, scope and objectives of the current research, research plan and organization of the thesis.

Chapter 2 gives an extensive literature review of existing rehabilitation methods and techniques highlighting recent strengthening methods and a reflection of the justification of research needs in improving strengthening techniques. Chapter 3 introduces the proposed new and innovative strengthening approach, which is the backbone of this research. It includes a detailed description of experiments conducted on beams strengthened by the proposed mechanically bonded steel plate.

Chapter 4 reports the development of numerical models based on experimental results using the finite element program, *ABAQUS*. It also addresses the parametric study

---

conducted to develop an authentic and viable numerical model that can be applicable to simulate any arbitrary beams with varying geometrical and material properties.

Chapter 5 presents the design aids and their performance validation through Code based procedures, other design oriented analyses and experimental results. Chapter 6 presents conclusions and future recommendations of the research. The references are provided at the end.

## **Chapter 2      Literature Review**

### **2.1.    Need for Strengthening Structures**

This chapter describes the work done by various researchers in the past and highlights the problems faced and outcomes of their research efforts. It includes brief insight into various theoretical models proposed for typical procedures adapted to strengthen reinforced concrete structures and their viability in practical applications and in design practices. This chapter also highlights the significance of the proposed strengthening technique in comparison with existing methodologies.

### **2.2.    Strengthening of Reinforced Concrete Beams with Adhesively Bonded Steel Plates**

The first documented application of externally bonded steel plate for repairing or strengthening of reinforced concrete (RC) structures was found in 1964, when the basement beams of an apartment complex in South Africa were strengthened with epoxy bonded steel plate because of accidental omission of steel reinforcements during construction (Xanthakos 1996). Thereafter, this technique was used to strengthen a variety of structures in various countries. The types of application of steel plate bonding based on the infrastructure statistics for the past 30 years are illustrated in Fig. 2.1 (Bonaci and Maalej 2000).

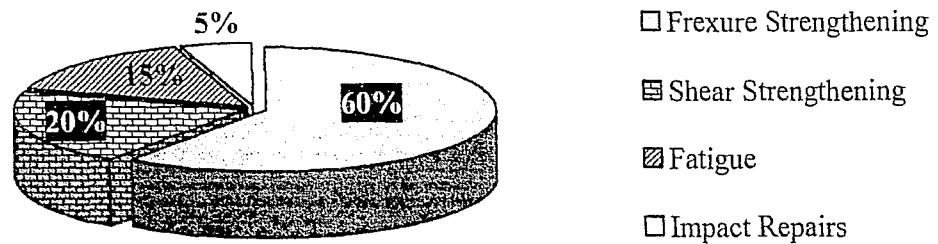


Fig. 2.1 Types of application of steel plate bonding according to infrastructure statistics (Bonaci and Maalej 2000)

### 2.2.1. Debonding of Steel Plates Due to Flexural and Shear Peeling Stresses

Reinforced concrete beams can be strengthened and stiffened by gluing steel plates to the tension face of the concrete. This procedure has been used to repair buildings (Van Gemert 1981) and to strengthen bridges (1978) and it has been used in various countries (Jones et al. 1988). Despite the overwhelming strength enhancement provided by the steel plate when bonded with epoxy resin, many of the research goes into studying because of the un-confinement of steel plate (not gripped) with concrete that results in peeling of the plate under increasing curvature of the beam as shown in Fig. 2.2 (Oehlers and Moran 1990).

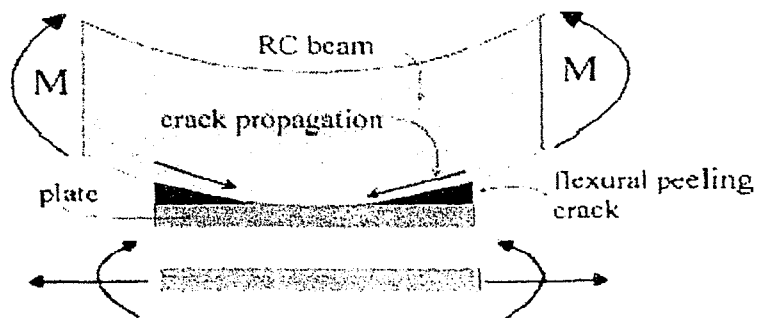


Fig. 2.2 Representation of flexural peeling mechanism (Oehlers and Moran 1990).



Hermite and Bresson (1967) carried out tests on concrete beams with steel plate bonded by epoxy resins to the tension surface. Tests were also performed on beams constructed by pouring concrete into U-shaped permanent forms coated with epoxy resin.

Solomon et al. (1976) working at the Wolfson Bridge Unit at Dundee University performed a series of flexural tests on double skin slabs and beams and investigated the suitability of the design procedures. Two types of specimens were considered, one where steel plates were glued on both faces of the hardened concrete core and the others where casting of concrete were performed directly against steel plates coated with adhesives in the mould. The failure of all beams took place after the slippage between the tensile plate and the concrete core at interface before the yielding in steel plate except in one test where yield stress was achieved. The strain in the upper steel plate remained well below the yield strength with no indication of buckling prior to failure reported. Mays and Smith (1980) updated the work carried out at the Wolfson Bridge Research Unit and confirmed the viability of bonded steel plates as a viable structural option but suggested further work was required on the long term durability and performance under actual traffic conditions.

Ong and Cusens (1982) noting the low stresses obtained on the upper flanges in the work of Solomon et al. (1976) carried out a series of tests using the cast-in-place technique by applying the adhesives to the steel and casting the concrete on top. They concluded that provided an efficient bond between the concrete and steel both slabs and beams behaved

compositely. For optimum strength and ductility, a 1-mm minimum adhesive thickness was suggested.

MacDonald (1978) reported on a series of tests on reinforced concrete beams with steel plates bonded to their tension flanges. The tests connected to the possible use for increasing the load capacity of existing bridges. An interesting result of the experiments was the failure of the beams at load similar to that of the unplated beams because of premature failure at the interface of the steel plate and the concrete. Variables such as type of resins, thickness of plate, the effect of load cycling had little effect on the load causing plate separation.

Based on the experimental study (Oehlers and Moran 1990), it was concluded that the presence of stirrups in reinforced concrete beams can increase the shear strength of beams by up to a factor of six but the load at which the peeling occurred does not increase. Therefore, it was assumed that the shear peeling is a function of shear strength of the beam without stirrups, which is the strength that can be found in most of the codes.

Oehlers (1992) found a very strong inter-relation between flexural and shear peeling of the plate. Based on the failure envelope plotted with the slope of one and through all the mean values of experimental results as shown in Fig. 2.3, the recommended design procedure as represented in Eq. 2.1, for plating the soffit of reinforced concrete beams so that the plate does not debond until the design load is reached.

$$\frac{M_p}{M_{up}} + \frac{V_p}{V_{uc}} < 1.17 \quad M_p < M_{up} \text{ and } V_p < V_{uc} \dots \dots \dots (2.1)$$

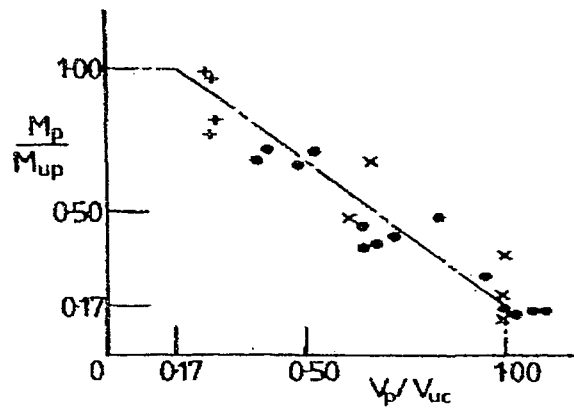


Fig. 2.3 Interaction between shear and flexure peeling, (Oehlers 1992).

where  $M_p$  and  $M_{up}$ , correspond to moment at the end of the plate when peeling occurred and ultimate moment at the end of plate when shear force is zero, respectively, whereas  $V_p$  and  $V_{uc}$  are the shear loads at the end of peeling when peeling occurred and shear strength of reinforced concrete beam without stirrups, respectively.

Hamoush and Ahmad (1990) developed a finite element model to investigate the failure mechanism by interface debonding of the plate and the adhesive layer due to high interface shear stresses, which exist at the interface. Investigation also includes the variation of critical strain energy release rate, which causes the interfacial crack to propagate.

It was concluded that the strain energy release rate peaks when the ratio of interfacial crack length to the half of beam span reaches 0.083 that correspond to the crack length of 100 mm (Hamoush and Ahmad 1990). This indicates that the shear stress distribution at the crack tip is maximum where the length of interfacial crack is approximately equal to

the height of flexural crack. It was also concluded that the presence of large number of flexural cracks (greater than five) releases the shear stresses at the interface and leads to the reduction of strain energy release rate and stress intensity factor. The proposed design rule represented by Eq. 2.2 includes the critical load ( $P_{cr}$ ) as a function of the applied load ( $P_{applied}$ ) and the strain energy release rates  $G_{cr}$  and  $G_{applied}$ . The term  $G_{cr}$  can be computed through experimental and analytical procedures.

$$P_{cr} = P_{applied} \times \sqrt{\frac{(G_{cr})}{(G_{applied})}} \dots\dots\dots (2.2)$$

Hussain et al. (1994) proposed a simple mathematical model as rational guidelines based on the strength design method, towards the designing of external steel plated singly reinforced beams for strengthening as represented in Eq. 2.3 and Eq. 2.4 based on Fig. 2.4.

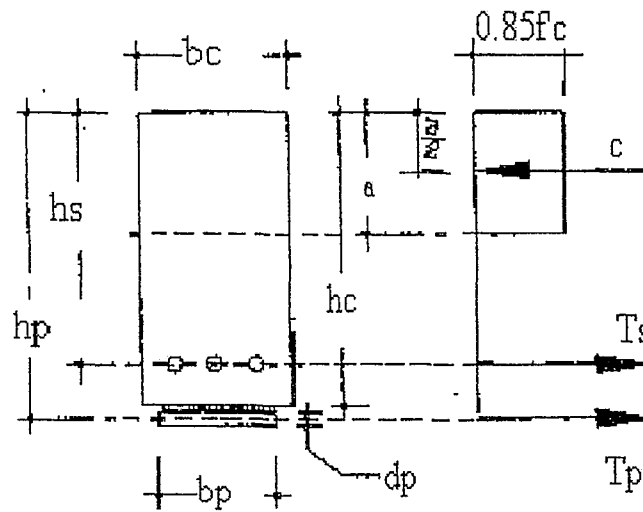


Fig. 2.4 Ultimate forces acting on a plated beam section (Hussain et al. 1994)

Where,

$$\frac{M_u}{\phi} = T_s \left[ h_s - \frac{a}{2} \right] + T_p \left[ h_p - \frac{a}{2} \right] \dots \dots \dots (2.3)$$

and the depth of rectangular stress block “a” is represented as;

$$a = \left( \frac{A_s f_y + b_p d_p f_{yp}}{0.85 f'_c b_c} \right) \dots \dots \dots (2.4)$$

Many of the research in the early 1990s were concentrated on the behavior of stress transfer through bond at the concrete-steel plate interface. Chajes et al. (1996) played a vital role in investigating the behavior of the force transfer through bond and length of plate required based on single lap shear test. According to the study, if the failure mode of the joint is governed by the shearing of the concrete directly beneath the bond, the value of ultimate bond strength will be proportional to  $\sqrt{f'_c}$ . The strain distribution along the bonded length decreases at fairly linear rate (especially at or below service load levels) meaning that the force transfer is largely uniform which lead to a constant value of bond resistance (R).

Täljsten (1996) concluded that the stress concentration was very high at the plate curtailment and quickly diminishes near the high moment varying zone. Furthermore, the biggest geometrical influence on the level of shear and peeling stresses is the distance between the support and the plate end. In order to minimize these stresses, the distance of plate end from the support should be kept minimum. Also, increasing stiffness of epoxy or steel plate increases shear and peeling stresses at the plate end.

Tadeu et al. (2000) showed the other factors such as temperature variation and type of concrete have a great influence on the occurrence of failure as they performed shear test under high temperature. According to them, at 60 °C, epoxy such as SIKA ICOSIT K-AC loses half of its strength, and at about 90 °C, the strength reduces to 24-29%. Moreover, at 120 °C, a film of water was observed on the surface of the concrete, in addition to the deterioration of the resin. This may be caused by the release of free water present within the concrete by evaporation at 100 °C. The migration of free water causes the appearance of pressure on the bond, contributing to the failures.

Aprile et al. (2001) used the bond slip model proposed by Spacone and Limkatanyu (2000) and developed a simple and accurate displacement-based fiber frame element to evaluate the shear stress distribution under increasing load by taking into account all the nonlinearity of material including tension stiffening of concrete. They concluded that the failure of plated beams always started by plate debonding, either at plate ends or somewhere in a cracked concrete zone.

Leung (2000) further worked out on a model based on fracture mechanics to find the combination of parameters affecting the delamination of steel plate with respect to shear stresses formed under increasing load. It was concluded that delamination was favored by large member sized, low adhesive thickness, low plate stiffness and small contact area between plate and adhesive. This was contrary to the statement of Oehlers and Ali (2003) that beams plated over part of their width had an increased flexural peeling strength.

Ali et al. (2001) developed a mathematical model, to quantify shear-peeling mechanism as shown in Fig. 2.5 based on Fig. 2.6.

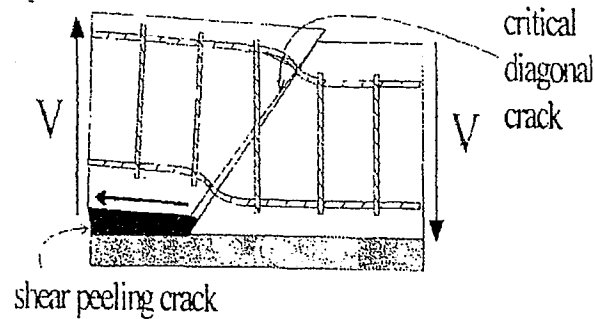


Fig. 2.5 Shear peeling mechanism (Ali et al. 2001).

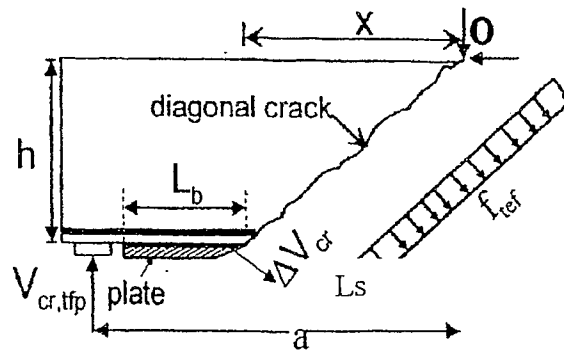


Fig. 2.6 Forces in cracked steel plated beams (Ali et al. 2001).

A new approach was implemented after realizing the fact that the brittle failure (shear bond failure) initiated, when the plate ends were placed in predominantly shear regions. The model proposed is represented in Eq. 2.5, which is based on plasticity concept for shear strength in reinforced concrete plated beams. The proposed diagonal cracking load can be obtained by taking moments of all the forces about point O, as shown in Fig. 2.6.

$$V_{cr} = \left( \frac{x^2 + h^2}{L_s} \right) \left( \frac{f_{tef} b}{2} + \frac{m f_t b t_p (h + 0.5 t_p)}{h^2} \right) \dots\dots\dots (2.5)$$

Hui-Shen and Yang (2001), found that all the previous theories about interfacial shear stress between steel plate and concrete had suffered from some limitations. It was observed that, the maximum value of the shear stress at adhesive-to-concrete interface is slightly greater than the plate-to-adhesive interface but the maximum value of normal stress at the concrete-to-adhesive interface is much greater than that of the plate-to-adhesive interface, indicating that the adhesive-to-concrete is much more critical interface for debonding failure.

Mukhopadhyaya and Swamy (2001) realized the urgent need for the development of a simple model for design against debonding of plated beams. To capture the influencing parameters that caused premature debonding failure, the experimental investigation done by Robert (1989) was carefully reviewed (Mukhopadhyaya and Swamy 2001). It was concluded that, the value of the shear stress at which plate debonding failure occurs was influenced by the elastic modulus of the plate material (E), stress-strain profile of the plate material, ratio of moment carries by the internal reinforcing bars to that of moment carries by external plate, geometry of beam, the shear span to depth ratio and also to a lesser extent, by the concrete strength.

It has also been documented that to prevent abrupt debonding failure at the plate end, bolt shear connectors can be used to increase the resistance against debonding of epoxy bonded steel plated beams. However, according to Ali and Oehlers (2003), it is not



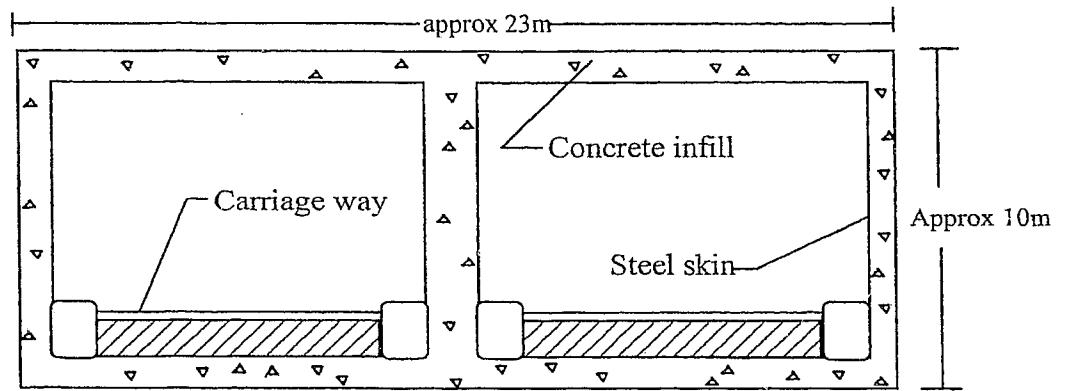
recommended to apply such a technique because the bolted shear connector requires interface slip to transfer shear stresses and hence adhesively bonded steel plate will debond before the bolts become active.

### **2.2.2. Strengthening of Reinforced Concrete Beams with Mechanically Bonded Steel Plates**

Parallel to adhesive bonded connections, mechanical connections have also been facilitated. Solomon (1976) & Solomon and Goplani (1979) described a series of 5 tests on beams externally reinforced by a single 1.84 mm thick mild steel sheet of 4 m length and 0.36 m width. The stirrups were welded to the surface of the sheet. The beams were tested under four points loading and deflection and strains in concrete and steel were recorded during the test. No bond failure at the steel concrete interface nor indication of shear cracking within the shear span was observed. All beams collapsed due to the failure of the upper concrete in flexural compression following tension yielding of the lower steel sheet. Solomon et al. (1979) concluded that the beams satisfied the ultimate and serviceability requirements and that the main economics of this approach would be in the ease of construction and the reduction in reinforcing steel and formwork.

One of the largest bodies of work investigating the application of double skin composite beams and columns where mechanical devices are used to secure bond between steel and concrete has been performed at the University of Wales College of Cardiff. The system was originally devised for submerged tube tunnels (Fig. 2.7) by a team of consultants in Cardiff (Tomlinson and Partners with Sir Alexander Gibb and Partners). The system proposed by Naraynan et al. (1987) consisted of a double-skin steel plated construction

secured by welding headed studs at suitable intervals anchored in a concrete infill. The spacing of the studs was used to control the local buckling of the steel sheets under loading.



Typical tunnel section

Fig. 2.7 Typical cross section of conventional tube tunnel (Naraynan et al. 1987).

The advantages over traditional reinforced concrete tunnels included fabrication in sections, speedier construction and better quality control. Also, in conventional concrete tube tunnels, an outer steel layer is required to ensure water tightness but with external steel skin reinforcements, this would not be required. Tests were performed on full and half scale models of the tunnel sections.

The half scale tests with a rectangular cross-section 250 mm deep x 800 mm wide and 4 m long had steel plates 6 mm and 3 mm thick secured to the outside and inside of the concrete by 6 mm diameter mild steel bolts. The failure of the beams in simply supported and cantilevered tests was exhibited by shear cracks developing in the concrete at the quarter span positions with steel plate buckling and yielding accompanied by stud shearing. The full-scale double skin composite beams had full size stud connections

spaced at 300 mm centres. The type of failure is similar to the half scale tests. Narayanan et al. (1987) concluded that the applications of the system were not limited to submerged tunnels but had wider general applications in construction.

Oduyemi and Wright (1989) reported on an investigation into the behavior of double sandwich beams. They tested 18 model beams of dimension 150 mm x 150 mm x 1500 mm under four point loading (Fig. 2.8) to investigate the effect of overlapping shear studs, steel skin thickness, spacing of top shear connector, amount of bottom shear connector and low concrete strength.

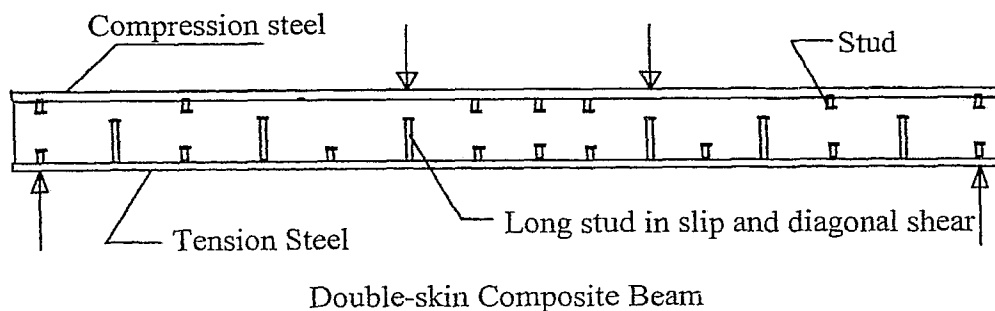


Fig. 2.8 Typical cross section of double skin composite beam (Oduyemi and Wright 1989).

The bond between the steel plate and the concrete was removed by greasing the inside faces allowing the studs alone to take the interface shear. The beams were expected to fail in either flexural, horizontal slip or vertical shear failure. When flexural failure of the beam occurred, the deflection was linear up to tensile stress of lower steel plate. After yielding, the beams behaved with a large amount of ductility until collapse produced by concrete crushing. Horizontal slip failure occurred after the flexural cracking of the concrete and an increasing rate of bottom slip. The failure was sudden with shearing of the bottom plate from concrete caused by stud failure. Vertical shear failure occurred in

the 'diagonal tension' manner with final collapse when the dowel action capacity of the steel plates was reached. This type of failure was prevented by introducing long studs to provide shear reinforcement. Local buckling of the compression plate reduced the value of ultimate load in some tests and so a maximum stud spacing/plate thickness ratio of 30 was proposed. Oduyemi and Wright (1989) concluded that flexural failure of the beam could be realized by providing short studs to transfer shear bond and long studs to carry diagonal tension stresses. In order to take account of the effects of combined shear, axial and bending stresses, the design strength of the shear studs was recommended to be 55% in the tension zone and 80% in the compression zone of the ultimate strength obtained from push-out tests.

Oduyemi and Wright (1990) continued the previous investigations by testing 12 scale model beam/column elements. There were three groups of 4 tests each. The first group of tests investigating the variations in the axial load failed in a flexural manner with cracks appearing at higher load levels for greater axial loads. In the second group, where the spacing between the connectors varied, those tests with the studs closely spaced failed in flexure while the later tests with studs further apart collapsed due to longitudinal shear. In the final group looking at the effect of thickness, the tests with thin plates failed in flexure because of yielding of the steel and the test with thickest plate shear studs failed, before yield, at the steel/concrete interface. The authors concluded that the shear connection at the tension plate was critical in determining the behavior of the element but with correct design, predictable critical loads could be achieved.

Kountoris (1990) produced design charts for the double skin composite elements based on the requirements of BS8110 with modifications to take account of failure at the steel/concrete interface. The design curves showed greater convergence to experimental as the load eccentricity increased probably because flexural rather than axial failure occurred.

Wright, Oduyemi and Evans (1991) described design developments based on the series of tests on double skin beams, columns and beam/columns. The design basis was similar to that of reinforced concrete but with the additional considerations of the possibility of plate buckling and adequate provision of shear connector. The ultimate strength in bending was based on the BS8110 stress block with a partial safety factor of 1.5 on the concrete and 1.15 of the steel strength. These equations assumed full connection between the steel plate and the concrete, which require sufficient shear connectors capable of transferring the full yield load to the steel. Design recommendations were made to avoid buckling of compression plate, for basic design shear strength and for combined axial and bending effects.

Oehlers (1992) and Oehlers, Wright and Burnet (1994) described a construction technique that uses profiled steel decking as permanent and integral shuttering for the sides and soffits of the reinforced concrete beams. In this form of construction, the profiled sheet is first fabricated into fully braced open box girders and reinforcing bars are added as required. The box section can be placed on site with a minimum of additional support, and the concrete can then be poured to form a composite profiled

beam. Previous research (Oehlers 1992) has shown that this system has many advantages: the side profiled sheets can substantially increase the flexural strength without loss of ductility and are more ductile than reinforced concrete beams of same flexural strength; the side sheets also increase the shear strength and shear ductility; encasement of concrete reduces shrinkage and creep of concrete, which can reduce deflections by as much as 40% and allow an increase in span/depth ratio of the order of 20%. Oehlers found that the flexural strength of the profiled beams can be affected by the local buckling of the sheet between the ribs of the decking.

Oehlers, Wright and Burnet (1994) developed simple design procedures to prevent local buckling of the profiled sheeting before the ultimate strength is reached, and to determine the flexural strength of the beam for various strength of shear bond which allows for the variation in the bond forces at the interface due to slip. They confirmed that the shear bond failure has only a small effect on the ultimate strength.

Foley and Buckhouse (1999) proposed a technique, which was very simple and devoid of complex formulas as basic principle of reinforced concrete was used in design. They successfully tried to increase the capacity and stiffness by bonding steel channels through bolts at regular intervals on the underside of concrete, but they also informed the lack of ductility at ultimate stages.

### **2.2.3. New Approach to Steel Plate Bonding**

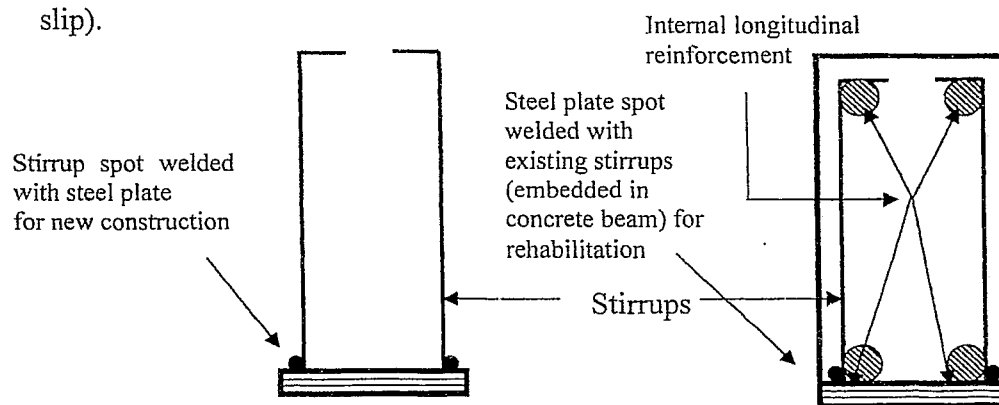
A new approach to steel plate bonding in which steel plate was welded to the legs of the uniformly distributed stirrups to alleviate the complexities associated with the peeling

stress developed in the epoxy bonded steel plate (Hossain 1999, Jim 1999, Nupiri 2000, Kashif et al. 2004) as shown in Fig. 2.9.

The advantages of this technique are to utilize the stirrups (embedded in concrete beams) for two purposes:

- (a) to provide adequate shear resistance
- (b) To provide plate with a strong mechanically bonded connections in resisting horizontal slip.

In this system, shear stirrups are supposed to act like a shear stud and provide resistance to both diagonal tension failure and horizontal slip at the connection. This technique also has a potential to be used to construct beams and girders in bridges and buildings. Failure of such beams was found to depend on the mode of interface connection, geometric dimensions of beams, and spacing of shear reinforcement and thickness of steel plate (Hossain 2001, Hossain 1999). Depending on the relative influence of such parameters, the beams failed either by tearing of steel plate or by interface failure (without horizontal slip).



(a) Stirrups plate assembly (b) Steel plate welded with existing stirrups of RC beam

Fig. 2.9 System components of mechanically bonded/welded strengthening system

Test results showed that beams welded with relatively thin plates (i.e. 0.5 mm etc.) failed by tearing of sheets rather than due to crushing of concrete at the top or by failure at the spot welded locations as found in beams welded with thicker steel plate (Hossain 1999).

The technique of welding steel plate with stud embedded in concrete shows a simple and straightforward procedure in designing double skin sandwich composite beams and columns. The failure associated with horizontal slip, buckling of composite plate was determined, and design guidelines have been proposed to overcome these kinds of failure modes (Wright, Oduyemi and Evans 1991). Similar to that approach, a procedure for strengthening reinforced concrete beams with welded steel plate to the legs of stirrups is proposed to overcome some of the problems associated with adhesively bonded composites techniques as discussed earlier.

This new strengthening system also has potential to be used as a new technique to effectively construct beams or girders in buildings, bridges and other forms of new construction. The problems associated with adhesives is removed using strong spot welded connection and the variation in temperature as well as complex design calculation for limiting adhesive thickness, extensive surface preparation and provision for adhesive drying time are completely eliminated. Moreover, the problem of flexural and shear peeling stress that can cause debonding of steel could be converged into two simple modes of failure such as tearing of plate and failure of spot weld. Failure of spot weld in beams welded with thicker plate was also reported (Hossain 1999, Nupiri 2000, Hossain 2001).



The literature review suggests the novelty of this form of construction. Currently design guidelines are not available for this new form of construction and hence, there is a need for the development of design guidelines. The current research will focus on this aspect. Comprehensive finite element analysis based on experimental results will be conducted in order to develop a reliable finite element model, which can be used to simulate numerous computer model beams with variable geometric and material properties. The results from computer model beams will be used to develop quick, simple and accurate design guidelines for practical applications.

# **Chapter 3      A New Approach to Steel Plate Bonding Technique: Review of Experimental Investigations**

## **3.1.    Introduction**

This chapter describes the proposed strengthening technique in details with its application procedures for frequent field applications and enlightens the significance of this technique over other prevailing techniques. Experiments conducted by Jim (1999) and Nupiri (2000) on beams with the proposed strengthening technique reported by Hossain (2001), are described in order to understand the overall behavior and failure modes of member strengthen with such a technique. Factors affecting the strength and failure modes of beams with the proposed strengthening technique are critically reviewed so that they can be used for efficient modeling of such a system by finite element analysis.

## **3.2.    Introduction of New Approach**

Conventional methods using epoxy bonded steel plates for strengthening reinforced concrete members have shown problems with epoxy, surface preparation techniques and premature debonding. The proposed method with steel plate mechanically bonded to the stirrup through welded connections (Fig. 2.9) can avoid deficiencies observed in conventional methods. The variables affecting the performance of such beams are the strength of weld, geometric properties of beam, thickness of the steel plate and the amount of longitudinal and shear reinforcement of the existing beam. Strength of spot weld can vary in order to achieve desired contact stiffness. Steel plate of optimum size

should be selected as welding may cause some material damage due to residual stress depending on the strength and thickness of steel plate. Compatibility of weld strength and the strength of steel plate and stirrups should be analyzed prior to implement this technique.

### **3.3. Characteristics of Proposed Technique**

This technique can avoid peeling of plates as well as temperature effects on bonding as observed in epoxy-bonded methods. The potential pre-fabrication of this technique and avoidance of extensive surface preparation for epoxy bonding or complex procedure associated with bolting of steel plate to concrete can be contributing factors to make this system as a simple and cost effective in construction. The use of unskilled labor and reduction in construction time can also lead to cost effective solution to upcoming needs for strengthening.

This strengthening technique offers different arrangement of steel plates for strengthening. Typical forms of such beams with various modes of mechanical connections are shown in Fig 3.1(a-d). Main reinforcement can also be used with steel plates to strengthen beams as shown in Fig. 3.1(b-c). Two steel plates can be used inside the stirrups for ease in casting of concrete as shown in Fig. 3.1(c). This form of arrangement has also a potential to be use in new construction. The stirrup-plate assembly acts as both shear and main reinforcement in such beams.

For retrofitting and strengthening, mechanical connection can be provided with various arrangements where the steel plate can be used either alone or with longitudinal

reinforcement inside the stirrups or outside the stirrups around the existing damaged beam as shown in Fig. 3.1(d). Other problems in such construction during retrofitting can be overcome without much difficulty. The problem of corrosion can be eliminated by providing sufficient concrete cover around the existing strengthened beam.

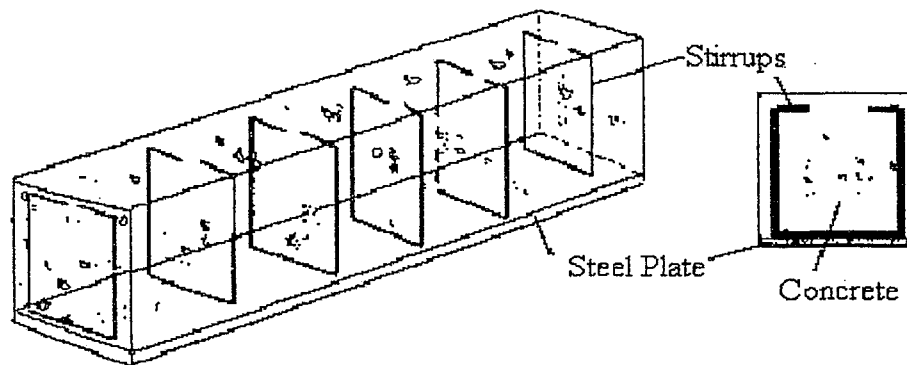


Fig 3.1 (a) Steel plate-stirrups assembly (Hossain 1999)

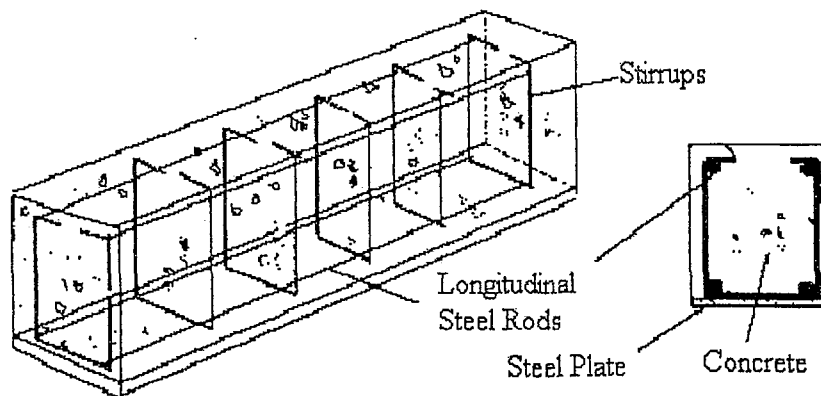


Fig 3.1 (b) Steel plate-stirrups assembly with longitudinal reinforcement (Hossain 1999)

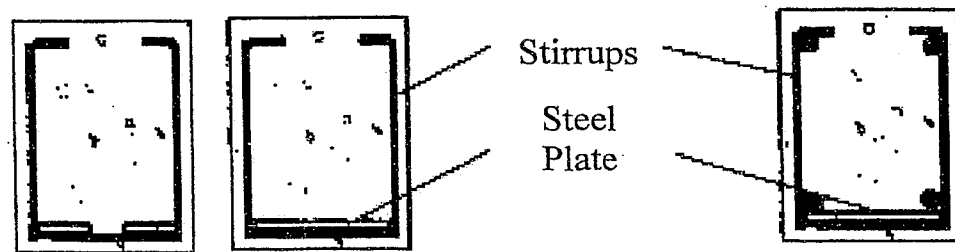


Fig 3.1 (c) Single and double plate assembly with and w/o internal reinforcement  
(Hossain 1999)

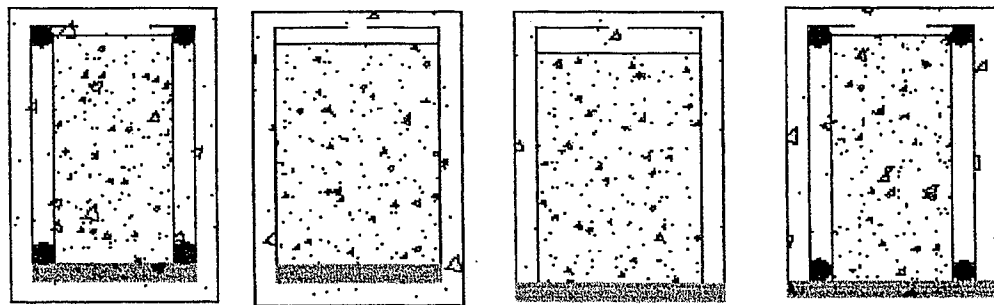


Fig 3.1 (d) Damage retrofitted beam (Hossain 1999)

Fig. 3.1 Mechanically plate bonding technique with different plate arrangement

### 3.4. Field Application Procedure

The proposed technique is simple to implement in retrofitting or strengthening damaged beams. Normally concrete cover from existing beams is chipped off to expose the steel stirrups. The stirrups are then cleaned with wire brush to remove dust and stains. The steel plate of optimum thickness (as per design) is then placed parallel to tension face of existing concrete members and welded to the legs of stirrups. More or less the same procedure can be adopted with different plate arrangement shown in Fig. 3.1(a-d). For ease in construction at site, the following procedure can be adopted: (a) steel plate-

stirrups or plate-stirrups-main reinforcement assembly can be prefabricated and then placed around the existing beam of interest, (b) the connection between existing beams and steel plate-stirrups assembly can be provided by welding stirrup of existing beams with those of assembly, and (c) finally, the process ends up by filling the spaces between formwork and steel plate, between steel plate and existing beam and assigned cover thickness using either shotcrete or a flowable concrete such as self-consolidating concrete.

### **3.5. Experimental Studies**

Comprehensive series of tests were conducted to investigate the behavior of such composite beams (Hossain 2001, Hossain 1999, Jim 1998, Nupiri 2000). Heavily instrumented tests provided details information on the load deflection response and failure modes of the system. Test parameters included were:

- Spacing of shear reinforcement,
- Mechanical bonding at interface,
- Thickness of steel plate, and
- Longitudinal reinforcement.

Two series of beams will be the focus of attention throughout the research and describe as series 1 and series 2 beams. Series 1 beams have steel plate-stirrups assembly without longitudinal reinforcement while series 2 beams have 5-mm diameter longitudinal reinforcement (Hossain 2001).

### 3.5.1. Beam Geometric Properties

Typical cross-section of tested beams are shown in Fig. 3.2. Detailed geometric properties of beams are summarized in Table 3.1. All test specimens had constant length “L”, width “b” and depth “d” to study the effect of variation in thickness of steel plate “ $t_p$ ”, spacing of shear reinforcement “S” and the presence of longitudinal reinforcements. All beams in Series 2 had 5-mm  $\Phi$  longitudinal reinforcement at top and bottom, while Series 1 had no longitudinal reinforcement. Both series of beams had 0.4-mm and 3-mm thick steel plate respectively welded at the bottom in addition to internal longitudinal steel reinforcement (in case of series 2 beams). Both series of beams had 5-mm diameter stirrups with spacing ranging from 50 mm to 180 mm.

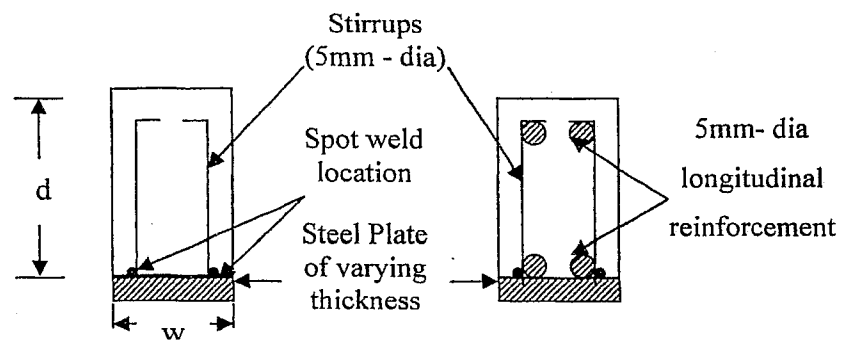


Fig. 3.2 Cross-section details of pilot beams.

Table 3.2 shows the material properties associated with concrete, internal longitudinal reinforcement and steel plate extracted from experimental studies and reinforcement details. The beams were named, for example, as  $S_1B_{50}$  where subscript of S represented the Series number and subscript of B represented the spacing of stirrups in mm followed by the plate thickness in mm.

	Effective Length	Width	Total Depth	Top Cover	Bottom Cover	Side Cover
	"L"	"b"	"h"			
	mm	mm	mm			
S <sub>1</sub> B <sub>50</sub> - 0.4mm	800	100	150	10	10	10
S <sub>1</sub> B <sub>100</sub> - 0.4mm	800	100	150	10	10	10
S <sub>1</sub> B <sub>150</sub> - 0.4mm	800	100	150	10	10	10
S <sub>1</sub> B <sub>180</sub> - 0.4mm	800	100	150	10	10	10
S <sub>1</sub> B <sub>50</sub> - 3mm	800	100	150	10	10	10
S <sub>1</sub> B <sub>100</sub> - 3mm	800	100	150	10	10	10
S <sub>1</sub> B <sub>150</sub> - 3mm	800	100	150	10	10	10
S <sub>1</sub> B <sub>180</sub> - 3mm	800	100	150	10	10	10
S <sub>2</sub> B <sub>50</sub> - 0.4mm	800	100	150	10	10	10
S <sub>2</sub> B <sub>100</sub> - 0.4mm	800	100	150	10	10	10
S <sub>2</sub> B <sub>150</sub> - 0.4mm	800	100	150	10	10	10
S <sub>2</sub> B <sub>180</sub> - 0.4mm	800	100	150	10	10	10
S <sub>2</sub> B <sub>50</sub> - 3mm	800	100	150	10	10	10
S <sub>2</sub> B <sub>100</sub> - 3mm	800	100	150	10	10	10
S <sub>2</sub> B <sub>150</sub> - 3mm	800	100	150	10	10	10
S <sub>2</sub> B <sub>180</sub> - 3mm	800	100	150	10	10	10

Table 3.1 Description of geometrical properties of test series

### 3.5.2. Fabrication, Casting, Curing and Material Properties

The stirrups-steel plate-main reinforcement assembly for each of beams was fabricated first (Hossain 2001). Connection between steel plate and stirrups was provided by spot welding. The whole assembly was then placed in wooden mould for casting concrete (Fig. 3.3). Compaction of concrete was done by poker vibrator in a single layer. Control concrete cylinders and cubes were cast at the same time for compressive strength test. The beams were remolded after 24 hours of casting and moist cured until tested at 30<sup>th</sup> day.



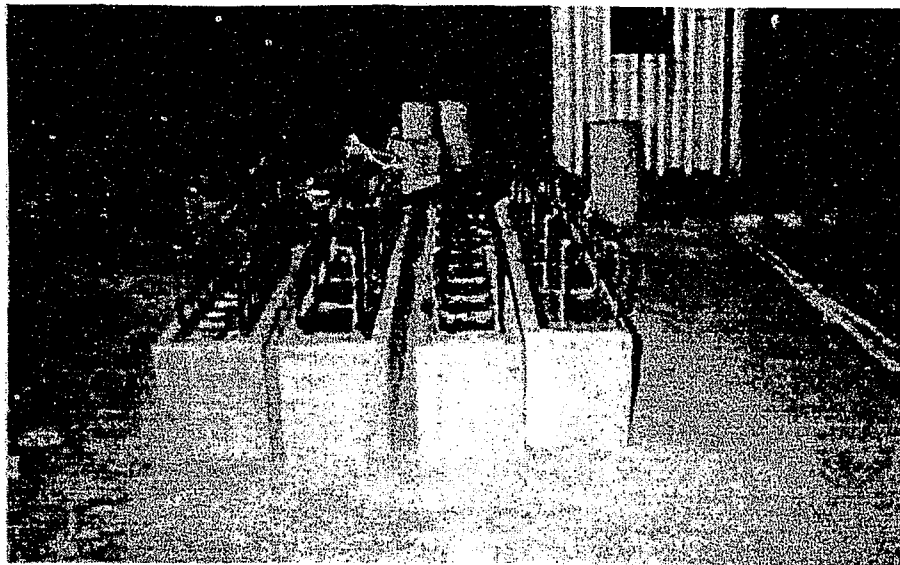


Fig. 3.3 Assembly of test specimens during casting (Hossain 2001)

Tensile tests were carried out on 0.5 mm and 3 mm thick plate and the corresponding yield strength ( $f_{yp}$ ) of steel plate with and without spot weld was determined (Fig. 3.4).

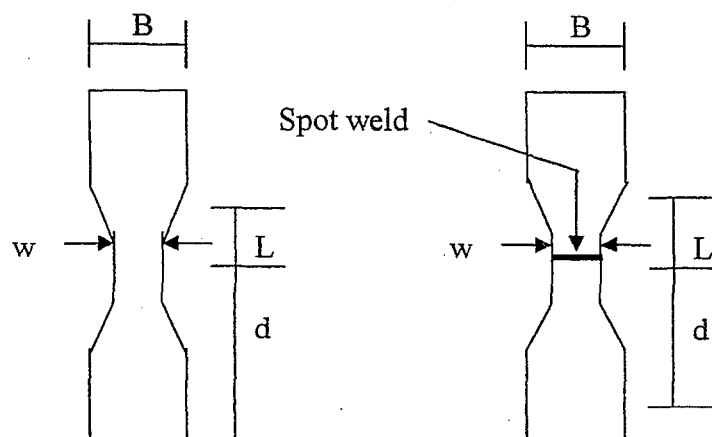


Fig. 3.4 Tensile test specimen (Hossain 2001)

Beam Designation		Material Properties			Reinforcement Details		
					5 mm - Diameter		Plate Th.
		$f_c$	$f_{ys}$	$f_{yp}$	Long. R/f	Stirrups Spacing	
		MPa	MPa	MPa	Details	mm	
S <sub>1</sub> B <sub>50</sub> - 0.4 mm	Jim 1999	38	455	360	-	50	0.4
S <sub>1</sub> B <sub>100</sub> - 0.4mm		38	455	360	-	100	0.4
S <sub>1</sub> B <sub>150</sub> - 0.4 mm		38	455	360	-	150	0.4
S <sub>1</sub> B <sub>180</sub> - 0.4mm		38	455	360	-	180	0.4
S <sub>1</sub> B <sub>50</sub> - 3 mm	Nupiri 2000	41	455	366	-	50	3
S <sub>1</sub> B <sub>100</sub> - 3mm		41	455	366	-	100	3
S <sub>1</sub> B <sub>150</sub> - 3 mm		38	455	366	-	150	3
S <sub>1</sub> B <sub>180</sub> - 3mm		38	455	366	-	180	3
S <sub>2</sub> B <sub>50</sub> - 0.4 mm	Jim 1999	38	455	360	2-B	50	0.4
S <sub>2</sub> B <sub>100</sub> - 0.4mm		38	455	360	2- T, 2-B	100	0.4
S <sub>2</sub> B <sub>150</sub> - 0.4 mm		38	455	360	2- T, 2-B	150	0.4
S <sub>2</sub> B <sub>180</sub> - 0.4 mm		38	455	360	2- T, 2-B	180	0.4
S <sub>2</sub> B <sub>50</sub> - 3 mm	Nupiri 2000	39	455	366	2- T, 2-B	50	3
S <sub>2</sub> B <sub>100</sub> - 3 mm		39	455	366	2- T, 2-B	100	3
S <sub>2</sub> B <sub>150</sub> - 3 mm		39	455	366	2- T, 2-B	150	3
S <sub>2</sub> B <sub>180</sub> - 3 mm		39	455	366	2- T, 2-B	180	3
Notation "T" and "B" in longitudinal reinforcement refer to as Top and Bottom reinforcement							

Table 3.2 Material properties of experimental reinforced concrete beams

Similar test was also performed on 5 mm diameter mild steel rods, which were used as longitudinal and shear reinforcements to determine the yield strength ( $f_{ys}$ ). Properties of concrete, steel plate and rods are presented in Table 3.2.

### 3.5.3. Instrumentation and Test Setup

Assembly of test setup is shown in Fig. 3.5 and schematic representation of test setup showing strain gauge location is presented in Fig. 3.6 (Hossain 1999, Hossain 2001). One strain gauge was installed at the center of the steel plate while the other was placed at 25 mm above the bottom of concrete.

Both strain gauges were installed at mid span of the beam. The beam was tested incrementally under four point loading system. At each increment of load, the dial gauge and electronic strain measuring equipment recorded deflection and strains, respectively.

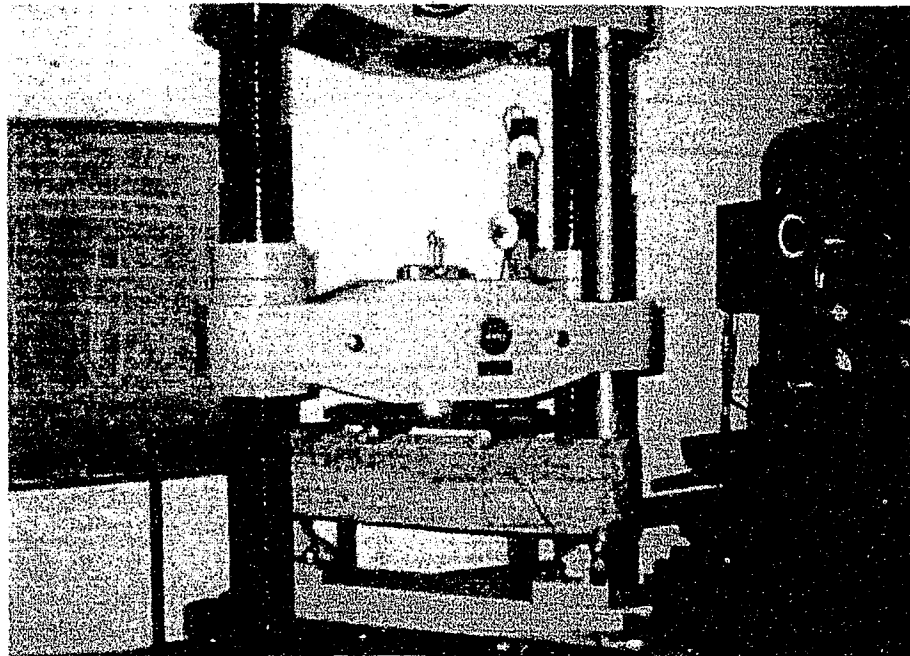


Fig. 3.5 Assembly of test setup (Hossain 1999, Hossain 2001)

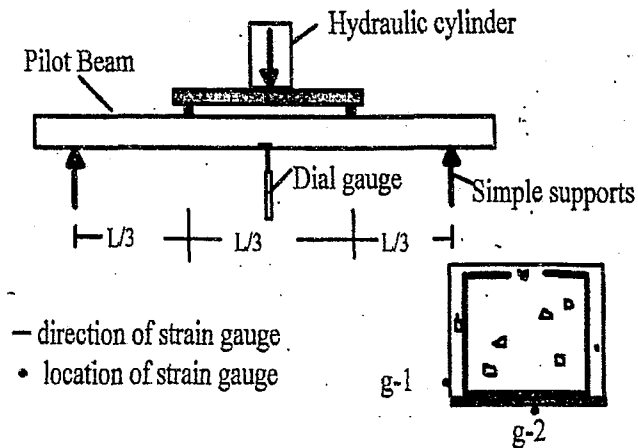


Fig. 3.6 Schematic of test set-up and instrumentation (Hossain 1999)

### 3.5.4. Failure Modes of Tested Beams

#### 3.5.4.1. Beams with 0.4-mm Thick Plate

Failure modes in all beams having 0.4-mm thick plate were initiated with the initial debonding of the steel plate between adjacent spot-weld locations. Progressive loading yielded further initiation of cracks starting from the bottom and propagating towards the center of the beam as represented in Fig. 3.7. Beam  $S_1B_{50}$  and  $S_1B_{100}$  failed by tearing of plate with cracking extended to the full depth of the beam.

For  $S_1B_{150}$  and  $S_1B_{180}$  beams, the failure was due to the insufficient shear reinforcement. Series 2 beams, failed by tearing of steel plate with the development of cracks extending up to full depth of beams. Failure of both Series 1 and Series 2 beams was predominantly due to tearing of plate because of excessive flexural stresses as shown in Fig 3.7 and Fig. 3.8.

It is worth noting that in all tested beams, failure was either due to the tearing of sheeting or weld failure.  $S_1B_{100}$  beam showed large deflection among those of series 1 beams. This might be due to the fact that the cracks propagated very quickly to the compression zone resulting in crushing at the top. Flexure cracks also induced interface shear between spot welded sections of the steel plate.  $S_2B_{50}$  failed predominantly in flexure due to tearing of plate followed by flexure cracks propagated straight to the top.  $S_2B_{100}$ ,  $S_2B_{150}$  and  $S_2B_{180}$  beams failed in a mixed mode of flexure-shear failure with tearing of plate as shown in Fig. 3.8.

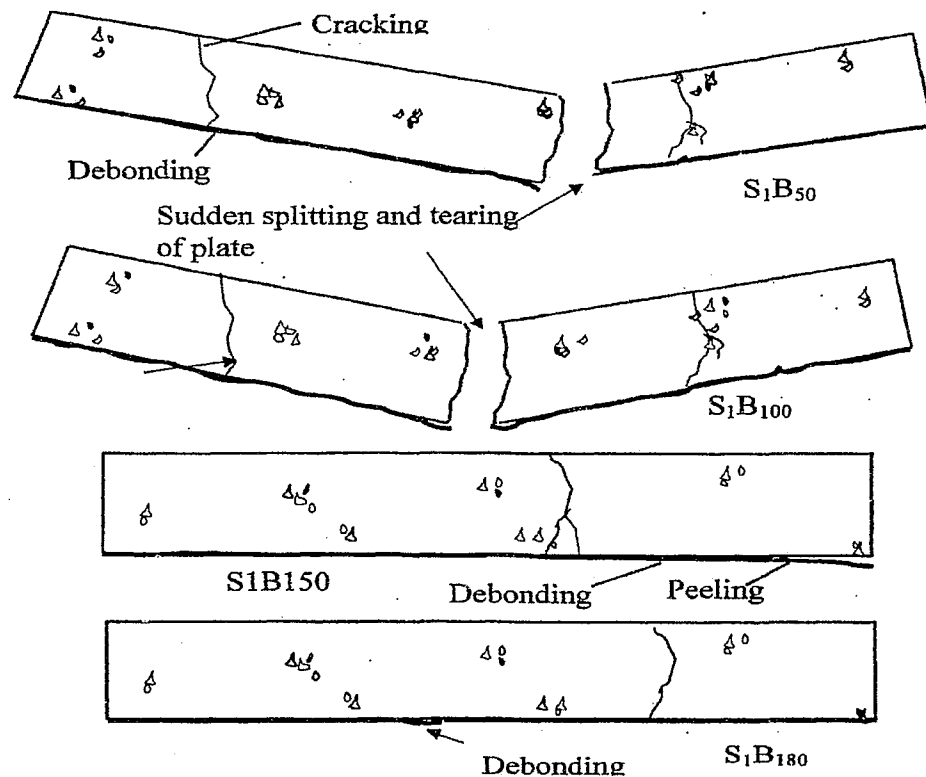


Fig. 3.7 Failure modes of Series 1 beams (Hossain 2001)

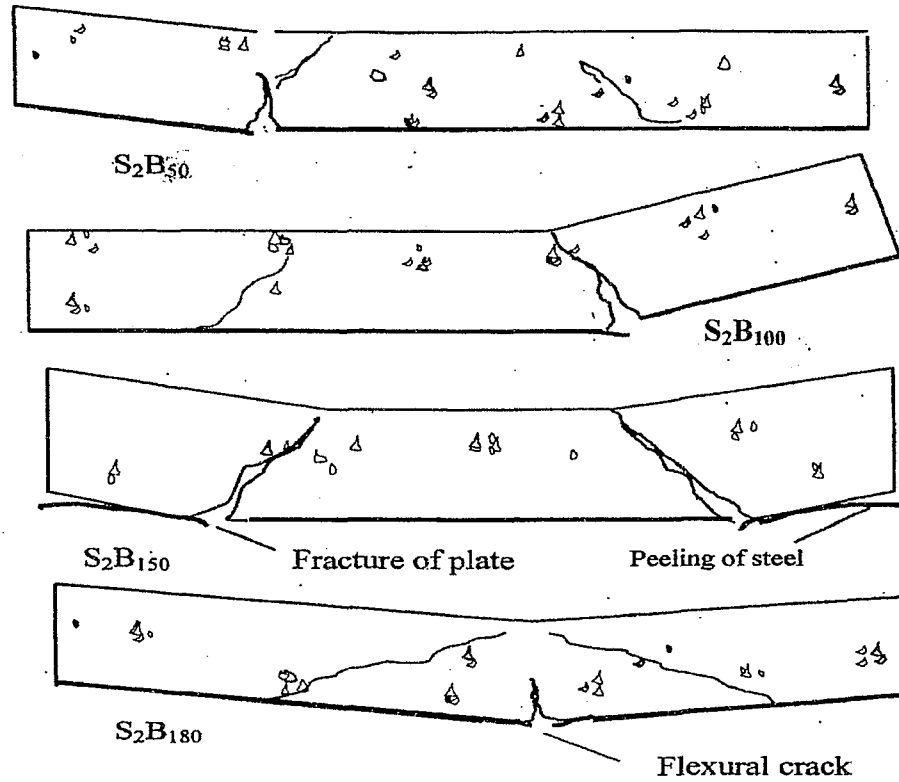
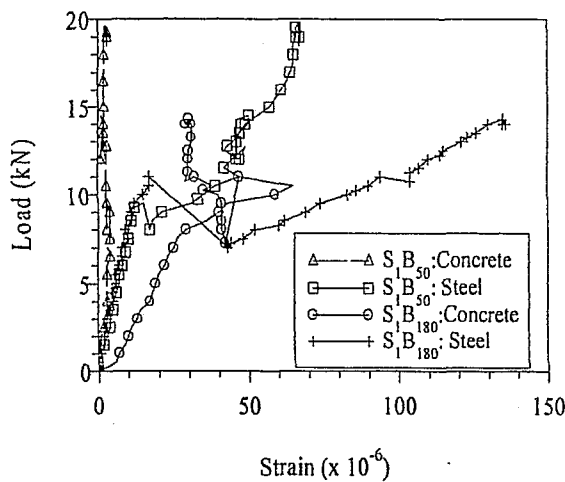
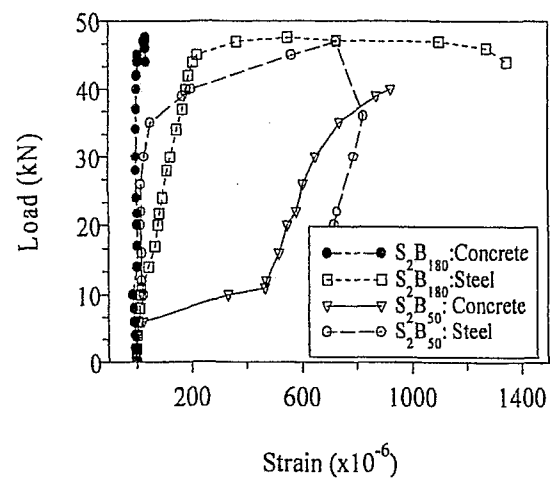


Fig. 3.8 Failure modes of Series 2 beams (Hossain 1999)



(a) Series 1 strain development



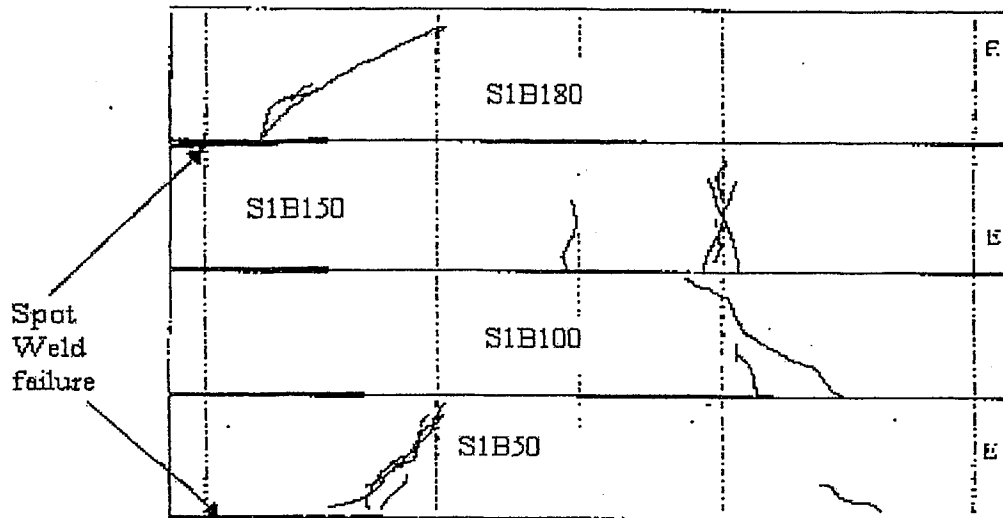
(b) Series 2 strain development

Fig. 3.9 Strain development in Series 1 and Series 2 beams (Hossain 2001)

Fig. 3.9(a-b) shows the variation of strain with load for Series 1 and Series 2 beams. The tensile strains in the steel in Series 2 beams were found to be greater than those in Series 1 beams. This may be due to the fact that the cracks in concrete propagated very quickly to the compression zone and crushing failure at the top eventually led to the fracture of steel plate and the beam collapsed.

#### 3.5.4.2. Beams with 3mm Thick Plate

All beams in Series 1, S<sub>1</sub>B<sub>50</sub>, S<sub>1</sub>B<sub>100</sub>, S<sub>1</sub>B<sub>150</sub> and S<sub>1</sub>B<sub>180</sub> failed due to peeling of steel plate as a result of spot weld failure and propagation of flexural cracks started from mechanical joint location up to the full depth of beam with some inclination towards the center. Peeling of the bottom steel plate as a consequence of spot weld failure extended from the supports towards the center as the beams reached its ultimate load carrying capacity as shown in Fig. 3.10.



**Fig. 3.10** Failure modes of series 1 beams with 3mm thick steel plate  
(Nupiri 2000, Hossain 2001)

In Series 2 beams, the failure was found to be due to the crushing of concrete because of flexural cracks that extended towards the top nearly about three quarters to the total depth of the beam during the loading history (Nupiri 2000 and Hossain 2001). These beams failed at much higher loads as compared to the beams without longitudinal reinforcements as shown in Table 3.3. It was also observed that beams with lower stirrup spacing such as S<sub>2</sub>B<sub>50</sub> and S<sub>2</sub>B<sub>100</sub>, initiated more flexural cracks than beams with 150 mm and 180 mm spacing of stirrups (Nupiri 2000 and Hossain 2001).

#### **3.5.4.3. Effect of Variable Parameters on Failure Modes of Pilot Beams**

Two kinds of failure modes were observed when analyzing two series of beams having steel plate without longitudinal reinforcement and steel plate with internal longitudinal reinforcement respectively, with varying steel plate thickness and stirrups spacing:

- (a) Debonding of spot weld,
- (b) Tearing of steel plate.

For beams having 0.4-mm thick steel plate of without longitudinal reinforcement, the load at which the first debonding occurred was higher as compared to the same beam having closely spaced stirrups (Table 3.3). However, beams with 3-mm thick steel plate with higher stirrup spacing showed higher first debonding load than those with less spacing stirrups. The presence of longitudinal reinforcement increased the loading carrying capacity of beams (Table 3.3).



For beams having thin steel plate (0.4-mm) with internal reinforcement, the failure occurred due to the tearing of plate as shown in Fig. 3.8, rather than failure of spot-weld connections. This might be due to the reason that the presence of longitudinal reinforcement gave relaxation to the shear/peeling stresses occurred at the interface connection of steel plate and concrete via spot weld.

Experiments had shown that by increasing the plate thickness (3-mm), the mode of failure of such beams had been shifted to shear rather than flexure in the presence of internal longitudinal reinforcement as the amount of tensile reinforcement in terms of greater thickness of steel plate was provided.

For beams without tensile reinforcement and reinforced with thick plate, failure happened due to the failure of weld as the stirrups alone were responsible for the strength of mechanical connection (Fig. 3.10). Moreover, failure of Series 2 beams (having internal longitudinal tensile reinforcement) due to tearing of the thin plate as shown in Fig. 3.8, can be eliminated by using steel plate of optimum thickness and high strength of spot weld.

Beam Series/Designation		1 <sup>st</sup> Debonding		Initial Concrete Crack		Ultimate/Peak		Failure
		Deflection	Load	Deflection	Load	Deflection	Load	Type
		( mm)	(kN)	( mm)	(kN)	( mm)	(kN)	F/S/T/W
Series 1 Beams	S <sub>1</sub> B <sub>50</sub> - 0.4mm	0.40	5.75	0.50	8.00	3.73	19.75	F with T
	S <sub>1</sub> B <sub>100</sub> - 0.4mm	1.50	13.50	2.30	13.67	6.50	22.00	F with T
	S <sub>1</sub> B <sub>150</sub> - 0.4mm	2.08	13.50	2.10	13.70	3.28	14.40	W
	S <sub>1</sub> B <sub>180</sub> - 0.4mm	2.03	11.00	2.03	11.00	2.78	15.07	F with T
	S <sub>1</sub> B <sub>50</sub> - 3mm	2.84	70.00	3.02	75.00	1.92	75.00	W
	S <sub>1</sub> B <sub>100</sub> - 3mm	1.28	35.00	1.59	45.00	1.62	55.00	W
	S <sub>1</sub> B <sub>150</sub> - 3mm	1.50	36.00	1.75	42.00	1.81	49.10	W
	S <sub>1</sub> B <sub>180</sub> - 3mm	2.14	32.00	2.14	34.00	1.50	34.60	W
Series 2 Beams	S <sub>2</sub> B <sub>50</sub> - 0.4mm	3.87	14.00	4.20	17.50	7.80	47.50	F with T
	S <sub>2</sub> B <sub>100</sub> - 0.4mm	1.10	10.50	1.39	11.50	10.40	47.00	F with T
	S <sub>2</sub> B <sub>150</sub> - 0.4mm	0.67	5.50	1.10	12.20	7.02	47.50	F with T
	S <sub>2</sub> B <sub>180</sub> - 0.4mm	3.70	12.00	4.19	14.00	8.00	46.00	F with T
	S <sub>2</sub> B <sub>50</sub> - 3mm	2.29	75.00	2.77	95.00	3.94	122.50	S
	S <sub>2</sub> B <sub>100</sub> - 3mm	3.40	65.00	3.57	70.00	2.95	71.50	S
	S <sub>2</sub> B <sub>150</sub> - 3mm	1.91	47.50	2.27	52.50	3.50	77.00	S
	S <sub>2</sub> B <sub>180</sub> - 3mm	2.50	50.00	2.78	55.00	3.93	57.50	S

where F = Flexure Failure, S = Shear Failure, T - Tearing of Steel Plate and W = Weld Failure

Table 3.3 Response of pilot beams during experiments (Hossain 2001)

### 3.5.5. Load-Deflection Responses of Beams

#### 3.5.5.1. Beams with 0.4mm Thick Plate

Load - deflection responses for Series 1 and Series 2 beams with 0.4 mm thick steel plate are compared in Fig. 3.10. For Series 1 beams, the ultimate load decreased with the increase of the spacing of stirrups as spacing of stirrups is directly associated with the strength of connection.

For Series 2 beams, the spacing of stirrups had little or negligible effect on the ultimate load, as the failure load of all beams was found to be the same as shown in Fig. 3.11. This

might be due to the fact that the strength enhancement due to the presence of longitudinal reinforcement superseded the benefit of thin gauge steel plate. It is well understood from the tested beams that the performance of such beams depends on the steel plate of optimum thickness and effective shear connection devices to avoid premature failure.

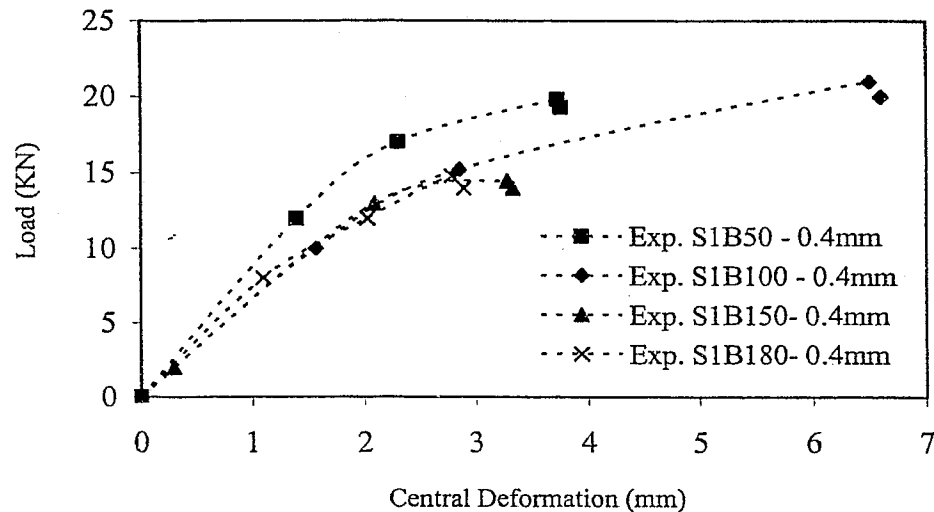


Fig. 3.11 Load deflection response of series 1 beams

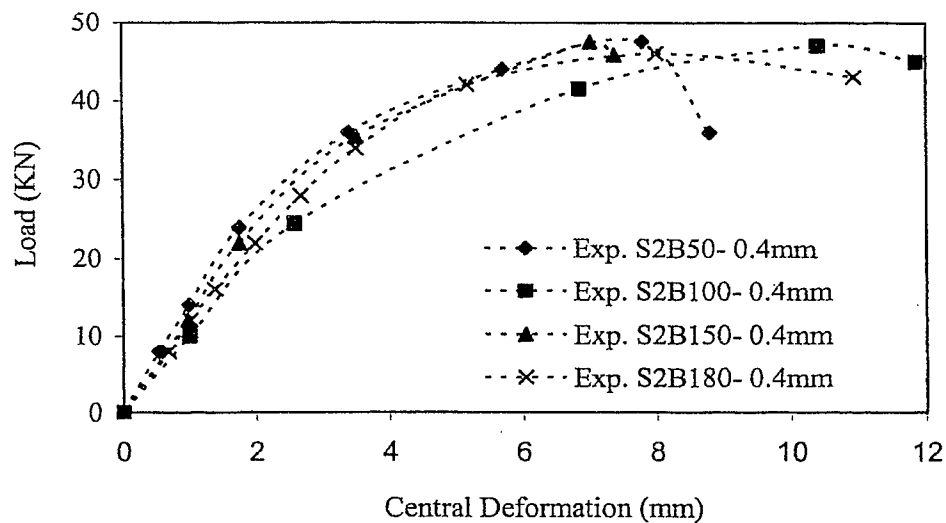


Fig. 3.12 Load deflection response of series 2 beams.

### 3.5.5.2. Beams with 3-mm Thick Plate

Load deflection responses of Series 1 and Series 2 beams are presented in Fig. 3.13. It is found clearly that the spacing of stirrups has great influence on ultimate load carrying capacity and corresponding deflection. Beams having closely spaced stirrups exhibited much higher load than beams with increased stirrup spacing. In addition, it was observed from both Series 1 and Series 2 beams that the ultimate load decreased proportionally with the increase of the stirrup spacing as shown in Fig. 3.13 and Fig. 3.14. S<sub>2</sub>B<sub>50</sub> beam failed at much higher load though it was a singly reinforced beam but it had closely spaced stirrups. S<sub>2</sub>B<sub>100</sub>, S<sub>2</sub>B<sub>150</sub> and S<sub>2</sub>B<sub>180</sub> beams showed proportional decrease in failure load with reduced deflection as these beams were doubly reinforced (Fig. 3.14). The increase in plate thickness in Series 2 beams, changed the mode of failure to brittle shear failure (leading to the debonding of plate due to weld failure) rather than plate tearing as additional plate thickness together with internal longitudinal reinforcement increased the reinforcement ratio corresponding to the cross section of the beam.

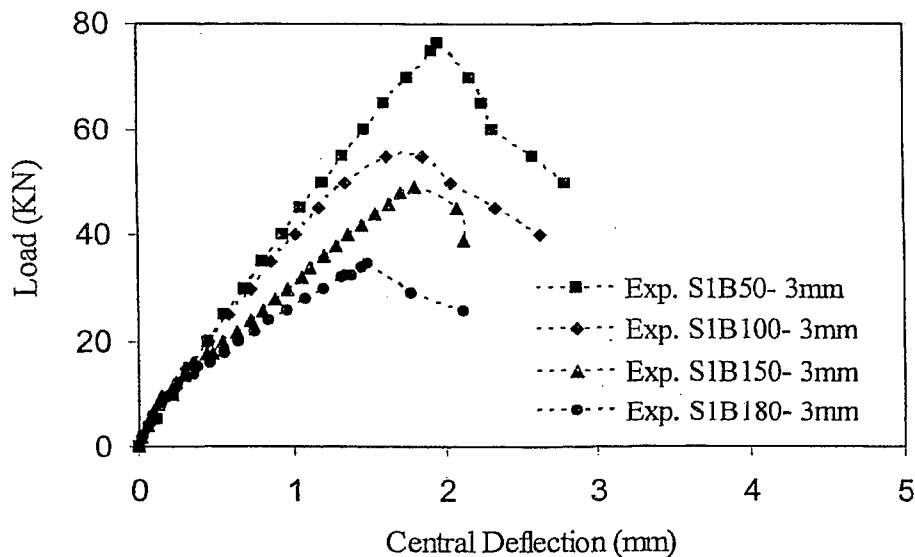


Fig. 3.13 Load-deflection response of series 1 beams

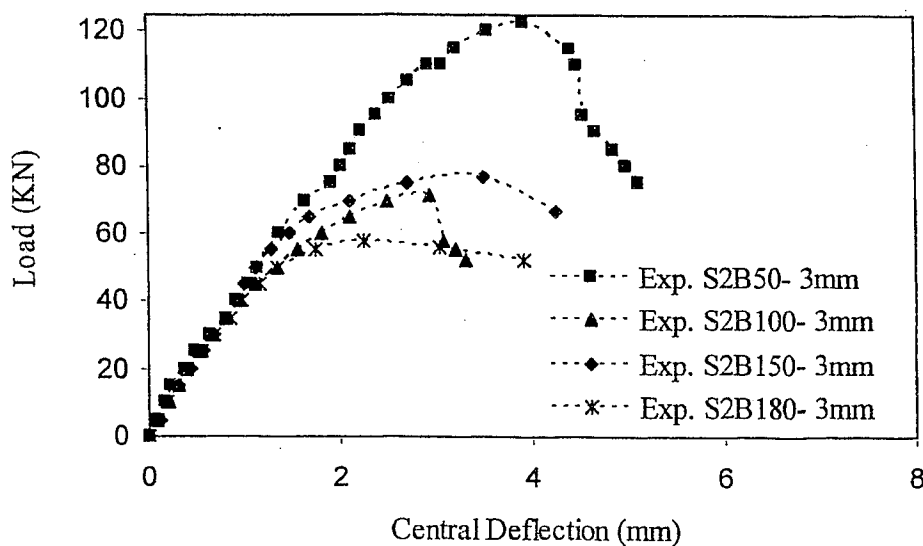


Fig. 3.14 Load deflection response of series 2 beams

### 3.5.5.3. Effect of Variable Parameters on Ultimate Load-Deflection Response

Comparative study to analyze the effect of the presence of internal longitudinal reinforcement on ultimate load and central deflection of beams is shown in Fig. 3.15 and Fig. 3.16. It is clearly seen from Fig. 3.15 and Fig. 3.16, that the presence of internal longitudinal reinforcement has a great influence on the ultimate load carrying capacity of the beam. Moreover, the stirrup spacing has small or negligible influence on the ultimate load of the beams with thin steel plate and with longitudinal reinforcement as compared to the beam without reinforcement. This might be due to the fact that the strength enhancement due to the presence of longitudinal reinforcement superseded the benefit of thin plate as tension reinforcement. Moreover, the presence of internal steel increases the ultimate deflection as depicted from Fig. 3.17 and Fig. 3.18.

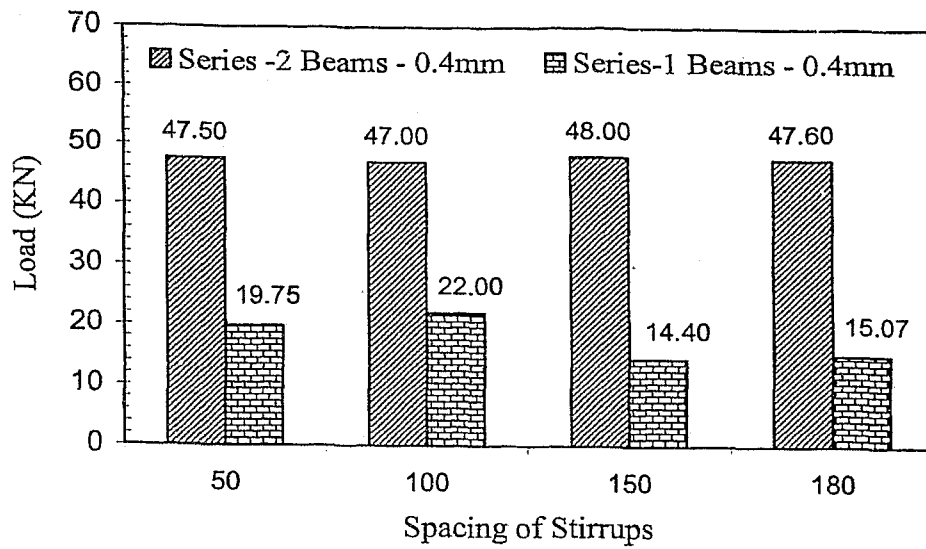


Fig. 3.15 Effect of internal tensile reinforcement on ultimate load capacity of beam with 0.4-mm thick steel plate

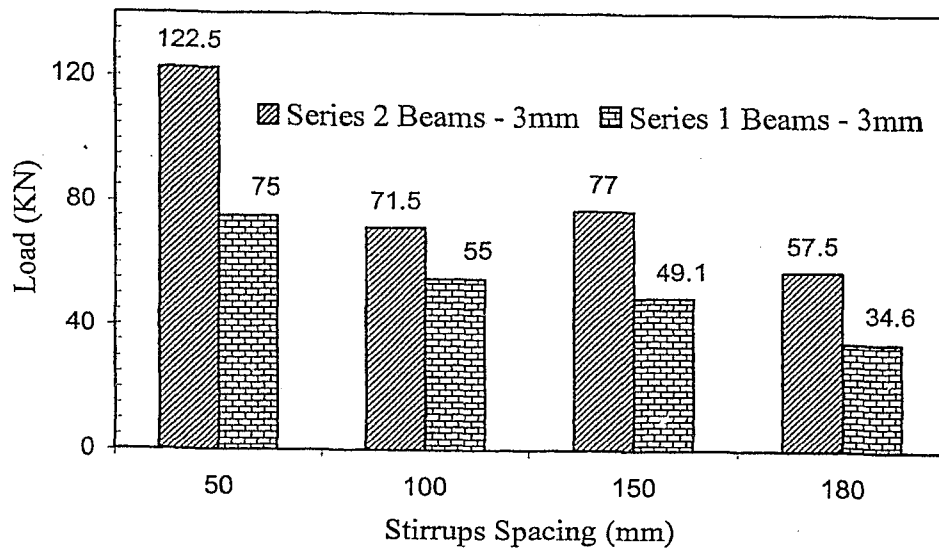


Fig. 3.16 Effect of internal tensile reinforcement on ultimate load capacity of beams with 3-mm thick steel plate

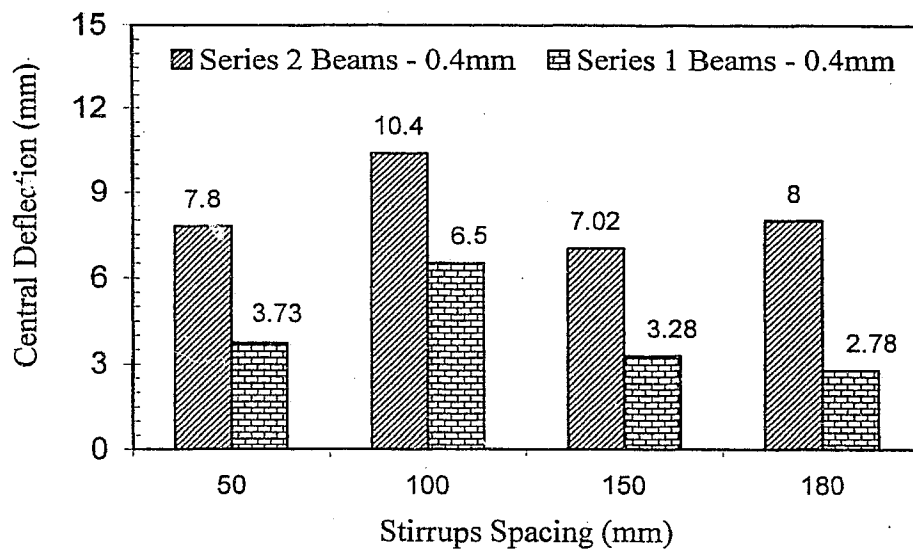


Fig. 3.17 Effect of internal tensile reinforcement on central deflection of beams with 0.4-mm thick steel plate

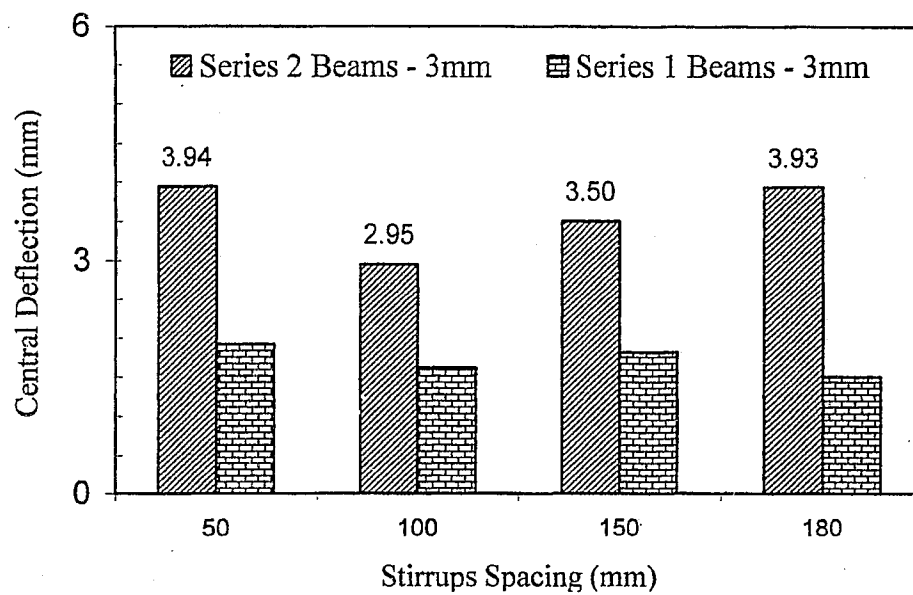


Fig. 3.18 Effect of internal tensile reinforcement on central deflection of beams with 3-mm thick steel plate

The influence of stirrup spacing has little or negligible effect on ultimate load carrying capacity and deflection associated with ultimate failure (Fig. 3.15) but their variation affected the mode of failure. For example, if closely spaced stirrups are used with thin plate, the mode of failure will be pure flexure with tearing of steel plate as concluded from Table 3.3. Increase in stirrup spacing can result in tearing of thin plate after that shear cracks heading towards the top of beam with certain inclination (Jim 1998, Hossain 2001).

More or less the beam will follow the same behavior if relatively thick steel plate is used but this time, failure will happen at the interface connection (weld location) rather than plate tearing due to increased capacity of thick steel plate (Fig. 3.10). Increasing of the spacing of stirrups for beams having thick plate may result in shear failure combined with peeling of plate due to weld failure (Table 3.3).

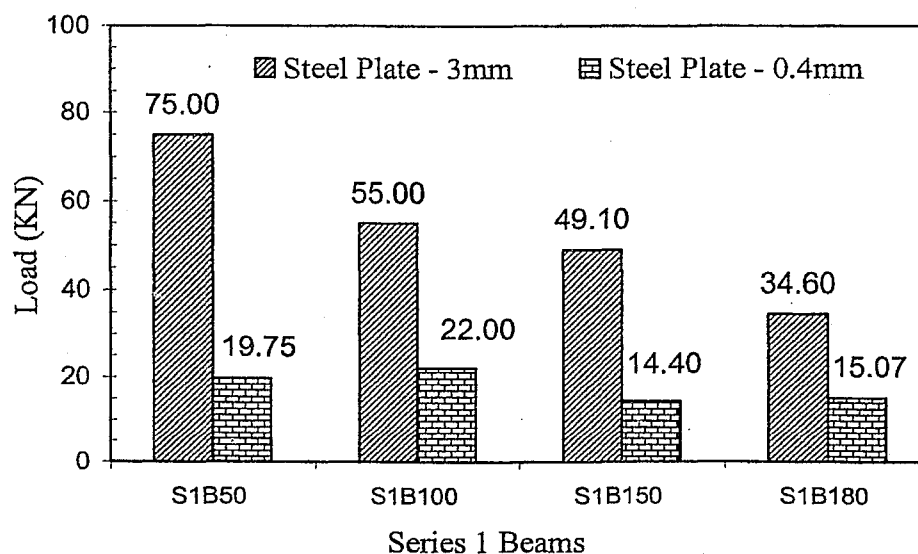


Fig. 3.19 Effect of plate thickness on ultimate load of Series 1 beams



As shown in Fig. 3.19 and Fig. 3.20, the ultimate load increases with the increase of plate thickness i.e. beam with thick plate (3-mm) failed at a higher load than those with thin plate (0.4 mm). Moreover, it is evident that the increase in plate thickness converts failure mode from ductile (flexure failure combined with tearing of plate) to brittle failure (peeling of plate due to welded failure at the interface of concrete and steel plate) as mentioned in Table 3.3.

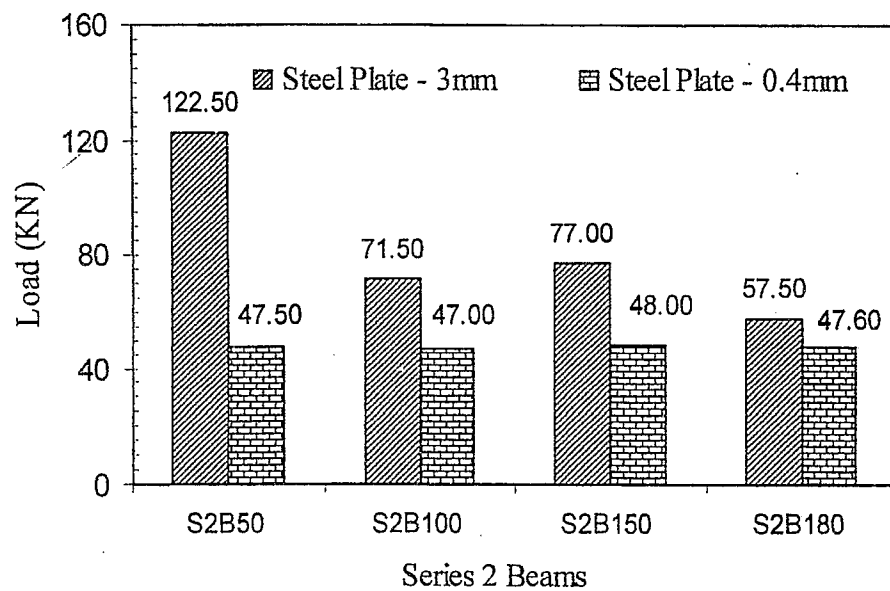


Fig. 3.20 Effect of plate thickness on ultimate load of series 2 beams

On the other hand, increasing plate thickness results in a decrease in deflection of beams as illustrated in Fig. 3.21 and Fig. 3.22. The effect of plate thickness on deflection of beams is much greater (40 to 50% reduction in deflection) than the effect of variable stirrup spacing in such beams.

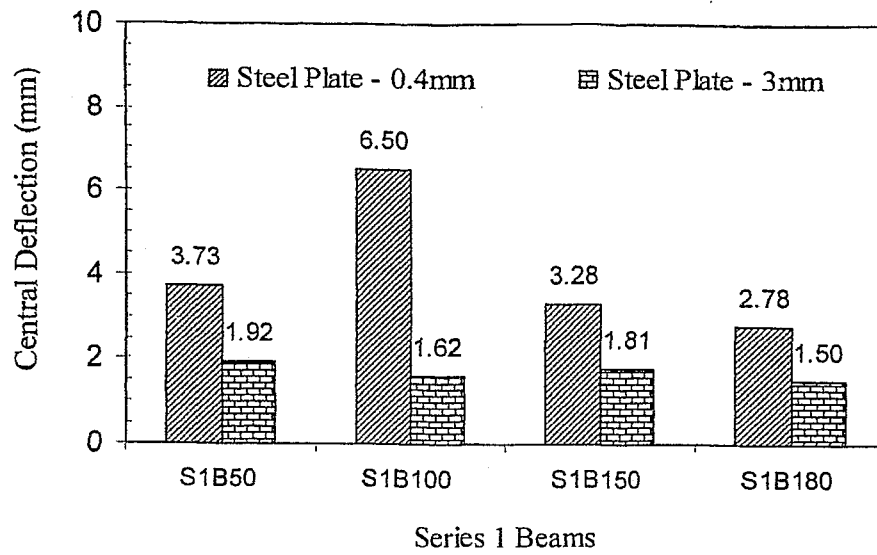


Fig. 3.21 Effect of plate thickness on central deflection of series 1 beams

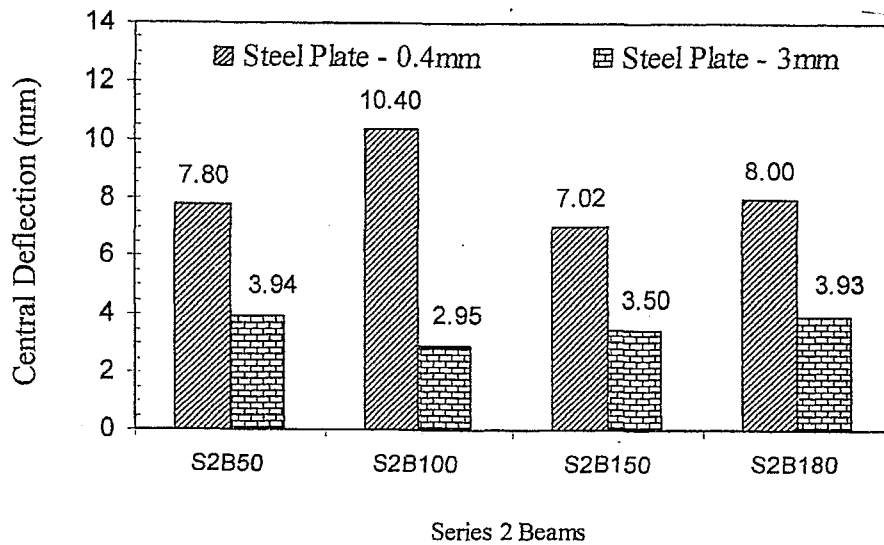


Fig. 3.22 Effect of plate thickness on central deflection of series 2 beams

An increase in load carrying capacity and reduction in deflection of experimental beams strengthened with mechanically bonded steel plate had been observed during experiments

with increasing plate thickness but failure mode had been changed from tearing of steel plate to debonding due to failure at spot welded connection (Jim 1999 and Nupiri 2000).

It was well understood from the tests that the performance of such beams depends on the steel plate of optimum thickness and effective shear connection devices that did not fail prematurely (Hossain 2001). The steel-plate stirrups assembly can be used for strengthening purposes instead of steel plate alone, with high strength spot weld to give more strength to this kind of mechanical connections.

From experimental observations, it is concluded that the factors such as variation in steel plate thickness, stirrups spacing and the presence of internal longitudinal reinforcement have great influence on the failure modes and ultimate strength of the such novel form beams. These factors are taken into consideration for the development of finite element model and design guidelines.

## Chapter 4 Development of Finite Element Model

### 4.1. Introduction

This chapter describes in details, the development of a finite element model to simulate the behavior of experimental beams discussed in Chapter 3, using general purpose finite element software, *ABAQUS* (Abaqus User's Manual Volume 1, 2004). In this chapter an arbitrary experimental beam ( $S_2B_{100}$ ) with 0.4-mm thick plate (Jim 1999), has been selected and idealized into numerical model using finite element and its performance has been checked using various types of elements and its compatibility with different types of interface connections. A finite element model is then selected to analyze the behavior of all 8-experimental beams (Jim 1999, Hossain 2001) with 0.4-mm thick steel plate and to validate the performance of the developed finite element model.

### 4.2. Development of a Finite Element Model

A schematic representation of general beam is shown in Fig. 4.1. Reinforced concrete beam having longitudinal bars embedded in the concrete while steel plate connected to different interface connections in order to check their performance. Shear reinforcements are introduced in terms of uniformly spaced steel stirrups.

An arbitrary experimental beam,  $S_2B_{100}$  (Jim 1999, Hossain 2001) of Chapter 3, having a cross-section of 100 mm x 150 mm with an effective length of 800 mm, is selected and idealized numerically using the finite element model.

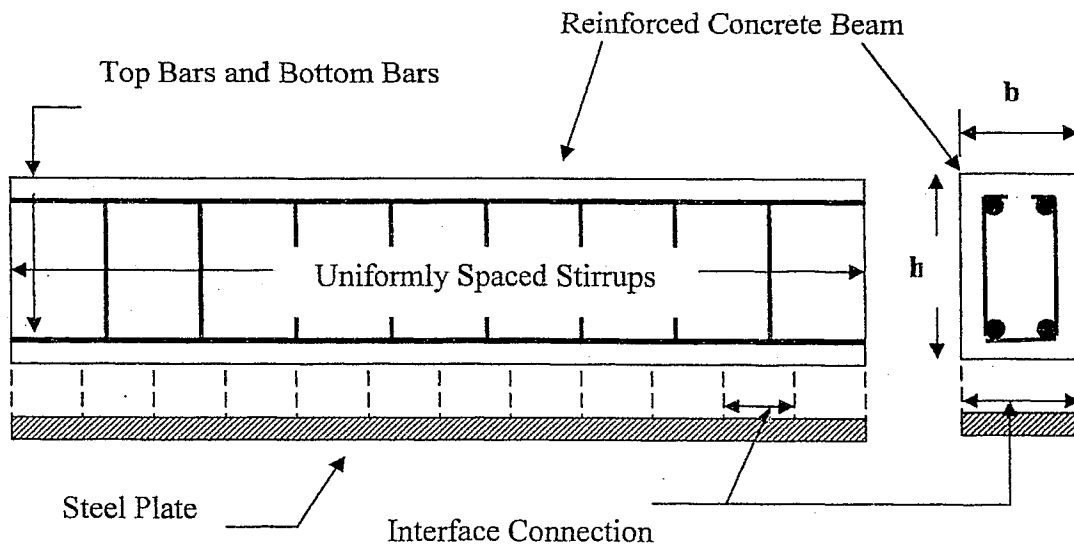


Fig. 4.1 Schematic of general reinforced concrete beam

#### 4.2.1. Beam Geometry, Loading and Boundary Conditions

The beam is reinforced with  $2 \times 20 \text{ mm}^2$  steel area corresponding to 2-5 mm diameter steel bars at both top and bottom with an offset of 10-mm from top and bottom to provide concrete cover. Shear reinforcement is provided in terms of 5 mm diameter steel stirrups spaced at 100-mm intervals. The beam was loaded under four-point loading configuration.

This beam simulated as simply supported with one hinged end and the other end is pinned. Fig. 4.2 illustrates a schematic representation of the beam under study (i.e. S<sub>2</sub>B<sub>100</sub>).

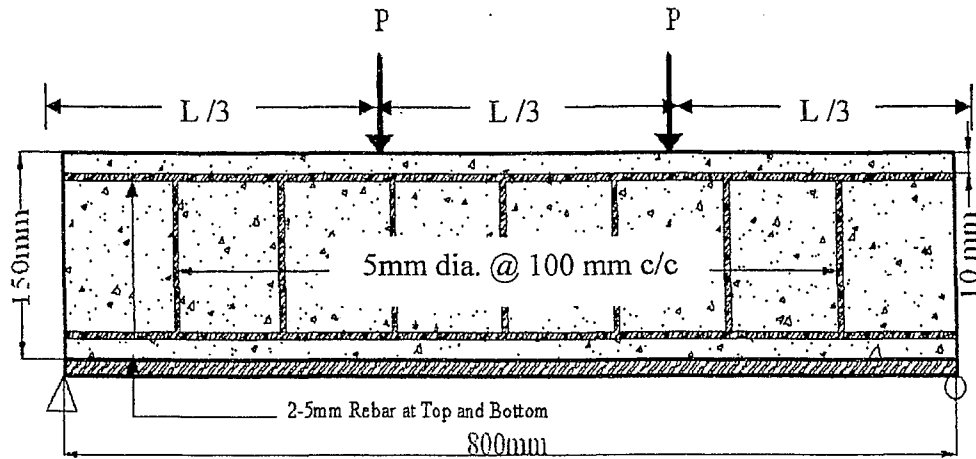


Fig. 4.2 Typical beam dimension (not to scale), loading and boundary conditions

#### 4.2.2. Modeling the Non-Linear Behavior of Concrete

##### 4.2.2.1. Cracking Behavior of Concrete

The development of a model for the behavior of concrete is a challenging task because it behaves differently under uni-axial and multi-axial loading conditions. In this model, concrete is assumed to be an isotropic material prior to cracking. The response of concrete that is incorporated in the model is illustrated by the uni-axial response of a specimen shown in Fig. 4.3.

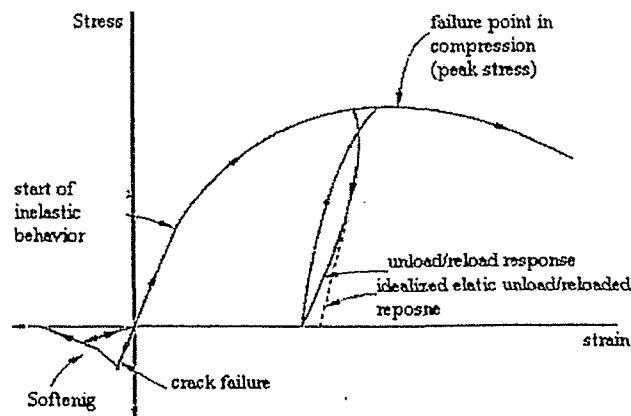


Fig. 4.3 Typical strength concrete under uni-axial tension and compression (Abaqus User's Manual Volume II 2004).

In multi-axial stress states, these observations can be generalized through the concept of surfaces of failure and of ultimate strength. These surfaces are defined in Fig. 4.4.

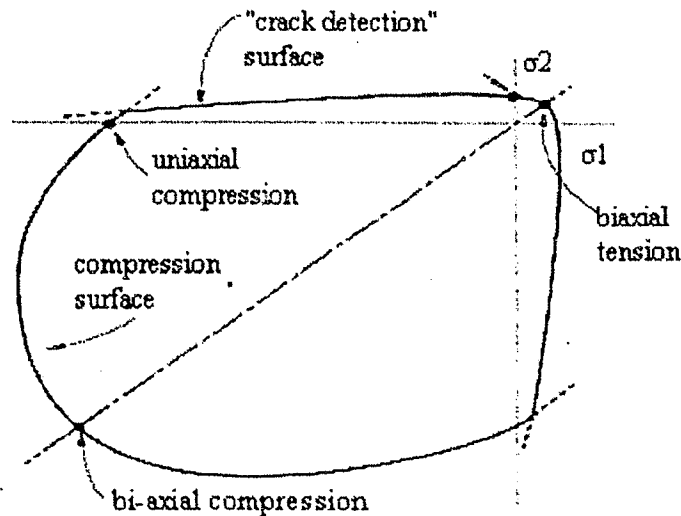


Fig. 4.4 Multi-axial state of stress in concrete (Abaqus User's Manual Volume II 2004).

A smeared cracking approach is used to represent the cracked concrete as an orthotropic material in the sense that it does not track individual "micro cracks". Consecutive calculations are performed independently at each integration point in the finite element model.

Cracking is assumed to occur when the stress reaches a failure surface called "crack detection surface" as illustrated in Fig. 4.4. The strength of concrete in bi-axial compression is greater than the uni-axial compression and generally taken as 105-107%

of its ultimate uni-axial compressive strength (MacGregor and Barlett 2000). The ultimate tensile strength ( $f_t$ ) is considered as the flexural strength of concrete ( $f_r$ ) and is taken according to Canadian Code, CSA A23.3 1994:

$$f_r = 0.6\lambda_c \sqrt{f'_c} \dots\dots\dots (4.1)$$

Even though researchers (Yang et al. 2003, Kachlakev and Miller 2001, Thevendran et al. 1999 and Sebastian et al. 2000) reported three different crack directions such as orthogonal cracks, rotating cracks and fixed multidirectional cracks, *ABAQUS* uses fixed orthogonal direction of cracks. In addition, *ABAQUS* allows orthogonal crack to be used with shear retention by modifying shear retention property so that the shear stresses tend to be zero with increasing crack openings. Traditionally, the shear retention model does not converge to zero whereas *ABAQUS* allows shear stresses to become zero as the deflection along the crack interface increases (Abaqus User's Manual Volume II 2004).

*ABAQUS* model defines the total shear stresses as a function of shear strain whereas traditional shear retention model define the shear stress-strain relationship by incremental form. In this way, it is possible to achieve a shear retention model, which will decrease shear stresses to zero when large deflection occurs. Therefore, orthogonal cracks are allowed with the shear retention model. These cracks are recoverable and they will remain in the calculation but it may open or close based on loading and unloading conditions.



#### 4.2.2.2. Tensile Behavior of Concrete

Concrete in tension is considered as a linear-elastic material until the uni-axial tensile strength, at which, the concrete cracks and later, exhibit a linear softening behavior. The tensile strength of concrete is typically 8-10% of the compressive strength (MacGregor and Barlett 2000).

A linear softening model has been used to represent the post failure behavior in tension. The softening behavior depends on the size of the element in a cracked region. The post failure behavior across cracks is modeled with \*TENSION STIFFENING option available in *ABAQUS*, which allows the definition of the strain-softening behavior for cracked concrete. This option allows for the effect of the interaction between embedded reinforcement and concrete. The tension stiffening model in *ABAQUS*, is represented in Fig. 4.5.

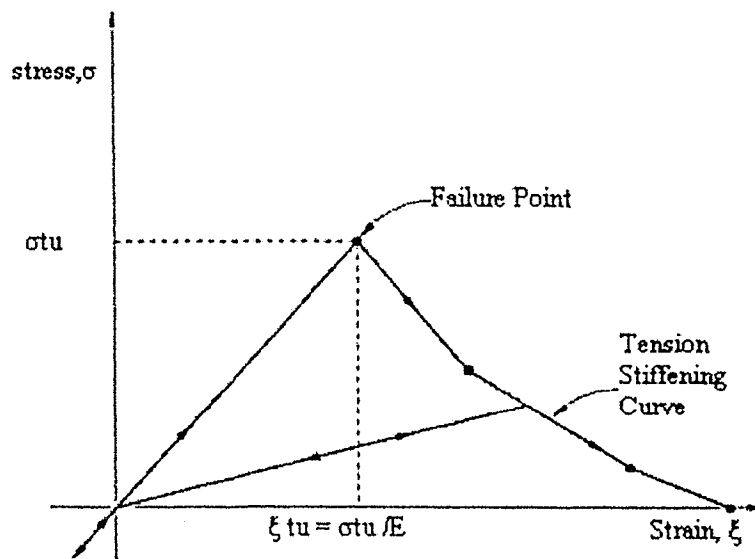


Fig. 4.5 Tension stiffening model for concrete (Abaqus User's Manual Volume II 2004).

A reasonable starting point for a relatively heavily reinforced concrete beam with fairly detailed mesh is to assume that the strain softening after failure reduces the stress linearly to zero at a total strain about 10 times the strain at failure. The strain at failure in conventional concrete is typically  $10^{-4}$ , which suggests that the tension stiffening that reduces the stress to zero at a total strain of about  $10^{-3}$  is reasonable (Abaqus User's Manual Volume II 2004).

#### 4.2.2.3. Compressive Behavior of Concrete

When the principal stress components are dominantly in compression, the response of the concrete is modeled by an elastic-plastic model using a simple form of the yield surface written in terms of equivalent pressure stress,  $p$ , and the Von-Mises equivalent stress,  $q$ . \*CONCRETE option in *ABAQUS* (Abaqus User's Manual Volume II, 2004) is used to define the stress-strain behavior of the concrete in an inelastic range. This option allows the user to define the compressive stress as a function of compressive stress-inelastic strain data in a tabular form.

The stress strain curve can be defined beyond the ultimate stress, into the strain-softening regime. In the selected model, the uni-axial stress strain curve is assumed to be linear up to  $0.3 f'_c$  (McGregor and Barlett 2000), beyond that point a model proposed by (Desayi and Krishnan 1964, Eq. 4.2) is used up to the stage when the concrete reaches its ultimate compressive stress,  $f'_c$ . The strain  $\epsilon_u$ , at which the maximum compressive stress occurs is generally taken as 0.002-0.0025 (McGregor and Barlett 2000), but in this study, the model proposed by (Desayi and Krishnan 1964, Eq. 4.3) is used.

Compressive stress in an inelastic range up to ultimate stage:

$$f = \frac{E_c \cdot \xi_c}{1 + \left( \frac{\xi_c}{\xi_{cu}} \right)^2} \quad (\text{Desayi and Krishnan 1964}) \dots\dots\dots (4.2)$$

Ultimate concrete compressive stress:

$$f'_c = \left( \frac{E_c \cdot \varepsilon_{cu}}{1.71} \right) \quad (\text{Desayi and Krishnan 1964}) \dots\dots\dots (4.3)$$

Compressive Stress in post failure region:

$$f = \frac{2f''_c \left( \frac{\xi_c}{\xi_{cu}} \right)}{1 + \left( \frac{\xi_c}{\xi_{cu}} \right)^2} \quad (\text{Todeschini, MacGregor 2000}) \dots\dots\dots (4.4)$$

Where,

$f'_c$  = Ultimate compressive strength of concrete

$f$  = Compressive stress at concrete extreme fiber

$E_c$  = Modulus of elasticity of concrete

$\xi_c$  = Compressive strain at concrete extreme compressive fiber

$\xi_{cu}$  = Ultimate compressive strain at concrete extreme compressive fiber

$$f''_c = 0.8 f'_c$$

Beyond that point, a model proposed by Todeschini, 2000 (Eq. 4.4) is used to define the post failure characteristics of concrete in compression, up to the limit where the crushing strain of concrete, which is generally ranging between 0.003 and 0.0035 (MacGregor and Barlett 1997), is reached. The simplified stress-strain curve as used in the selected model is constructed from seven points connected by straight lines as shown in Fig. 4.6.

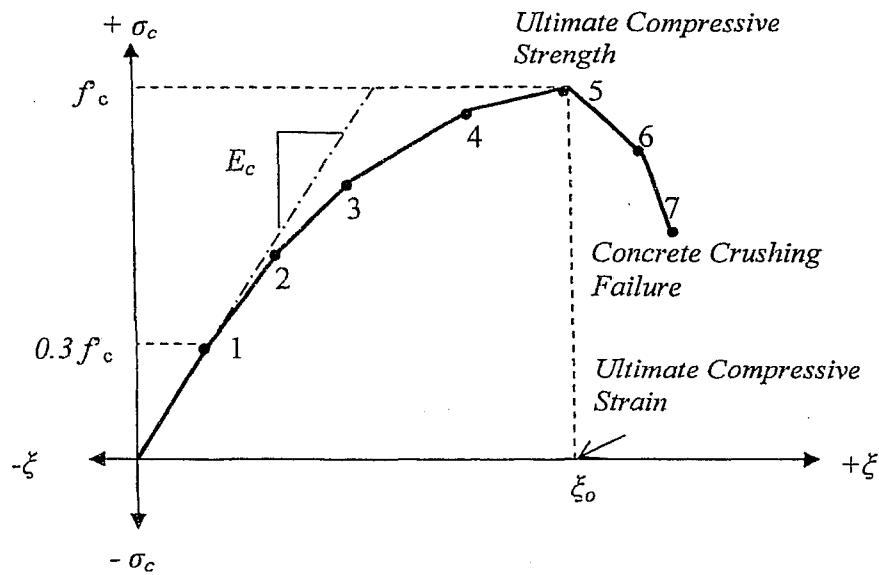


Fig. 4.6 Adapted model of uni-axial curve for concrete in compression

The Modulus of elasticity of concrete ( $E_c$ ) has been calculated using the Canadian code (CSA A23.3 - Cl. 8.6.2.3) and addressed in Eq. 4.5.

$$E_c = (4500\sqrt{f'_c}) \dots\dots\dots(4.5)$$

where  $f'_c$  is in MPa.

#### 4.2.2.4. Modeling of Shear Retention in Concrete

As concrete cracks, its shear stiffness diminishes. This effect is called shear retention and is defined by invoking \*SHEAR RETENTION option exclusively available in *ABAQUS* (Abaqus User's Manual Volume II 2004) as a function of strain across the cracks. The decrease of shear transfer capability of concrete across the crack is taken into account by introducing a factor "p", a function of tensile strain across the crack. The shear retention

model assumes that the stiffness of open cracks reduces linearly to zero as the crack opening increases as shown in Fig. 4.7.

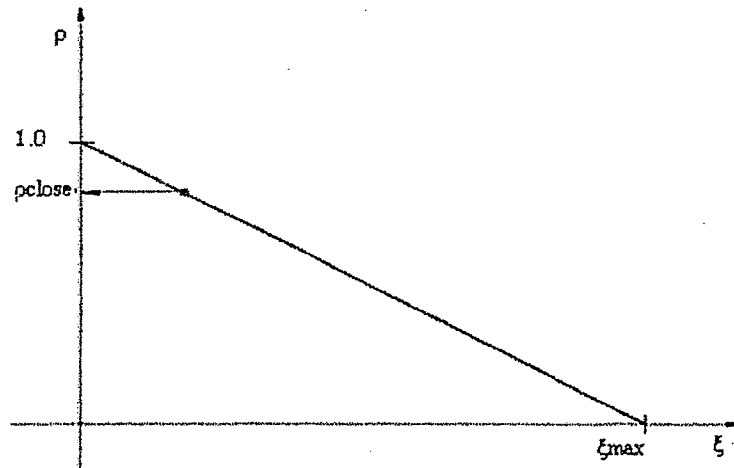


Fig. 4.7 Shear retention model (Abaqus User's Manual Volume II 2004).

The shear modulus of concrete is taken as  $\rho G$  and it is represented in Eq. 4.6.

$$\rho = \left( 1 - \frac{\xi_c}{\xi_{c \max}} \right) \text{ for } \xi_c < \xi_{c \max}, \text{ and } \rho = 0 \text{ for } \xi_c > \xi_{c \max} \dots\dots\dots (4.6)$$

Where,

$G$  = Shear modulus of concrete

$\xi_c$  = Ultimate compressive strain at concrete extreme compressive fiber (0.0015-0.0025)

$\xi_{c \max}$  = Crushing strain at concrete extreme compressive fiber (0.003 -0.0035)

#### 4.2.3. Modeling the Behavior of Longitudinal Steel Reinforcement

Reinforcement in the concrete is defined by the \*REBAR option in *ABAQUS* (Abaqus User's Manual Volume I 2004). Rebar is considered as one-dimensional strain element. It is typically used with the metal plasticity model to describe the behavior of steel rebars

and superimposed on the mesh of standard element type used for modeling the concrete. With this approach, the concrete behavior is considered independent of the steel rebars. The effect associated with the rebar/concrete interface is difficult to model with this approach. This effect however, can be modeled approximately by introducing "Tension Stiffening" into the concrete model to simulate the load transfer across the crack through rebars assuming perfect bond between steel and concrete.

The rebar is defined as smeared layer of uniformly spaced reinforcing bars in shell and solid elements. Such layer thickness is equal to the area of reinforcing bar divided by the spacing between each rebar. Reinforcement can be defined as single rebar in solid element or in a layer of rebars having uniform spacing. The rebars in three-dimensional continuum elements are defined as layers lying in surfaces (Abaqus User Manual Volume II 2004).

The steel in the finite element model was generally assumed to be an elastic-perfectly plastic material and identical in tension and compression with a Poisson's ratio generally taken as 0.3 (MacGregor and Barlett 2000). Typical representation of the stress-strain response used by different researchers (Yang et al. 2003, Yang and Ye 2002, Kachlakev and Miller 2001, Tedesco et al. 1999) is shown in Fig. 4.8.

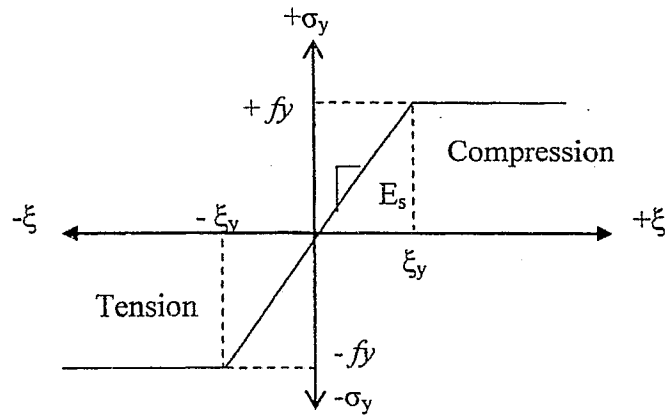


Fig. 4.8 General stress-strain relation for steel reinforcement.

#### 4.2.4. Non-Linear Solution

Since considerable nonlinearities may occur in terms of both material and geometry, resulting in the formation of negative stiffness matrix by the load deflection response, a static equilibrium states during the unstable phase of the responses can be achieved by using the “Modified Riks Method (mRA)”. This method is used where the loading is proportional; that is, where the load magnitudes are governed by a single scale vector. This method can provide solution even for the complex, unstable response shown in Fig. 4.9.

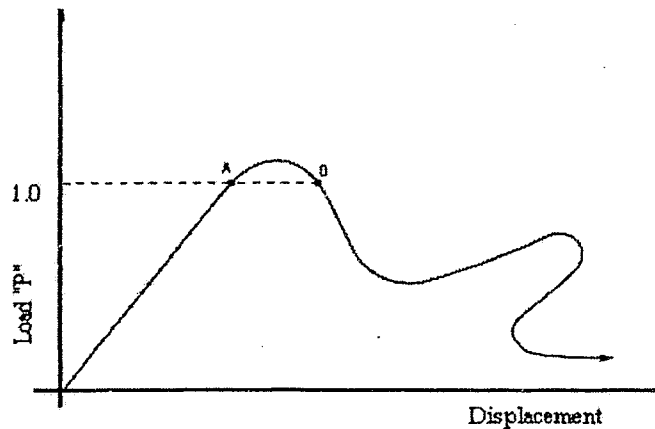


Fig. 4.9 Proportional loading with unstable response (Abaqus User's Manual Volume II 2004).

The Riks method uses the load magnitude as an additional unknown; it solves simultaneously for load and displacement. Therefore, another quantity must be used to measure the progress of the solution; *ABAQUS* uses arc length “L”, along static equilibrium path in load displacement space. This approach provides solution regardless of whether the response is stable or unstable (Abaqus User Manual Volume I 2004).

The loading during the Riks step is always proportional and the current load magnitude,  $P_{total}$  is defined by:

$$P_{total} = P_o + \lambda(P_{ref} - P_o) \dots\dots\dots (4.7)$$

Where  $P_o$  is the initial incremental load,  $P_{ref}$  is the reference load vector and “ $\lambda$ ” is the “load proportionality factor and it is found as a part of the solution. Riks Method uses only 1% of extrapolation of the solution increment. An initial increment of arc length is given on the data line called “ $\Delta l_{in}$ ”. The initial load proportionality factor is calculated by:

$$\Delta l_{in} = \frac{\Delta l_{in(i)}}{l_{period}} \dots\dots\dots (4.8)$$

Where  $l_{period}$  is a total arc length scale factor (typically set to 1) given on the data line of \*STATIC option.

For all subsequent iteration and increments, the value of “ $\lambda$ ” is computed automatically in such way that the user has no control over the load magnitude (recommended by *ABAQUS* program) but maximum and minimum arc length can be defined to control the



increment. In nonlinear analysis, the total load applied to a finite element model is divided into a series of load increments called load steps. At the completion of each incremental solution, the stiffness matrix of the model is adjusted to reflect nonlinear changes in structural stiffness before proceeding to the next load increment.

The *ABAQUS* program uses Newton-Raphson equilibrium iterations for updating the model stiffness. Newton-Raphson equilibrium iterations provide convergence at the end of each load increment within tolerance limits. Fig. 4.13, shows the use of the Newton-Raphson approach in a single degree of freedom nonlinear analysis for two load steps.

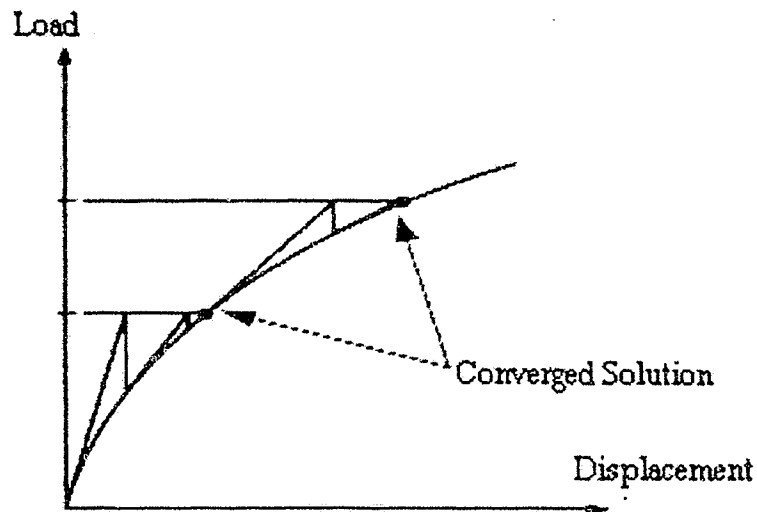


Fig. 4.10 Newton-Raphson iterative solution for 2 load increments (Abaqus User's Manual Volume II 2004).

#### 4.2.5. Load Steps and Response of Finite Element Model

For the nonlinear analysis, automatic time stepping in the *ABAQUS* program predicts and controls load step sizes. Based on the previous solution history and the physics of the

model, if the convergence behavior is smooth, automatic time stepping will increase the load increment up to a selected maximum load step size. If the convergence behavior is abrupt, automatic time stepping will bisect the load increment until it is equal to a selected minimum load step size. The maximum and minimum load step sizes are required for the automatic time stepping.

Prior to each solution, the Newton-Raphson approach assesses the out-of-balance load vector, which is the difference between the restoring forces (the loads corresponding to the element stresses) and the applied loads. Subsequently, the program carries out a linear solution, using the out-of-balance loads, and checks for convergence. If convergence criteria's are not satisfied, the out-of-balance load vector is re-evaluated, the stiffness matrix is updated, and a new solution is attained. This iterative procedure continues until the problem converges.

#### **4.2.6. Finite Element Analysis with Various Interface Models**

Two interface models have been used in the finite element analysis to simulate the behavior of experimental beams discussed in Chapter 3 and to develop a FE model for prediction purposes.

##### **4.2.6.1. Use of 2D Shell Element**

Initially, connector elements are used to create a link between steel stirrups and steel plate through welded options (Fig. 4.11) but problems have been faced to connect these connector elements with the steel stirrups as shear reinforcements are modeled using \*REBAR option which creates rebars as hypothetical elements embedded in concrete

using \*EMBEDDED option in *ABAQUS* (Abaqus User Manual Volume II 2004). Therefore, it is impossible with this type of modeling to get discrete element of rebar and their associated nodes to achieve a physical interface connection required to simulate the actual behavior of experimental beams.

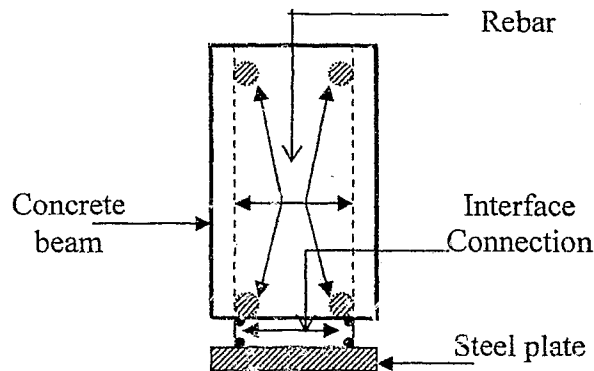


Fig. 4.11 Connection of hypothetical rebar with steel plate using connector element

The experimental beams described in Chapter 3 showed no horizontal interface/slip failure (Hossain 2001). These phenomena eventually reinforce the assumption that full interaction between concrete and steel plate can provide a reliable simulation of the behavior of experimental beams. Therefore for simplicity, failure of spot weld in model 1 is assumed to happen at a level where yield strength of steel plate is reached. For this reason, reduced yield strength of steel plate (i.e. reduce by 8%) due to residual stress at the time of welding at spot weld location obtained from experimental coupon test is used. Moreover, the tearing failure of steel plate rather than weld failure of experimental beams suggests that this type mechanical connection can be idealized assuming full interaction between concrete and steel plate.

In many instances, connector elements perform the same functions similar to multi-point constraint available with \*MPC option in *ABAQUS* (Abaqus Standard User's Manual Volume III 2004) and are more efficient than connector elements (ABAQUS Standard, User's Manual Volume II 2004). MPCs are preferred and used in this study instead of connectors, after a careful performance study on experimental beams. The use of multipoint constraint has been previously reported by Nethercot and Ahmed (1996) for the analysis of composite connections and composite frames with full interaction.

Since all nodes lying on the tension face of concrete and steel plate (Fig. 4.12), is constrained to be intact at all stages of load increment, it is assumed that there will be a full interaction between concrete and steel plate. This ensures full transfer of all stresses from the concrete to the steel plate causing steel plate to yield.

As an initial step, a finite element model requires discretization of the structure. The structure is divided into a number of small elements, and after loading, stresses and strains at integration points of these small elements as well as force and displacement at nodes are obtained (Bathe 1996; Nethercot and Ahmed 1996).

In developing Model 1, both concrete and steel plate is modeled using 2-dimensional shell elements. Typical FE discretization of an experimental beam (S<sub>2</sub>B<sub>100</sub>) with 4-node shell elements connected using multi-point constraint is shown in Fig. 4.12.

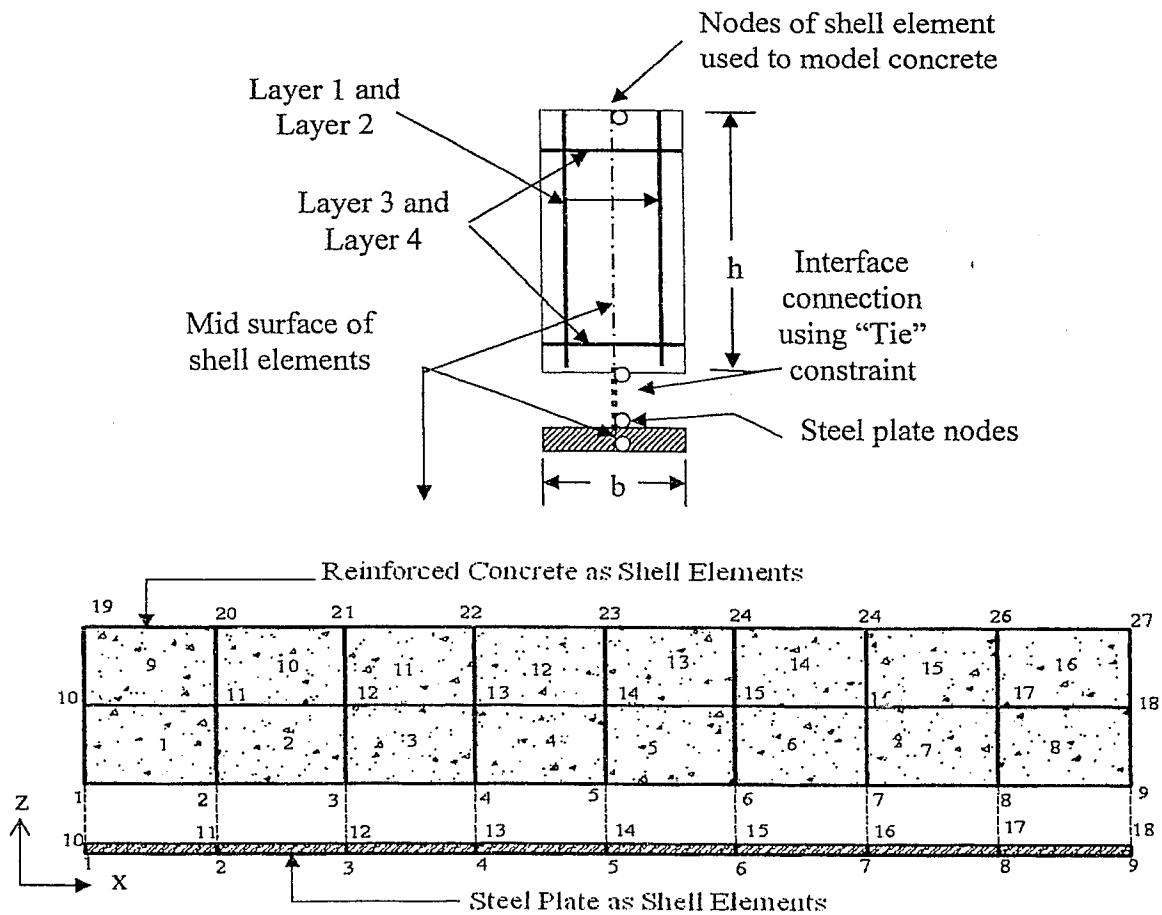


Fig. 4.12 Typical finite element discretization with 4-node shell elements

Both longitudinal and transverse reinforcement are modeled using smeared layer embedded in shell element using \*REBAR LAYER. Layer 1 and layer 2 have an area of  $20\text{-mm}^2$  corresponding to 5-mm diameter stirrups uniformly spaced at 100-mm (in case of S<sub>2</sub>B<sub>100</sub>) while layer 3 and layer 4 have an area of  $20\text{-mm}^2$  spaced at 100 mm in order to provide 2-5 mm diameter rebars. These rebar layers have been provided with reference to mid surface of shell elements as shown in Fig. 4.12.

An important step in finite element modeling is the selection of the mesh density, which can be performed through mesh and element type optimization process. A convergence of results is obtained when an adequate number of elements are used in the model. This is practically achieved when an increase in the mesh density has a negligible effect on the results (Sebastian 2000).

An extensive parametric finite element analysis is carried out to optimize the mesh size to achieve an appropriate mesh density. In order to optimize the interface connections with different types of MPCs, both concrete and steel plate are modeled using 4 and 8 node shell elements such as S4, S4R, S8 and S8R. The First letter, S, corresponds to a shell element followed by the number of nodes associated with the shell element and R, represent the reduced integration scheme. A normal 4 node shell element (S4) has 4- integration points while 4-node shell element with reduce integration (i.e. S4R) has only 1- integration point whereas, S8R has 4- integration points instead of 8- integration points (Abaqus User Manual Volume I 2004).

In order to check the performance of various shell elements available in *ABAQUS*, an arbitrary mesh size with 50-mm for both concrete and steel plate has been chosen for this study and tie constraint has been selected to provide an interface connection.

The performance of different types of shell elements is checked against the ultimate load capacity (47 KN) and the central deflection (10.47 mm) of the experimental beam, S<sub>2</sub>B<sub>100</sub>, with 0.4 mm thick plate (Table 3.3). Fig. 4.13 shows the percentage error obtained

against the various types of shell elements. It can be seen from Fig. 4.13 that the performance of S4 elements is good to predict the ultimate load but for ultimate central deflection, the model is very much stiffer than the result obtained from experiments (error of 93.50%). Fig. 4.14 compares the load versus central deflection curves obtained numerically with experimental one. It can be seen that almost all numerical beams exhibit lower ductility when compared with the experimental beam with 0.4-mm thick plate.

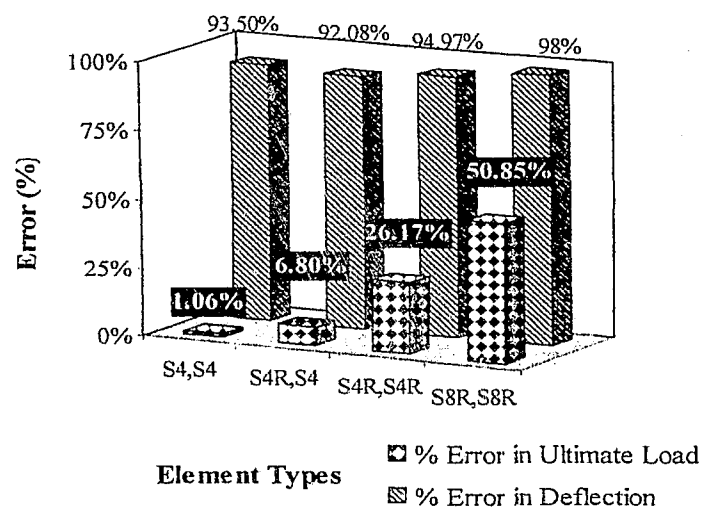


Fig. 4.13 Optimization of element type using various shell elements for S<sub>2</sub>B<sub>100</sub>

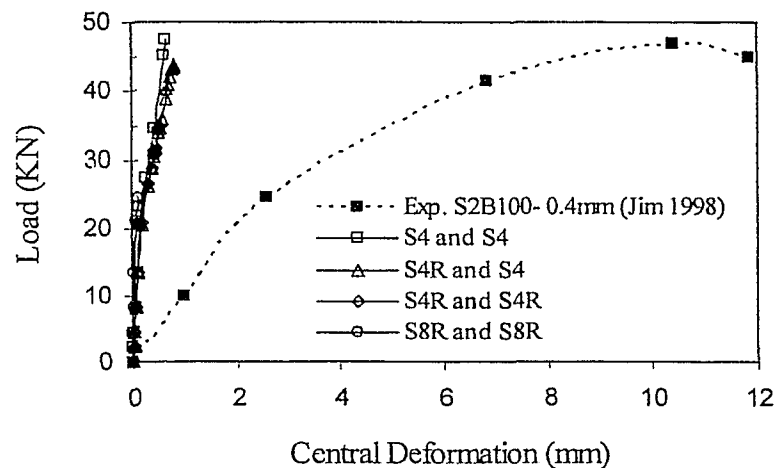


Fig. 4.14 Load Vs central deflection response of numerical beam for selection of element type.

After studying the performance of various shell elements and their impact on the load – central deflection response, the linear 4-node shell element is further optimized to select the appropriate mesh. A bar chart is plotted and illustrated in Fig. 4.15 with the percentage error obtained both the ultimate load and central deflection when the mesh size is varied.

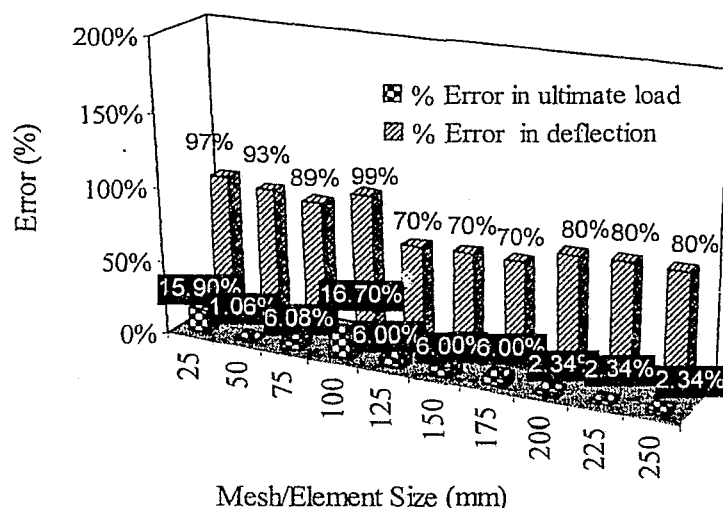


Fig. 4.15 Effect of mesh size on ultimate load versus central deflection.

#### 4.2.6.2. Combined Use of 3D Solid and 2D Shell Elements

Based on the poor performance of the model with two dimensional shell elements, it was decided to use hexagonal solid/brick element having six degrees of freedom at each node for concrete and 2D shell elements for the steel plate. Tie constraint is used to represent the connections between the steel plate and the concrete for the development of the finite element model. Tie constraint was used because of its good performance in simulating the steel plate - concrete interface as confirmed from the parametric study of model with 2D shell elements.



Both longitudinal and transverse reinforcement were modeled using a smeared layer embedded in the solid element used to model the concrete beam. A typical finite element discretization of beams in this model is shown in Fig.4.16.

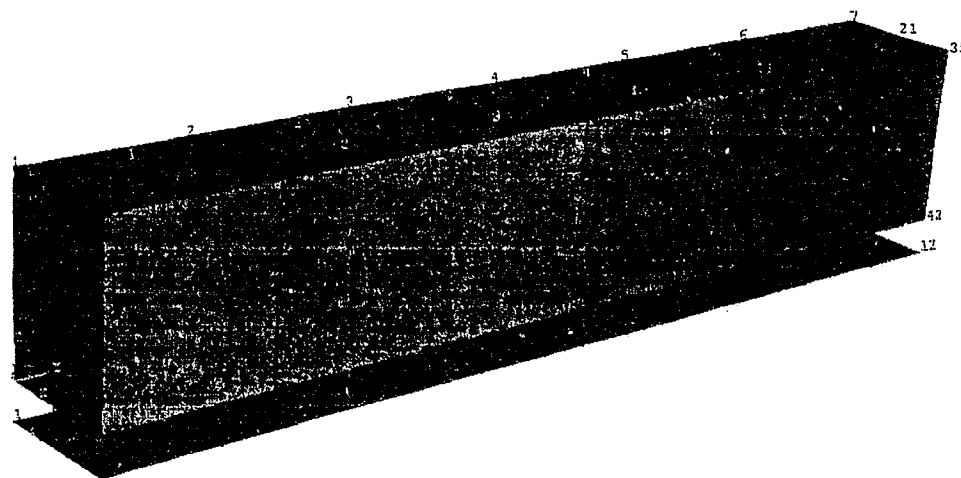


Fig. 4.16 Typical Finite Element discretization of the beam with mixed solid and shell elements

A parametric study was conducted to investigate the performance of the model with different elements and mesh sizes. The  $S_2B_{100}$  beam having 0.4-mm thick plate (Jim 1999) was also selected for the numerical investigation.

There are various types of linear and quadratic solid elements available by *ABAQUS* for the numerical modeling, some of them are listed as C3D8, C3D8R, C3D8I, C3D8H, C3D20R, C3D20H and C3D20RH. The First letter C; corresponds to a Continuum/Solid element followed by 2D or 3D, which corresponds to the 2D or 3D nature of the solid element. The second number denotes the number of nodes followed by an alphabet R, I,

or H, which denotes that either a solid element has reduced integration points, is hybrid or incompatible in nature.

In the first stage, the prediction of the numerical model is checked by using various mesh sizes ranging from 25 to 225 mm. A 3-dimensional solid element having 8 nodes with reduced integration scheme (i.e. C3D8R) is arbitrary selected to model the concrete beam and 4-node linear shell element (i.e. S4) is used to model the steel plate.

Tie constraint, because of its better performance has been used to create an interaction between the elements lying on the concrete tension face and the steel plate, which is kept constant throughout the development of the mixed model. The effect of varying the mesh size on the load-central deflection response of the beam is shown in Fig. 4.17.

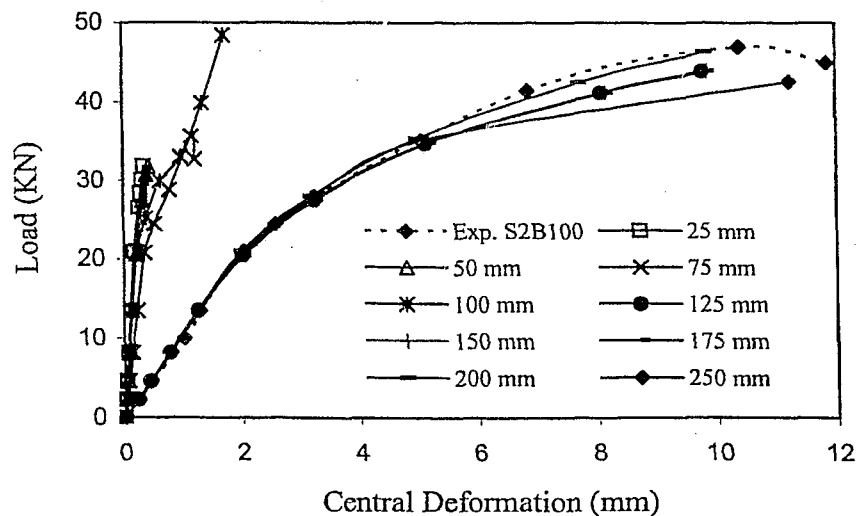


Fig. 4.17 Effect of mesh size on load-deflection response of FEA-S<sub>2</sub>B<sub>100</sub> beam

As illustrated in Fig. 4.17, it can be seen that the combined use of 3D solid and 2D shell elements in the model gives good results. Comparative study is illustrated in Fig. 4.18,

which shows that the percentage error obtained for the ultimate load and the central deflection is reasonably good for the mesh size ranging from 125 to 200 mm.

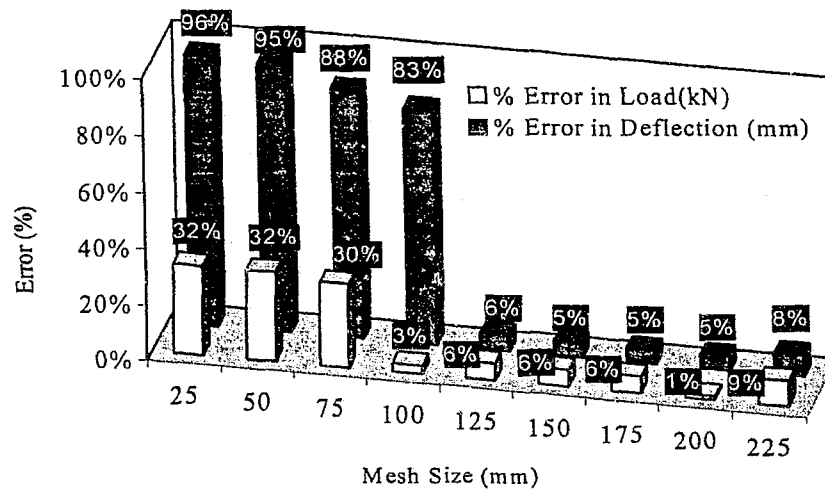


Fig. 4.18 Comparative study on various mesh size used with mixed model

Based on this, it was decided to use solid elements with 200 mm for both the concrete and the steel plate. Once the mesh/element size is optimized, the next step is to optimize the element type as *ABAQUS* offers a number of solid and shell elements with respect to their nodal configurations.

It was decided to keep the 4-node shell element (S4) which was used to model the steel plate, to check the performance of various solid elements with regards to the ultimate load-deflection response of the numerical  $S_2B_{100}$  beam. Optimization of element type for concrete is shown in Fig.4.19 and Fig. 4.20.

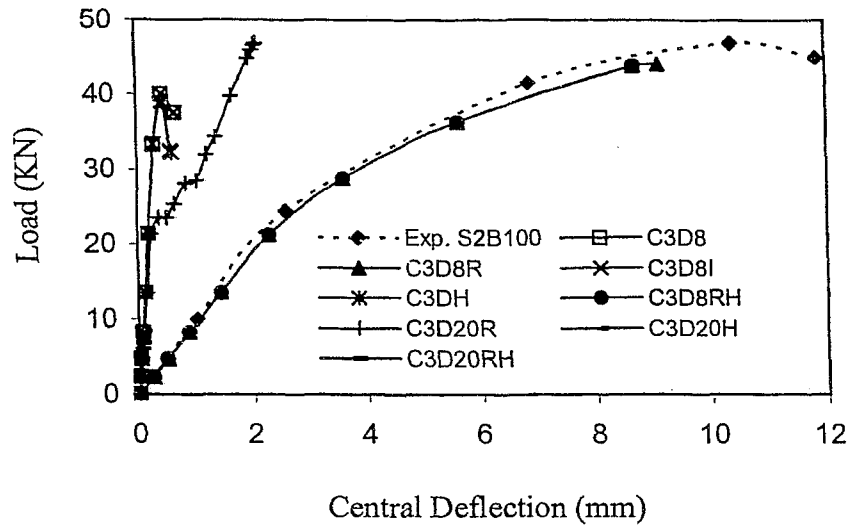


Fig. 4.19 Effect of different types of solid elements on load-deflection response

The performance of various types of solid/brick elements is shown in Fig. 4.19 and Fig. 4.20. Quadratic element with reduce integration such as C3D20R yield much better results in terms of the experimental results but its performance to predict the ultimate deflection is relatively poor as shown in Fig. 4.19 and Fig. 4.20.

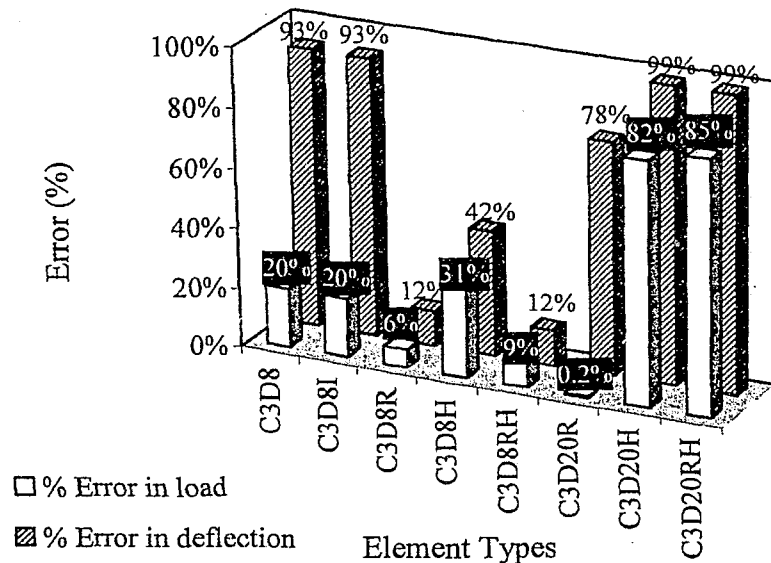


Fig. 4.20 Error obtained with different solid element

On the other hand, it can be seen that the performance of linear 8-node solid element with reduced integration (C3D8R) is comparatively much better than other elements.

After selecting the C3D8R element to model the concrete beam, further optimization is done to obtain an appropriate shell element to model the steel plate. For this purpose, shell elements of various types are used while using C3D8R element constant, to model concrete and the tie constraint to simulate the interface between the concrete and the steel plate.

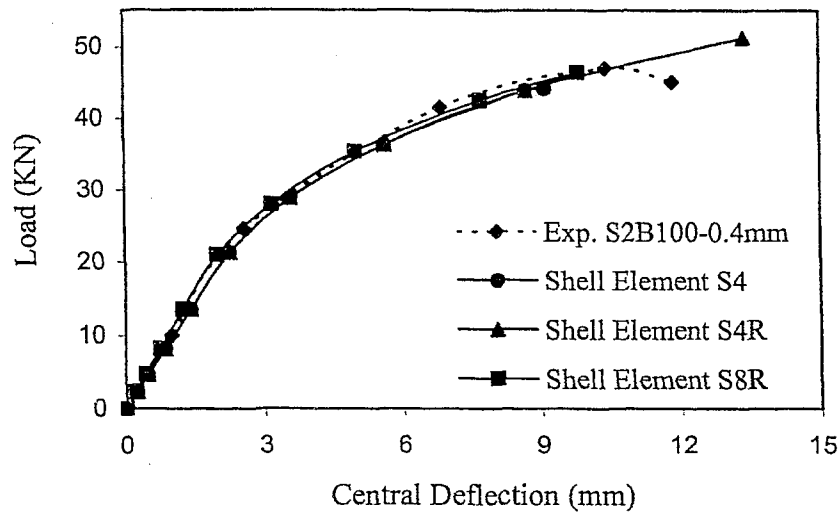


Fig. 4.21 Effect of shell element types on load-deflection response

The load-deflection response for the S<sub>2</sub>b<sub>100</sub> beam is given in Fig. 4.21 for various 2D shell elements used to model the steel plate. It can be seen that among the different types of shell elements, the linear 8-node shell element with reduce integration (S8R) yields excellent results that correspond to an error of 1% and 5% (Fig. 4.22) for the ultimate load and central deflection respectively.

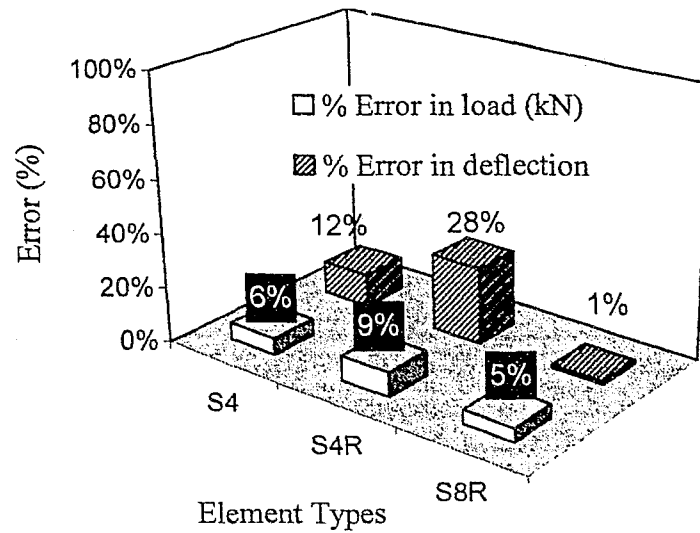


Fig. 4.22 Optimization of element type for steel plate

Based on the result obtained, a 3D 8-node solid element with reduce integration (C3D8R) is used to model the concrete part and an 8-node shell element with reduced integration (S8R) is used to model the steel plate in all beams with an optimized mesh size of 200-mm. Tie constraint is also kept constant at the interface of concrete and the steel plate. This optimized mixed model is then implemented to model all beams tested by Jim (1999). Load-deflection responses comparing experimental results with those obtained from FE analysis are shown in Fig. 4.23 to Fig. 4.26. From Fig. 4.23 to Fig. 4.26, it can be seen that the numerical analysis with mixed model approach yield close results to those obtained experimentally.

Tensile stress contours at the ultimate stage in the longitudinal direction for the  $S_2B_{100}$  beam with 0.4-mm thick plate are shown in Fig. 4.27. All numerical beams failed due to yielding of steel plate when modeled with mixed (solid-shell) element approach.

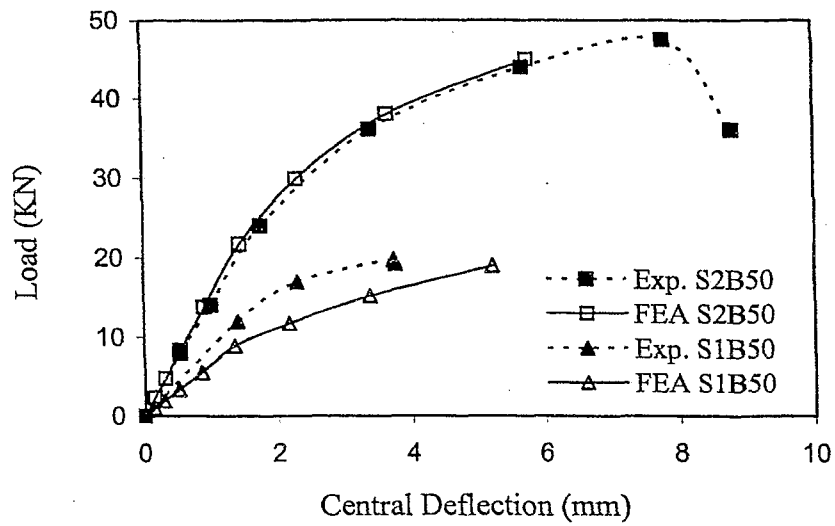


Fig. 4.23 Load vs. central deflection response for  $S_2B_{50}$  and  $S_1B_{50}$  Beams

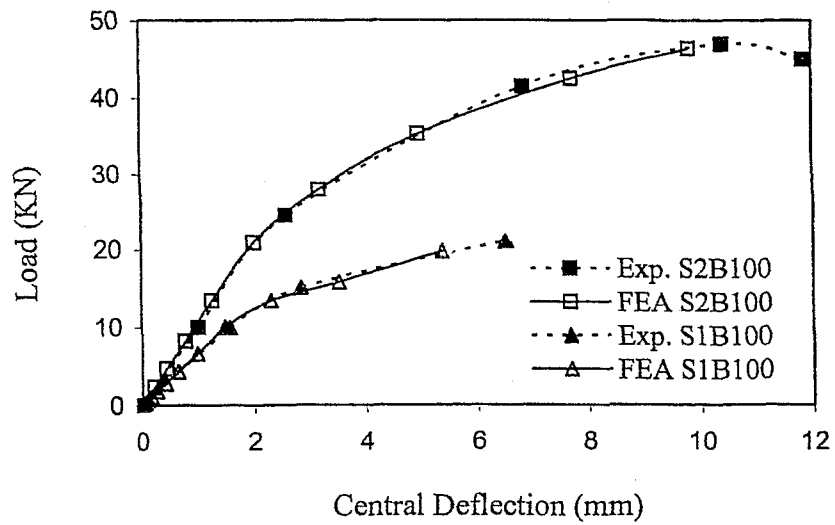


Fig. 4.24 Load vs. central deflection response for  $S_1B_{100}$  and  $S_2B_{100}$  Beams

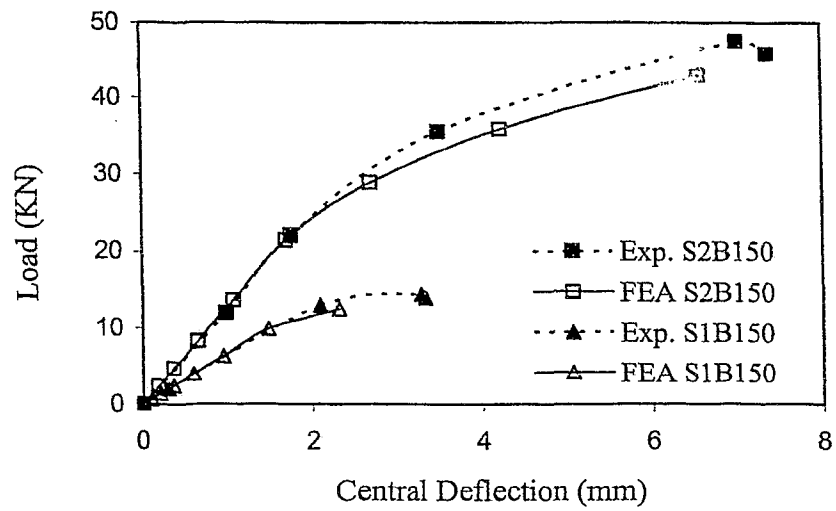


Fig. 4.25 Load vs. central deflection for  $S_1B_{150}$  and  $S_2B_{150}$  Beams

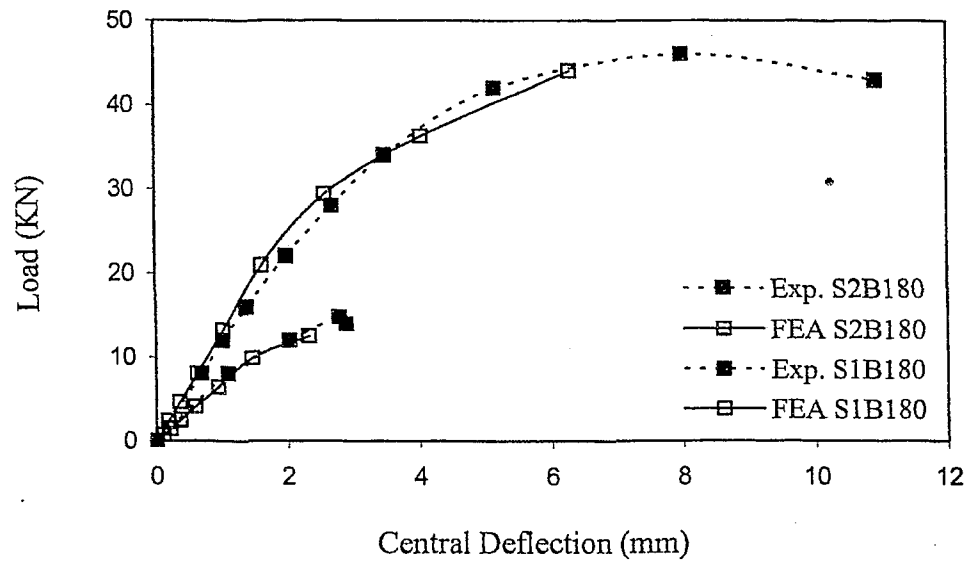


Fig. 4.26 Load vs. Central Deflection for  $S_1B_{180}$  and  $S_2B_{180}$  Beams



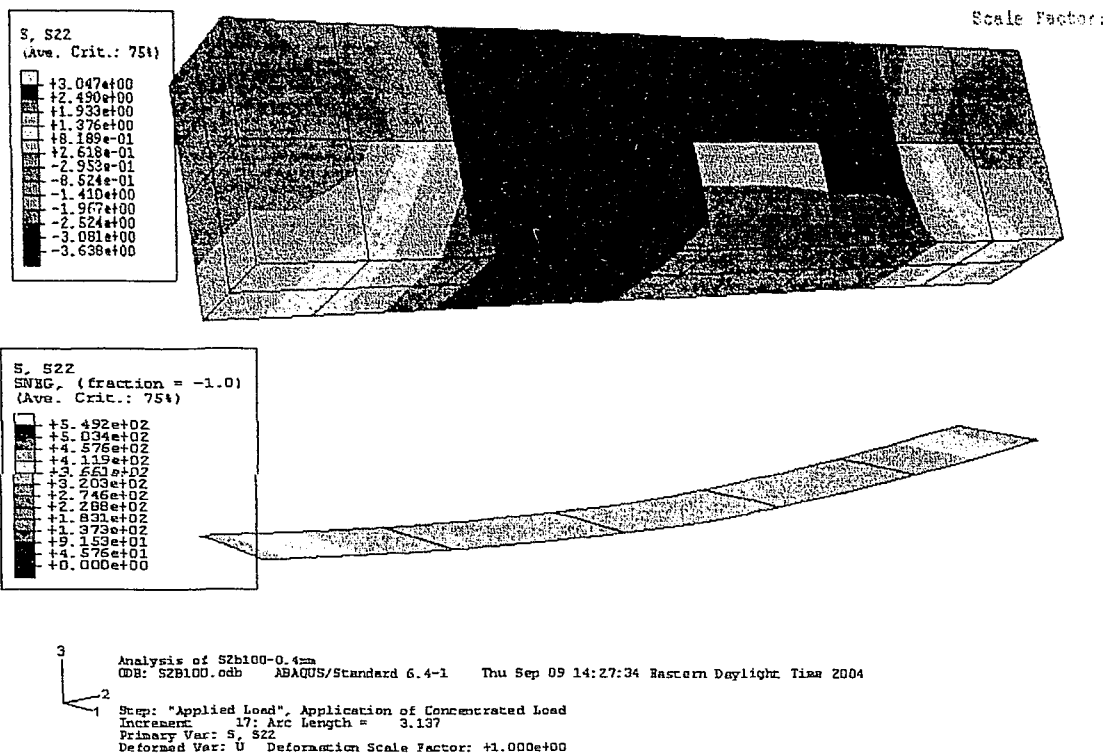


Fig. 4.27 Tensile stress contours in typical  $S_2B_{100}$  beam

#### 4.2.6.3. Shear-Stud Model

For this part, a 3D shear-stud model has been used to simulate the behavior at the concrete-steel interface. As shell element offers only mid surface with respect to the thickness of the steel plate and the use of shell elements can only provide an imaginary connection between the steel plate and stirrups, the concrete and the steel plate are idealized separately using, 8-node linear brick elements having six degrees of freedom at each node. The use of 3D brick elements for the steel plate instead of shell elements can provide a real connection between the top surface of the steel plate and stirrups through connector elements. The longitudinal reinforcements are simulated in concrete elements using the \*REBAR option in *ABAQUS*. Shear reinforcements are assumed to act as shear

studs connected to the steel plate using welded connection and are modeled independently with two node linear 3-D truss element as shown in Fig. 4.28. These shear stirrups are embedded in the concrete using \*EMBEDDED option available in *ABAQUS* and assumed to be fully bonded with concrete. Schematic presentation of shear-stud model is shown in Fig. 4.29.

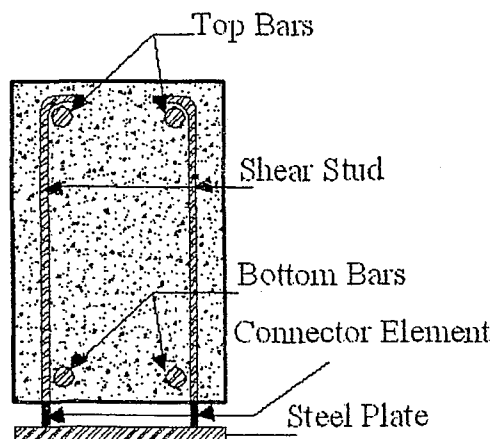


Fig. 4.28 Cross-section of beam with Shear - Stud Model

Welded connections between stirrups and the steel plate are idealized using 2-node, 3-D connector elements having six degrees of freedom at each node. The elements are equipped with load-displacement relations obtained from actual experiments conducted on actual steel plate-stirrup welded specimens. This allows the simulation of actual load-slip characteristics at the steel-concrete interface and failure of the interface. A typical load-slip relationship of such specimens is shown in Fig. 4.30.

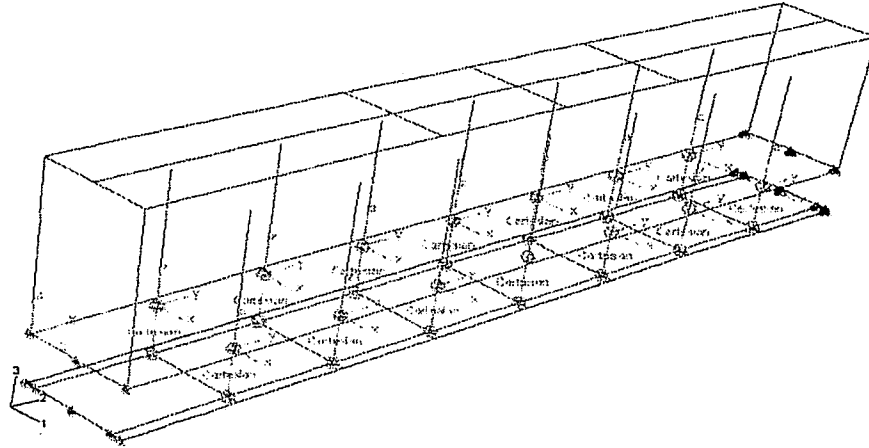


Fig. 4.29 Schematic of interface connection in shear-stud model.

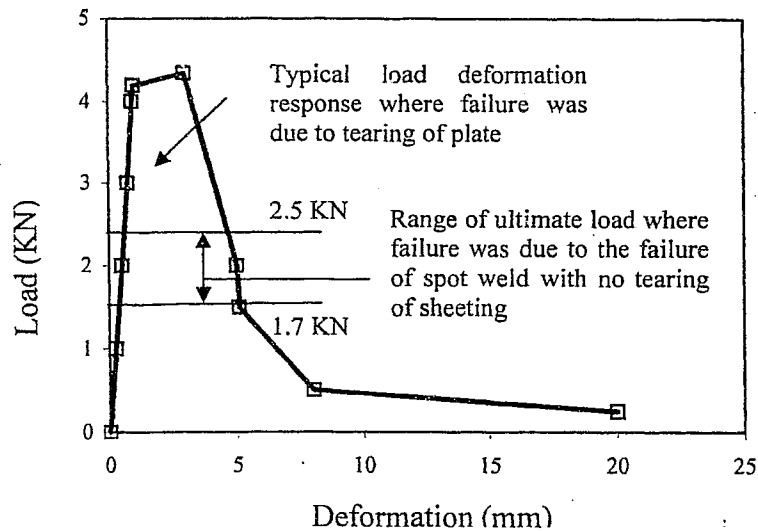


Fig. 4.30 Properties of Spot-welded plates in Lap-Shear Test (Hossain 2001)

A validation process has been conducted to optimize the model performance in simulating experimental results. A 3-D linear solid element having 8-node with six degrees of freedom per node (C3D8R) was used for both the concrete and the steel plate to analyze the effect of different mesh size on the load-deflection response of the  $S_2B_{100}$  beam with 0.4-mm thick plate. Fig. 4.31, shows the error obtained for both the ultimate

load and central deflection for the  $S_2B_{100}$ -0.4 mm beam. It can be seen that a mesh size of 100-mm or less is required to achieve good results by the FE model.

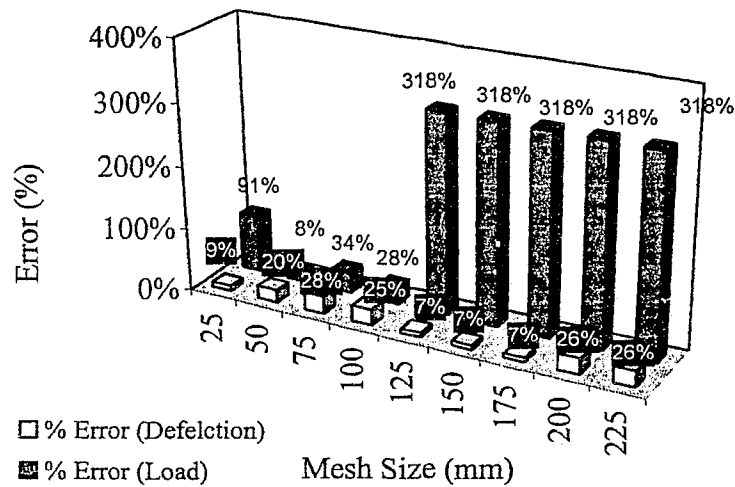


Fig. 4.31 Optimization of element type for Shear -Stud Model.

The mesh size of 50 mm has been selected on the basis of optimization process mentioned previously, for the modeling of both the concrete and the steel plate with solid elements. Therefore, both the concrete and the steel plate are modeled using solid elements of various types. C3D8 solid element were used for the steel plate while different solid elements were used for the concrete part.

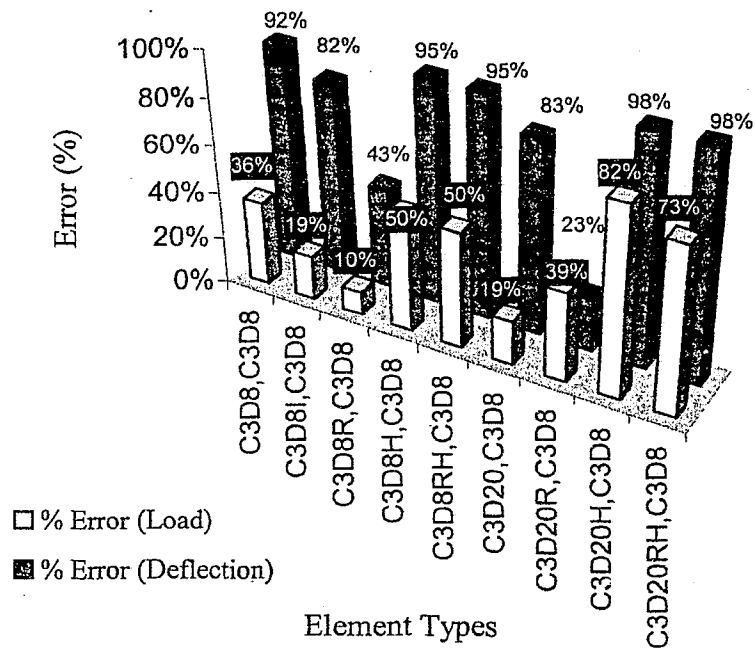


Fig. 4.32 Optimization of solid element types to model the concrete part in  $S_2B_{100}$  beam

Fig. 4.32 shows a comparative study in terms of percentage of error obtained when comparing the experimental response to those obtained numerically for the  $S_2B_{100}$  beam with 0.4-mm thick steel plate. It can be seen that the prediction based on the concrete part modeled with the linear 8-node solid element with reduced integration yields the best results. Therefore, the C3D8R element is selected to model the concrete part to further optimize the type of element use to for the steel plate.

Fig. 4.33 shows the effect of using different types of elements to model the modeled steel plate. It can be seen from Fig. 4.33, that the steel plate can be adequately modeled using C3D8R solid element.

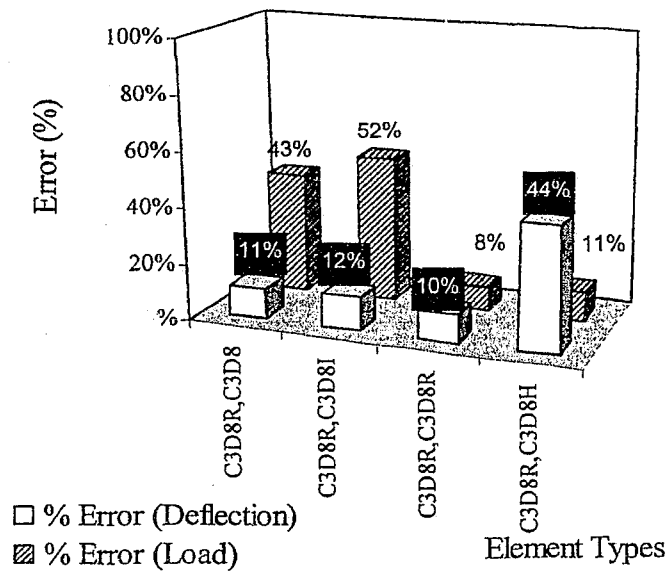


Fig. 4.33 Optimization of element type to model the steel plate in the shear stud model

This optimized model (Shear-Stud) is then implemented to simulate all experimental beams having 0.4-mm thin steel plate (Jim 1999). Simulated load-deflection responses of all 8 experimental beams using this model are shown in Fig. 4.34 to Fig. 4.37. From these figures it can be concluded that the shear-stud model is not suitable for the prediction of beams especially those in Series 1 category.

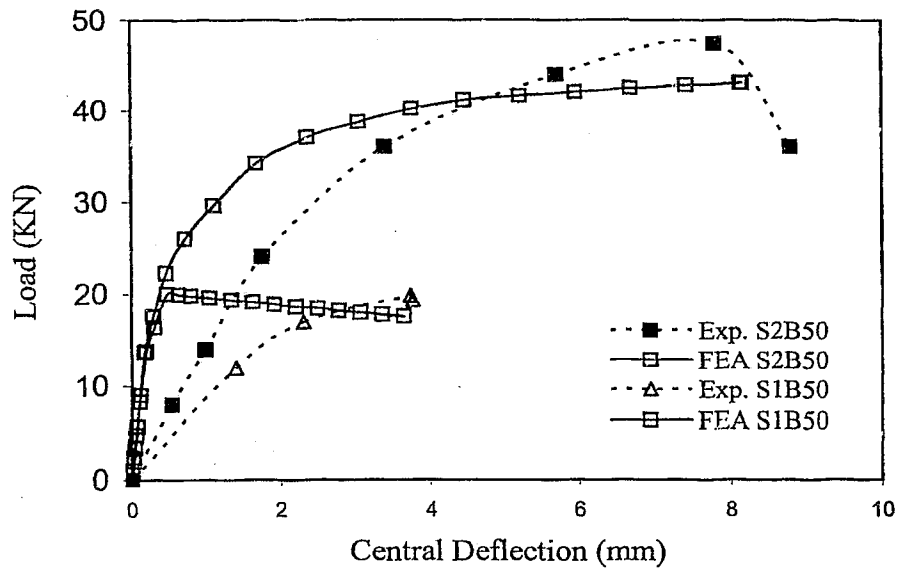


Fig. 4.34 Load vs. central deflection response of S<sub>2</sub>B<sub>50</sub> and S<sub>1</sub>B<sub>50</sub> beam using Shear-Stud Model

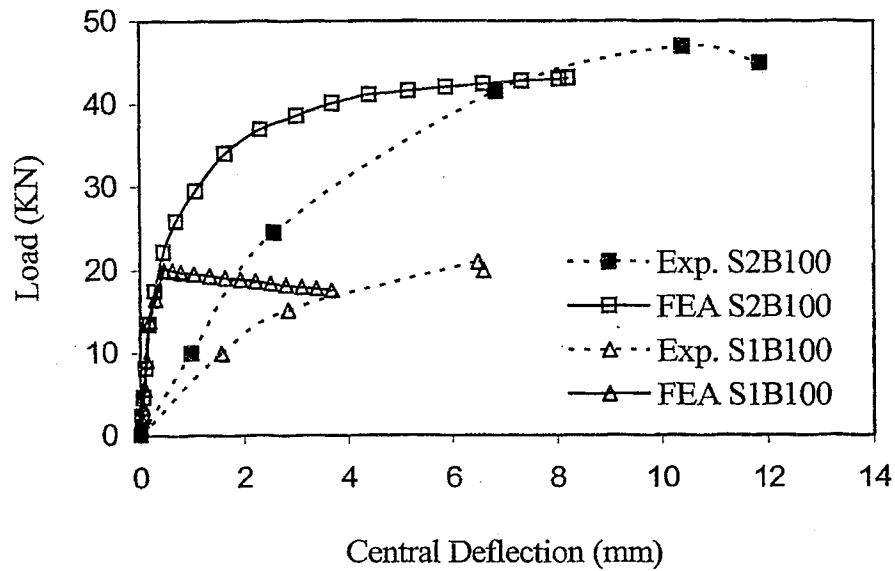


Fig. 4.35 Load vs. central deflection response of S<sub>2</sub>B<sub>100</sub> and S<sub>1</sub>B<sub>100</sub> beam using Shear-Stud Model

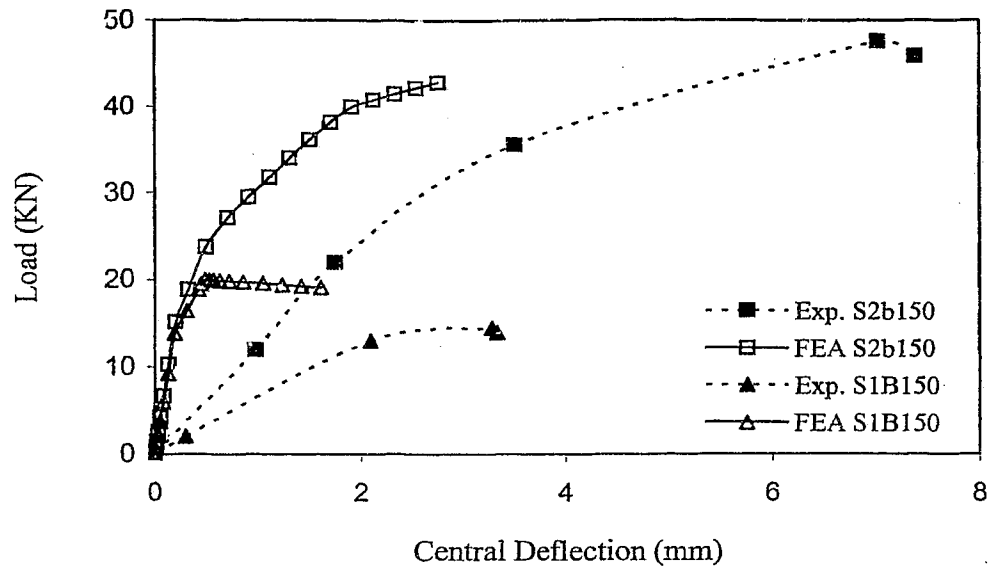


Fig. 4.36 Load vs. central deflection response of S<sub>2</sub>B<sub>150</sub> and S<sub>1</sub>B<sub>150</sub> beam using Shear-Stud Model

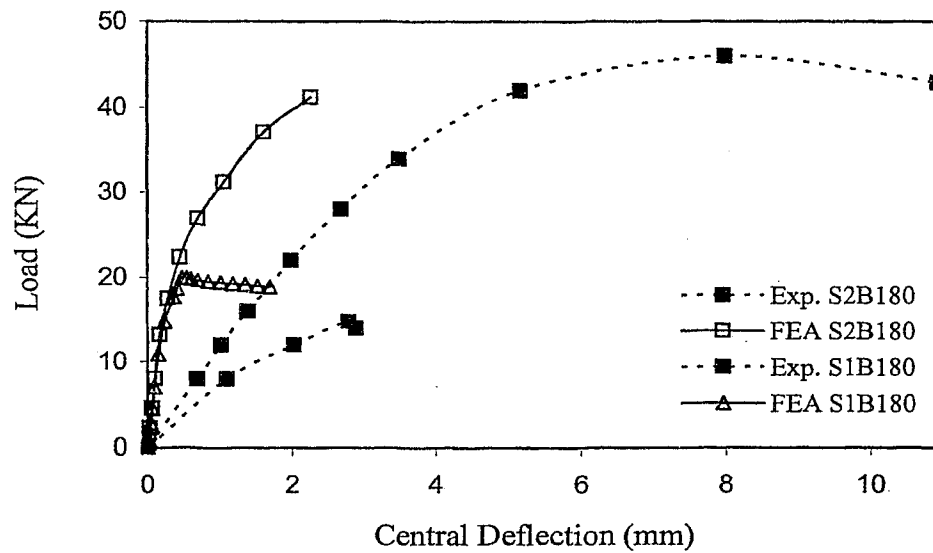


Fig. 4.37 Load vs. central deflection response on S<sub>2</sub>B<sub>180</sub> and S<sub>1</sub>B<sub>180</sub> beam using Shear-Stud Model



Tensile stress contours at the ultimate stages in the longitudinal direction for the  $S_2B_{100}$  beam with 0.4-mm thick plate are shown in Fig. 4.38. In all cases, failure of spot weld, modeled with connectors element results in punching of the reinforced concrete beam into steel plate when the ultimate strength of weld is reached (Fig. 4.39).

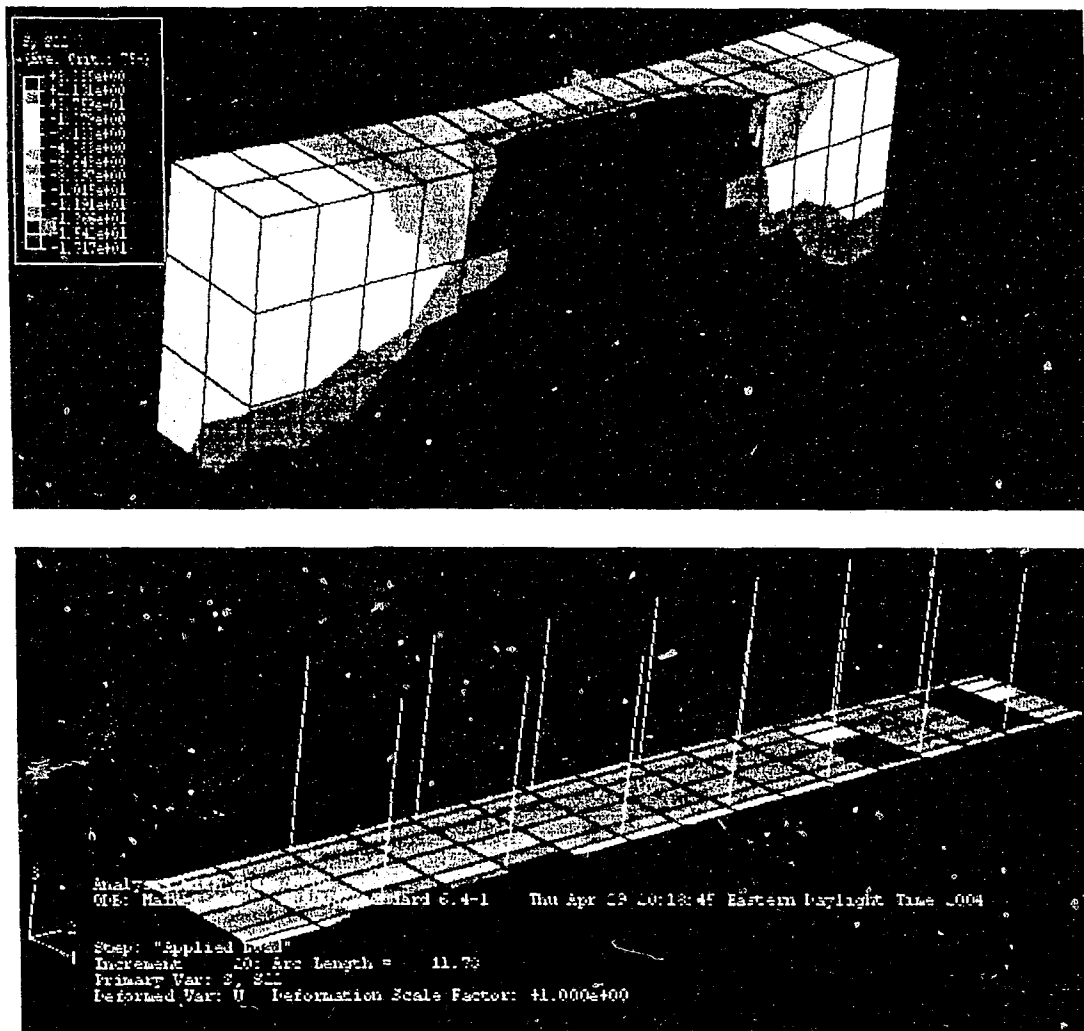


Fig. 4.38 Typical stress contour corresponding to the beam longitudinal direction

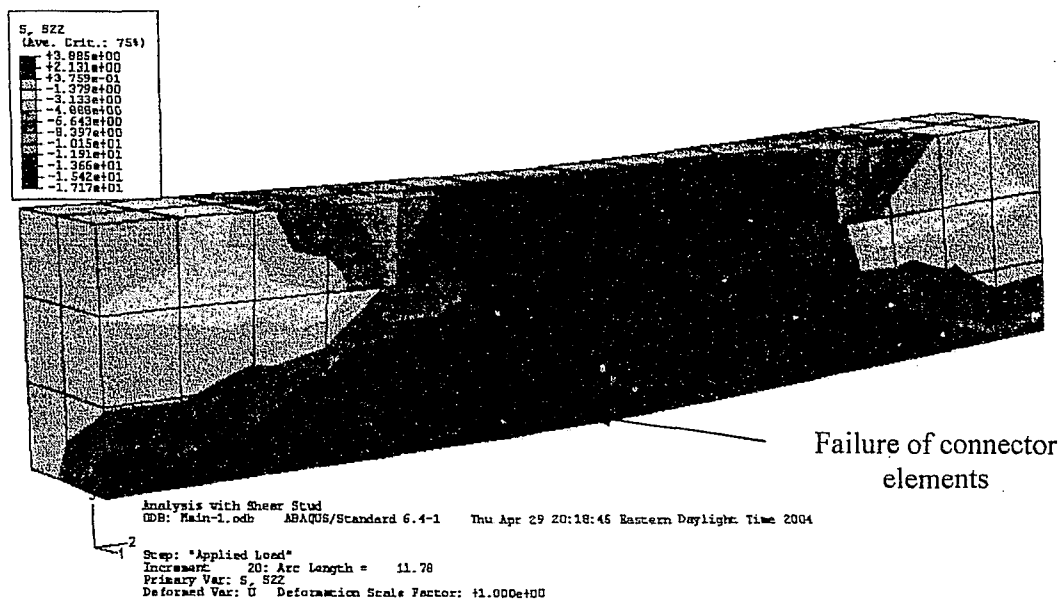


Fig. 4.39 Punching failure of concrete node into steel plate nodes in numerical beams.

### 4.3. Comparative Study on Finite Element Models

The results of simulations using different finite element models are presented in Table 4.1. The results of all numerical models presented in Table 4.1 are also compared with the experimental results (Jim 1999) in Table 4.2. The comparative study shows that the numerical results obtained with shell elements in Model-1 with shell elements predicts the ultimate load carrying capacity of beams reasonably well with an average experiment-to-predicted ultimate load ratio of 0.98 while under predict the ultimate deflection with an average factor of 5. The same can be said for the shear-stud model. The model using the mixed element approach gives the best results in predicting both the ultimate load and the central deflection. The mixed model predict reasonably well the ultimate load and the central deflection with an average experimental to predicted load and deflection ratio of 1.08 and 1.16, respectively as shown in Table 4.2.

Beam (Series)	Experimental Response		FEA		FEA		FEA	
			With Shell Elements		With Mixed Model		With Shear-Stud Model	
	Load (KN)	Central Deflection (mm)	Load (KN)	Central Deflection (mm)	Load (KN)	Central Deflection (mm)	Load (KN)	Central Deflection (mm)
S <sub>1</sub> B <sub>50</sub>	19.80	3.73	20.00	0.48	19.04	5.20	20.25	0.47
S <sub>1</sub> B <sub>100</sub>	21.00	6.50	20.03	0.48	19.80	5.38	20.02	0.36
S <sub>1</sub> B <sub>150</sub>	14.50	3.28	20.50	0.63	12.51	2.30	20.01	0.57
S <sub>1</sub> B <sub>180</sub>	14.80	2.78	19.98	0.47	12.50	2.30	19.97	0.40
S <sub>2</sub> B <sub>50</sub>	47.50	7.80	43.08	8.16	45.03	5.76	43.08	8.16
S <sub>2</sub> B <sub>100</sub>	47.00	10.40	43.10	8.23	46.39	9.81	43.10	8.68
S <sub>2</sub> B <sub>150</sub>	47.50	7.02	42.83	2.76	42.90	6.50	42.80	2.76
S <sub>2</sub> B <sub>180</sub>	46.00	8.00	41.26	2.26	44.10	6.29	41.26	2.26

Table 4.1 Prediction of ultimate load and central deflection using different FE models

Beam (Series)	Experiment /Model (Shell Element)		Experiment / Model (Mixed Model)		Experiment / Model (Shear-Stud Model)	
	Load	Central Deflection	Load	Central Deflection	Load	Central Deflection
S <sub>1</sub> B <sub>50</sub>	0.99	7.77	1.04	0.72	0.98	7.94
S <sub>1</sub> B <sub>100</sub>	1.05	13.54	1.06	1.21	1.05	18.06
S <sub>1</sub> B <sub>150</sub>	0.71	5.21	1.16	1.43	0.72	5.75
S <sub>1</sub> B <sub>180</sub>	0.74	5.91	1.18	1.21	0.74	6.95
S <sub>2</sub> B <sub>50</sub>	1.10	0.96	1.05	1.35	1.10	0.96
S <sub>2</sub> B <sub>100</sub>	1.09	1.26	1.01	1.06	1.09	1.20
S <sub>2</sub> B <sub>150</sub>	1.11	2.54	1.11	1.08	1.11	2.54
S <sub>2</sub> B <sub>180</sub>	1.11	3.54	1.04	1.27	1.11	3.54
Mean Value	0.98	5.09	1.08	1.16	0.98	5.86

Table 4.2 Comparative study on finite element models

# **Chapter 5      Development of Design Guidelines and Performance Validation**

## **5.1.    Introduction**

This chapter describes the development of design guidelines that can be used during the process of strengthening reinforced concrete beams with mechanically bonded steel plates. Discussions on the effect of some parameters, on the ultimate load carrying capacity of numerically simulated beams are also presented. Design guidelines are presented in terms of Design Charts developed from a large number of computer models and their performance validation is made against the prediction of 16 experimented beams (Jim 1999 and Nupiri 2000). To highlight the significance of these Design Charts for quick and accurate prediction of the strength of mechanically bonded strengthened beam, a design example is presented at the end of this chapter to assist potential users.

## **5.2.    Development of Design Guidelines**

Normally, there are three possible solutions to design and predict the ultimate strength of novel form of structural members and those are as follows:

- Experimental investigation;
- Code based mathematical models/governing equations;
- Finite element modeling leading to design charts and graphs.

Finite element modeling has the advantage over the other two methods. Experimental investigation can be time consuming and expensive. On the other hand, existing Code

based procedures may not be suitable for the prediction of ultimate strength of novel forms of structural elements and may lead to unreliable design. The development of a finite element model whose performance is validated through selective experimental results on novel form of structural elements and its subsequent use in the simulation of large number of such numerical structural elements can provide a cost-effective means of developing design guidelines.

The finite element using the mixed element approach, presented in Chapter 4, is used to simulate thousands of beams with mechanically bonded steel plates by varying material and geometric properties in order to develop design guidelines for such beams. The performance of developing design guidelines is validated through further experimental results of such beams, experimental results from other researcher and various Codes based design procedures.

### **5.3. Development of Design Charts by Finite Element Predictions**

The finite element model is used for developing design guidelines by generating a database of load-deflection response for over 9000 cases of steel plated beams by varying material and geometrical properties. Such design charts could serve for quick and accurate ultimate strength determination of such beams. The establishment of a reliable finite element model that is capable of giving quick and accurate prediction of strength of structural elements has many implications. The database can be used for the development of knowledge based system or neural network for the design of proposed steel plated beams (Famiyesin and Hossain 1998a, 1998b; Famiyesin et al. 2001).

Table 5.1 gives a summary of geometric and material parameters, which can influence the strength of such beams. The ranges of geometric and material properties used in the simulation of 9000 numerical beams are also presented in Table 5.1.

The longitudinal reinforcement is mainly based on its contribution with 20% provided at the top while 80% provided at the bottom with respect to the steel ratio as summarized in Table 5.1.

Parameters	Notation	Min.	Max.	Unit
Width of Beam	w	100	400	mm
Total Depth of Beams	h	150	650	mm
Spacing of Stirrups	S	50	200	mm
Longitudinal Steel Ratio	$\rho$	$0.15 \rho_b$	$0.55 \rho_b$	ratio
Compressive Strength of Concrete	$f'_c$	25	45	MPa
Yield Strength of Steel	$f_{ys}$	300	450	MPa
Yield Strength of Steel plate	$f_{yp}$	300	350	MPa
Steel Plate Thickness	$T_p$	0.5	10	mm
Stirrups Steel Area/Spacing	$A_v/S$	0.2	3.14	ratio
Length-to-Depth ratio	$L/h$	6	12	ratio
Concrete Cover	10% of "h"			mm

Table 5.1 Parameters of numerically simulated computer beams

Nine variables are used in developing theoretical computer model beams with varying aspect ratios, length to depth ratios, steel plate thickness, spacing of stirrups, concrete

strengths, reinforcement ratio (as percentage of balanced steel ratio for a particular section), yield strength for both the longitudinal reinforcement and the steel plate.

The computer model beams are analyzed as simply supported with one end pinned and the other on roller to allow relative movement. Cover to the internal steel reinforcement is assumed to be as 10% of the overall depth "h" of the beams with consideration of interior and exterior exposures.

Load-deflection responses of all 9000 computer model beams are simulated using *ABAQUS*. A typical INPUT file for finite element model (Mixed model) is also presented in Appendix A. Flexural strength of all experimental beams are calculated using various codes and presented in Appendix B. Peak loads derived from the finite element simulation are used to calculate the moment or flexural capacity of all beams. Detailed results showing strength of all computer model beams in terms of their moment resisting capacity are presented in Appendix C.

#### **5.4. Influence of Various Parameters on Ultimate Moment Capacity**

Influence of aspect ratios, length to depth ratios, plate thickness, spacing of stirrups, concrete strengths, reinforcement ratio, and yield strength for both longitudinal reinforcement and steel plate is discussed below.

#### 5.4.1. Effect of the Compressive Strength of Concrete ( $f'_c$ ) on the Ultimate Moment Capacity

To study the effect of compressive strength of concrete, 3 beams having a cross section of 100 mm x 650 mm (Beam-1), 100 mm x 500 mm (Beam-2) and 100 mm x 350 mm (Beam-3) with length-to-depth ratio of 12 are arbitrary selected. Reinforcement ratio of 15% of the balanced steel ratio calculated for these typical beams using the Canadian Code (CSA 1994) is kept constant together with 6.5-mm thick steel plate with tensile yield strength of 400 MPa for both steel rebars and the steel plate. Transverse reinforcement is provided using stirrups of 10-mm diameter bars with a uniform spacing of 50-mm giving a ratio of stirrup steel area to stirrups spacing,  $A_v/S$ , of 3.14.

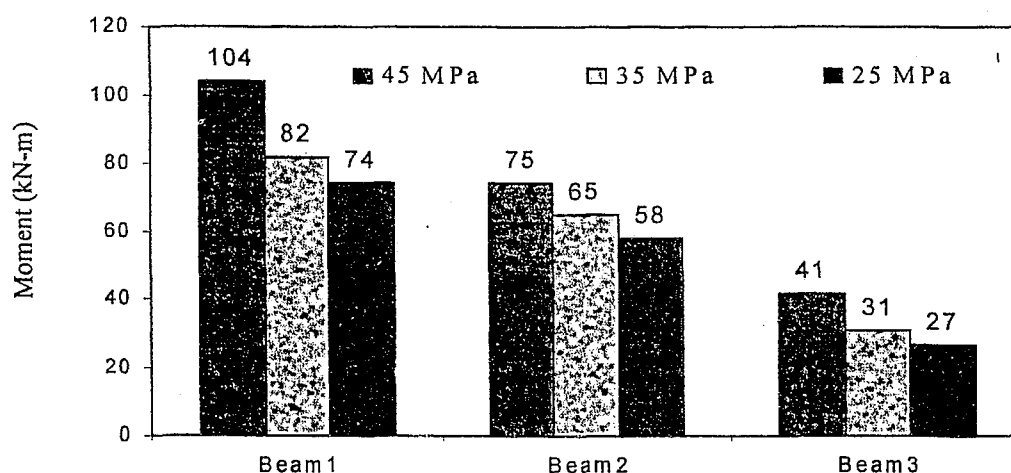


Fig. 5.1 Effect of compressive strength of concrete ( $f'_c$ ) on ultimate moment capacity

The effect of varying the compressive strength of concrete on the ultimate moment capacity of Beam-1, Beam-2 and Beam-3 is shown in Fig. 5.1. It can be seen that the moment capacity decreases almost linearly as the compressive strength of concrete



decreases. Therefore, the compressive strength concrete can be considered as an important factor for strengthening this novel forms of beams

#### 5.4.2. Effect of Yield Strength of Steel Reinforcement on Ultimate Moment Capacity

To study the effect of the yield strength of steel reinforcement on ultimate moment capacity beams, 3 beams having a cross section of 200 mm x 650 mm (Beam-1), 200 mm x 500 mm (Beam-2) and 200 mm x 350 mm (Beam-3) with length-to-depth ratio of 12 are arbitrary selected. The compressive strength of concrete is kept constant with a value of 25 MPa. The rest of the parameters used in the previous study are also kept constant to analyze the influence of yield strength of steel moment capacity of the studied beams. A comparative study is shown in Fig. 5.2.

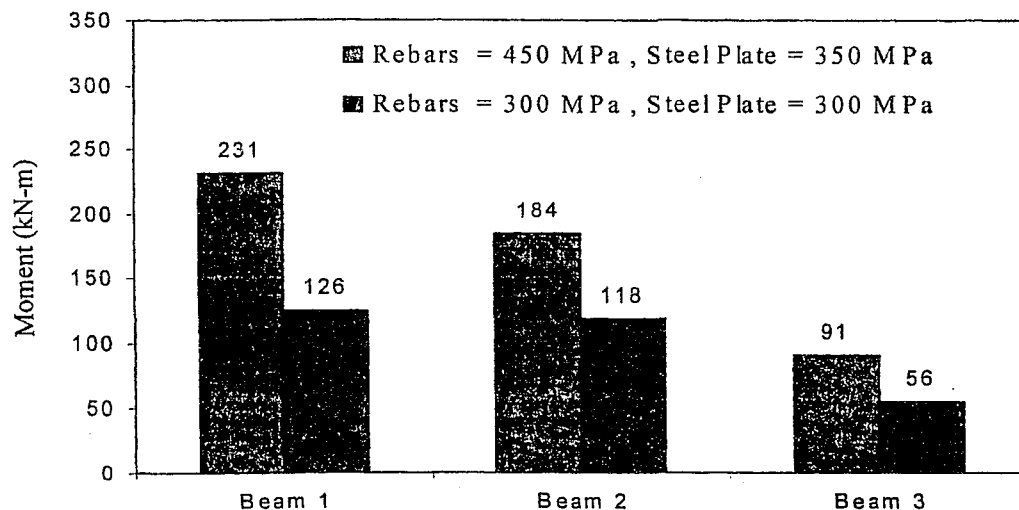


Fig. 5.2 Effect of yield strength of steel rebar ( $f_{y_s}$ ) and steel plate ( $f_{y_p}$ ) on ultimate moment capacity

From Fig. 5.2, it can be noted that the yield strength of reinforcement provided in terms of rebar and steel plate has great influence on the moment capacity of studied beams. Their strength decreases drastically with the decrease in yield strength of both longitudinal reinforcement and steel plate.

#### 5.4.3. Effect of Longitudinal Reinforcement Ratio ( $\rho$ ) on the Ultimate Moment Capacity

To study the effect of reinforcement ratio on the ultimate moment capacity, 3 beams having a cross section of 100 mm x 650 mm (Beam-1), 100 mm x 500 mm (Beam-2) and 100 mm x 350 mm (Beam-3) with length-to-depth of 12 are arbitrary selected with 0.5-mm thick steel plate. The concrete compressive strength is kept constant to a value of 25 MPa for all three beams together 300 MPa yield strength of internal longitudinal rebars and steel plate. The rest of the parameters used in the previous study are kept constant. The reinforcement ratio,  $\rho$ , varied from 15 to 55% of the balanced steel ratio calculated according to the Canadian code.

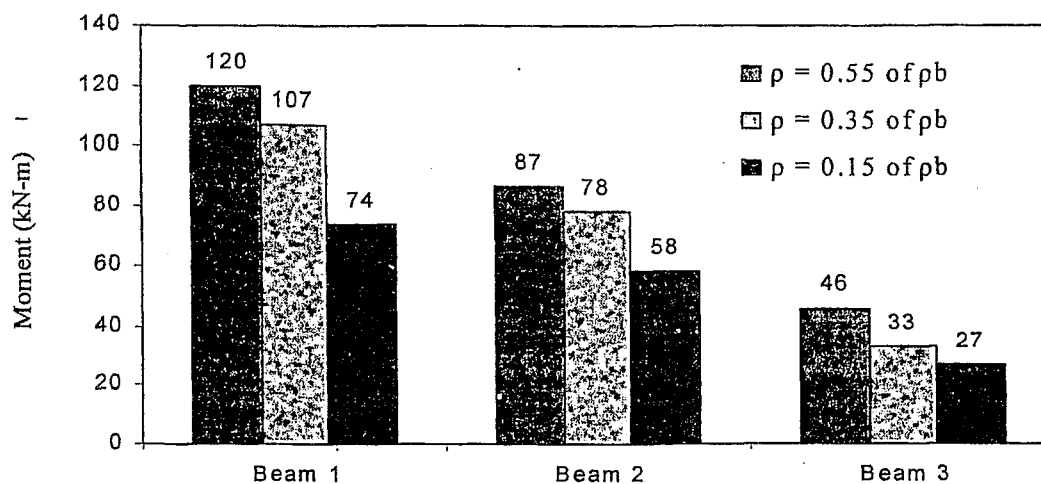


Fig. 5.3 Effect of internal reinforcement ratio ( $\rho$ ) on ultimate moment capacity

A comparative study showing the effect of the variation in internal steel ratios for typical beams is shown in Fig. 5.3. It can be noted that by increasing the reinforcement ratio, the strength of the beam increases.

#### 5.4.4. Effect of Stirrups Spacing "S" on the Ultimate Moment Capacity

To study the effect of stirrups spacing on ultimate moment capacity, 3 beams having a cross section of 100 mm x 650 mm (Beam-1), 100 mm x 500 mm (Beam-2) and 100 mm x 350 mm (Beam-3) with length-to-depth of 12 are arbitrary selected with a steel plate of 0.5-mm thickness. The ratio of stirrup rebar area to spacing is varied between ranges of 0.78 and 3.14. The ratio of steel reinforcement is kept constant to values of 15% of balanced steel ratio calculated using Canadian code. Compressive strength and yield strength of 25 MPa and 300 MPa are used respectively, for concrete, rebars and steel plate together. Comparative study showing the effect of stirrups spacing is presented in Fig. 5.4.

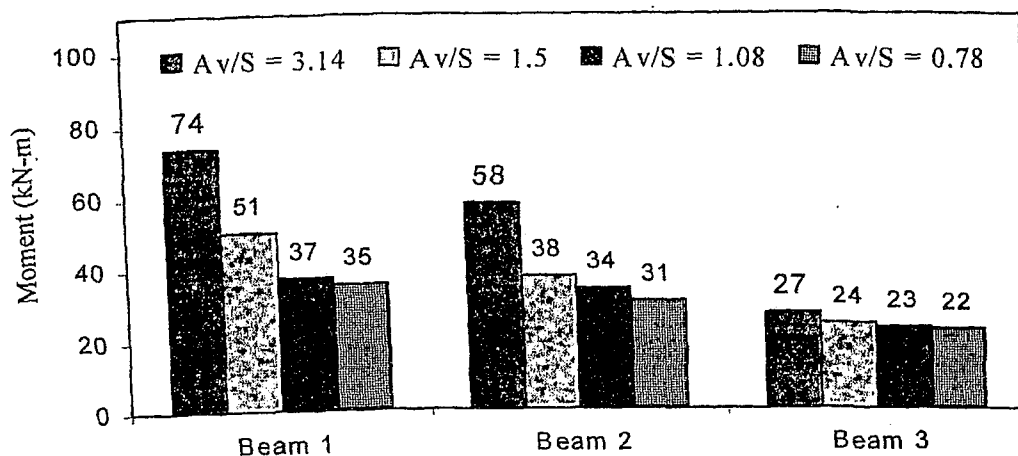


Fig. 5.4 Effect of stirrups spacing (S) on ultimate moment capacity

From Fig. 5.4, it can be noted that ultimate moment capacity decreases with increasing the spacing of stirrups.

#### 5.4.5. Effect of the Beam Width on the Ultimate Moment Capacity

To study the effect of beam width on ultimate moment capacity, 3 beams having constant depth of 650 was used. Beam 1 consists of length to depth ratio of 12 while Beam 2 and Beam 3 are of 9 and 6 respectively. Width of beam is varied between 100-mm to 400-mm. The ratio of stirrups steel area to spacing of stirrup is kept constant to a value of 3.14. The longitudinal reinforcement ratio is kept constant to a value of 15% of balanced steel ratio calculated using Canadian code. Concrete strength of 25MPa and yield strength of 300 MPa is used for concrete, internal longitudinal rebars and steel plate.

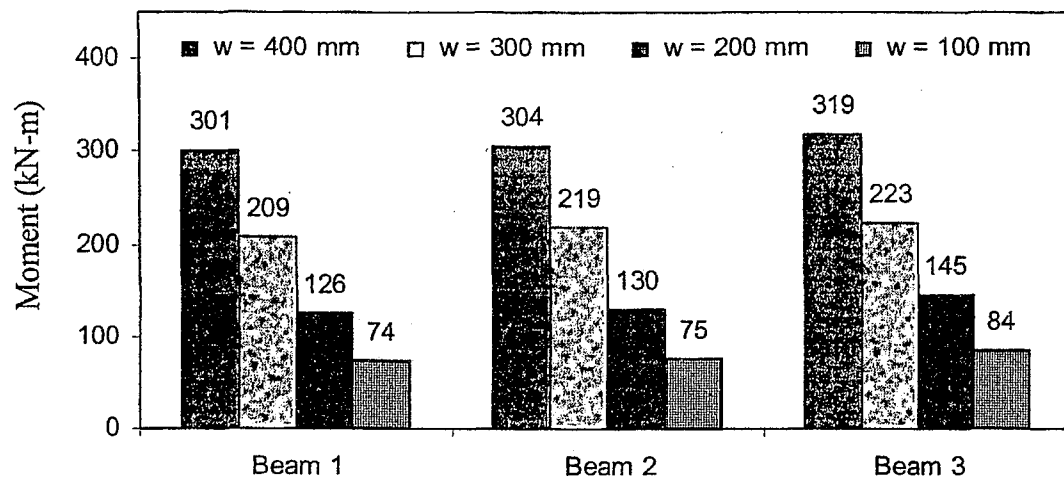


Fig. 5.5 Effect of width of beam on ultimate moment capacity

It can be noted that the width of beam is one of the important parameter affecting the ultimate strength of the beams (Fig. 5.5). The ultimate moment capacity of the beams

increases with increase in beam width, which might be due to the fact area of steel plate increases with the width of beams as steel plate of same width is used to strengthen reinforced concrete beams in all computer models.

#### 5.4.6. Effect of the Beam Depth on the Ultimate Moment Capacity

To study the effect of beam depth on ultimate moment capacity, 3 beams having constant width of 100-mm is used. Beam 1 consists of length to depth ratio of 12 while Beam 2 and Beam 3 are of 9 and 6 respectively, with 0.5-mm thick steel plate. Depth of beam is varied between ranges of 150-mm to 650-mm. The ratio of steel stirrup area to spacing of stirrups is kept constant to a value of 3.14. The longitudinal reinforcement ratio is taken as 15% of balanced steel ratio calculated using Canadian code. Concrete strength of 25MPa and yield strength of 300 MPa is used for internal longitudinal rebars and steel plate respectively.

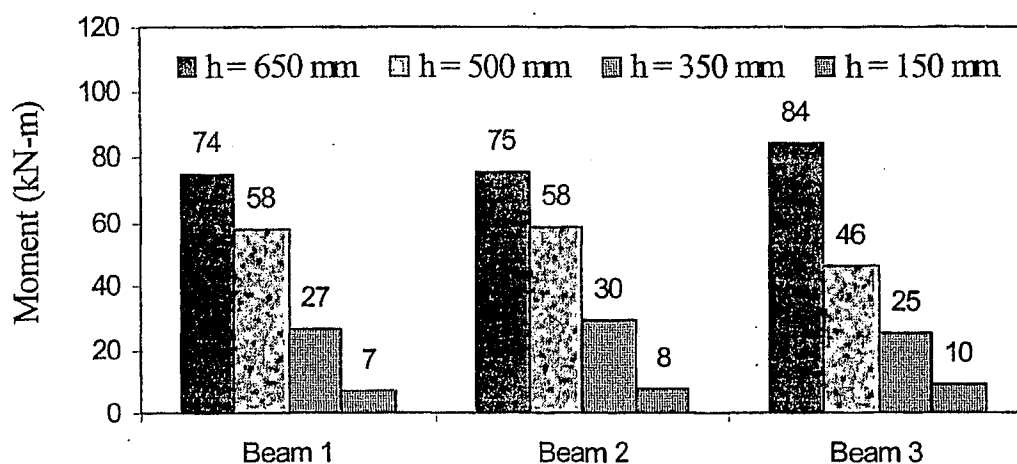


Fig. 5.6 Effect of beam depth (h) on ultimate moment capacity

It can be seen that moment capacity increases with the increase in depth of the beam (Fig. 5.6).

#### 5.4.7. Effect of Length-to-Depth ratio on Ultimate Moment Capacity of Finite Element Models.

To study the effect of length-to-depth ratio ( $L/h$ ) on the ultimate strength of numerical beams, 4 beams having constant geometrical section of 100 mm x 650 mm are used. Steel plate of 10-mm, 5-mm, 3-mm and 1.5-mm are used to strengthen Beam 1, Beam 2, Beam 3 and beam 4, respectively. The ratio of stirrups area to spacing of stirrups is kept constant to a value of 3.14. The longitudinal reinforcement ratio is taken as 15% of balanced steel ratio calculated using Canadian code. Concrete strength of 25 MPa and steel having yield strength of 300 MPa are used. The ultimate moment capacity of numerical beams is checked against variable length-to-depth ratio that ranges between 6 and 12. Comparative study shows in Fig. 5.7 indicated that moment capacity decreases with decrease in  $L/h$  ratio of beams.

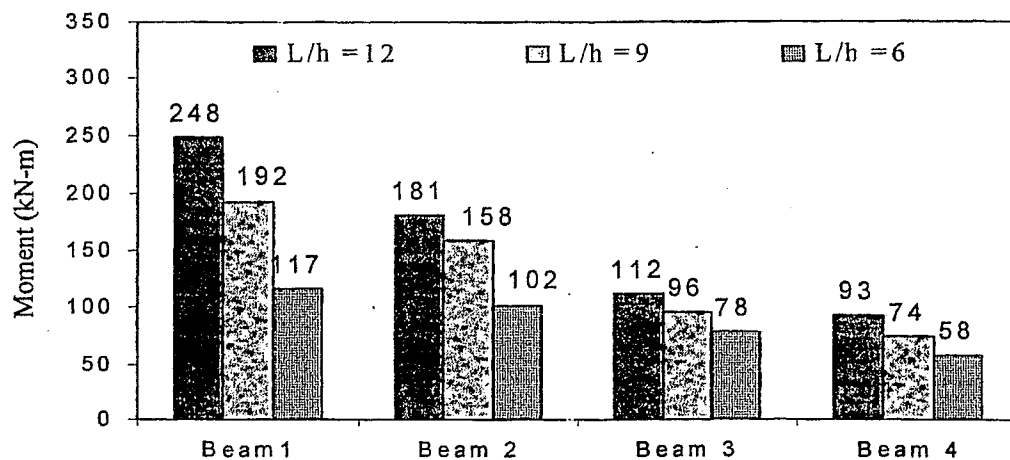


Fig. 5.7 Effect of length-to-depth ratio ( $L/h$ ) on ultimate moment capacity

#### 5.4.8. Effect of the Plate Thickness on the Ultimate Moment

To study the effect of steel plate thickness on ultimate moment capacity, 3 beams having constant width of 100 mm x 650 mm are used. Beam 1 consists of length to depth ratio of 12 while Beam 2 and Beam 3 are of 9 and 6 respectively. The ratio of steel stirrup area to spacing of stirrups is kept constant to a value of 3.14. The longitudinal reinforcement ratio is taken as 15% of the balanced steel ratio calculated using Canadian code. Concrete compressive strength of 25 MPa and yield strength of 300 MPa are used for both the internal longitudinal rebars and steel plate respectively.

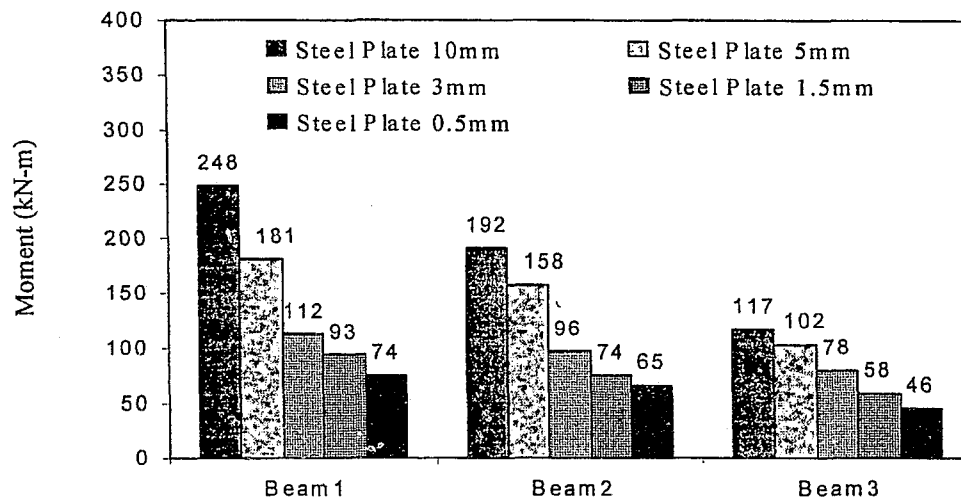


Fig. 5.8 Effect steel plate thickness ( $t_p$ ) on ultimate moment capacity

It can be seen from the comparative study shown in Fig. 5.8 that, the thickness of the steel plate increases the moment carrying capacity of the beams but care must be taken in order to prevent beams from being over reinforced.

## 5.5. Design Charts

From the results obtained through finite element simulation of 9000 computer model beams, 200 design charts are developed to facilitate the design of such beams with various material and geometric properties. Design charts consists of 2<sup>nd</sup> degree polynomial curves (trend lines) fitted through the data points and can be used to predict the moment capacity of an arbitrary beam when its material and geometric properties are known. A polynomial trend line is a curved line that is used when data fluctuates.  $R^2$  value (coefficient of correlation) is an indicator from 0 to 1 that reveals how closely the estimated value of a trend line to our actual data obtained from finite element simulations. A trend line is more reliable when the  $R^2$  value is near to 1. The coefficient of correlation ( $R^2$ ) of all 9000 computer models ranges between 0.94 and 0.98. A typical design chart with  $R^2$  is shown in Fig. 5.9.

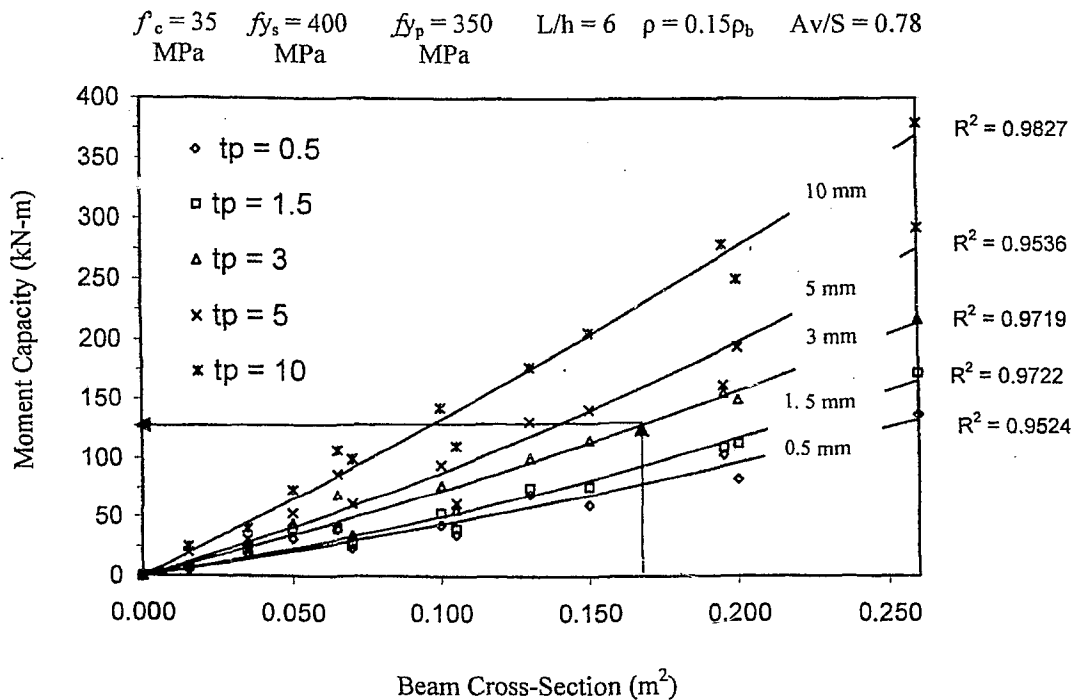


Fig. 5.9 Typical design chart showing prediction of moment capacity



The design chart has been established for a particular concrete cylinder strength  $f'_c$ , yield strength of steel reinforcement  $f_{ys}$ , yield strength of composite steel plate  $f_{yp}$ , length to depth ratio  $L/h$ , reinforcement ratio " $\rho$ " and thickness of steel plate  $t_p$  (shown on the chart). Design moments are expressed as a function of cross-sectional area of beams varying from 0 to  $0.25 \text{ m}^2$ . The combination of beam cross-section area and ratio of total length to depth ( $L/h$ ) helps the user to select  $b$  and  $h$  of the designed beam.

The geometrical properties and area of internal reinforcement are known for the case of an existing reinforced concrete beam to strengthen. Based on parameters mentioned on top of each design charts, a user can select appropriate design chart for a typical beam to be strengthened. The ultimate moment capacity can be determined by selecting the required steel plate thickness corresponding to the cross-sectional area of the beam using a trial and error analysis. The user must design the beam under study for shear prior to use the proposed design chart for the prediction of moment capacity.

#### **5.6. Performance Validation of Design Chart**

The performance of design charts in the prediction of moments is validated through further test results (Hossain 2001 and Nupiri 2000), results obtained from direct finite element analysis of experimental beams reported by Jim (1998) and various code based design procedures such as ACI (318-2002), CSA (1994), Australian Code (AS 3600-1988) and Euro Code-2 and are summarized in Table 5.3.

In addition to the eight beams having 0.4-mm thick steel plate tested by Jim (1999) and eight new experimental beams having 3-mm steel plate (Hossain 2001 and Nupiri 2000) are used to validate the performance of developed design charts. The description of all 16- beams is presented in Table 5.2. The use of design charts in predicting the moment capacity of beams strengthened with steel plates is illustrated in Figs. 5.10 to Fig. 5.25. Experimental moment capacities of such beams are also shown on the chart for comparative purpose.

Beam Designation	Material Properties			Beam Cross Section (b x h)	L / h	Av / S	% x ρ <sub>b</sub>
	$f_c$	$f_{ys}$	$f_{yp}$				
	MPa	MPa	MPa	mm			
Series -1 Beams							
S <sub>1</sub> B <sub>50</sub> - 0.4 mm	37.75	455	360	150 x 150	5	0.78	-
S <sub>1</sub> B <sub>100</sub> -0.4 mm	37.75	455	360	150 x 150	5	0.39	-
S <sub>1</sub> B <sub>150</sub> -0.4 mm	37.75	455	360	150 x 150	5	0.26	-
S <sub>1</sub> B <sub>180</sub> -0.4 mm	37.75	455	360	150 x 150	5	0.22	-
S <sub>1</sub> B <sub>50</sub> -3 mm	40.89	455	360	150 x 150	5	0.78	-
S <sub>1</sub> B <sub>100</sub> -3 mm	40.89	455	360	150 x 150	5	0.39	-
S <sub>1</sub> B <sub>150</sub> -3 mm	37.75	455	360	150 x 150	5	0.26	-
S <sub>1</sub> B <sub>180</sub> -3 mm	37.75	455	360	150 x 150	5	0.22	-
Series - 2 Beams							
S <sub>2</sub> B <sub>50</sub> -0.4 mm	37.75	455	360	150 x 150	5	0.78	0.21
S <sub>2</sub> B <sub>100</sub> -0.4 mm	37.75	455	360	150 x 150	5	0.39	0.21
S <sub>2</sub> B <sub>150</sub> -0.4 mm	37.75	455	360	150 x 150	5	0.26	0.21
S <sub>2</sub> B <sub>180</sub> -0.4 mm	37.75	455	360	150 x 150	5	0.22	0.21
S <sub>2</sub> B <sub>50</sub> -3 mm	38.76	455	366	150 x 150	5	0.78	0.20
S <sub>2</sub> B <sub>100</sub> -3 mm	38.76	455	366	150 x 150	5	0.39	0.20
S <sub>2</sub> B <sub>150</sub> -3 mm	38.89	455	366	150 x 150	5	0.26	0.21
S <sub>2</sub> B <sub>180</sub> -3 mm	38.4	455	366	150 x 150	5	0.22	0.21

Table 5.2 Properties of beam tested by Jim (1999) and Nupiri (2000)

In using Code based design procedures, the steel plated beams are idealized as reinforced concrete beams where the contribution of the steel plate is represented by tensile reinforcement together with internal longitudinal reinforcement. Detailed description of code based analysis is presented in Appendix B.

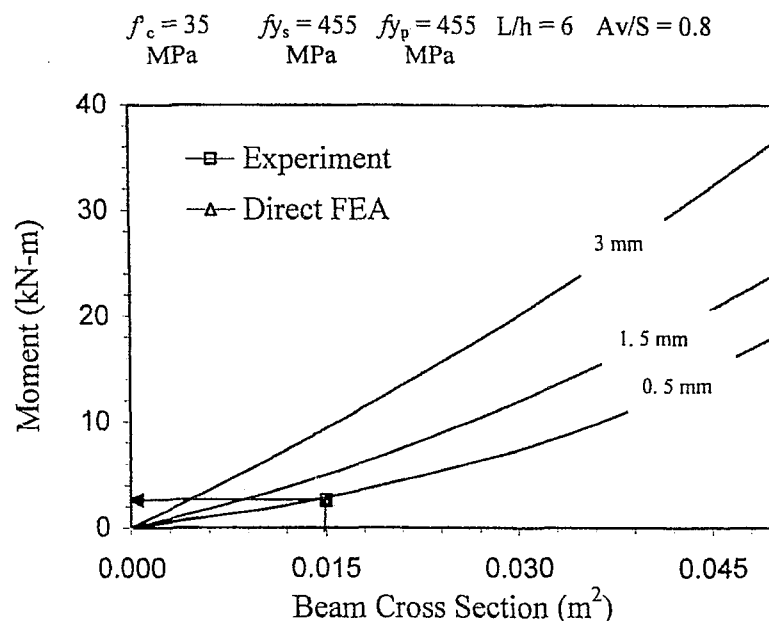


Fig. 5.10 Chart and F.E prediction of S<sub>1</sub>B<sub>50</sub>-0.4 mm Beam

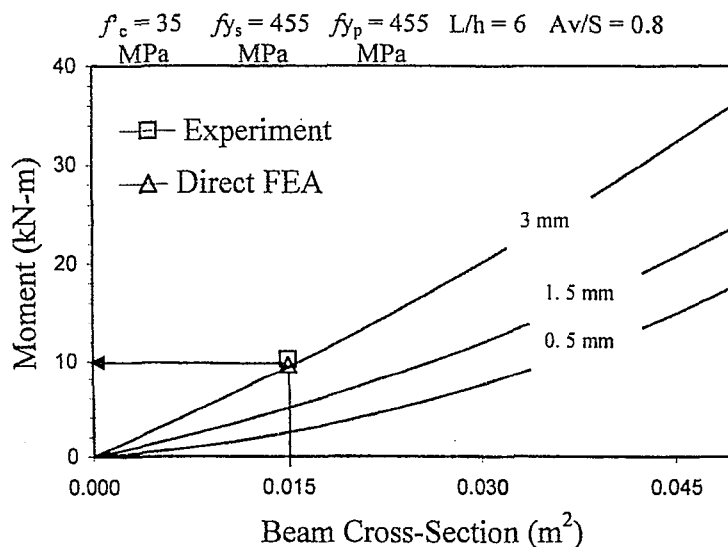


Fig. 5.11 Chart and F.E prediction of S<sub>1</sub>B<sub>50</sub>- 3 mm Beam

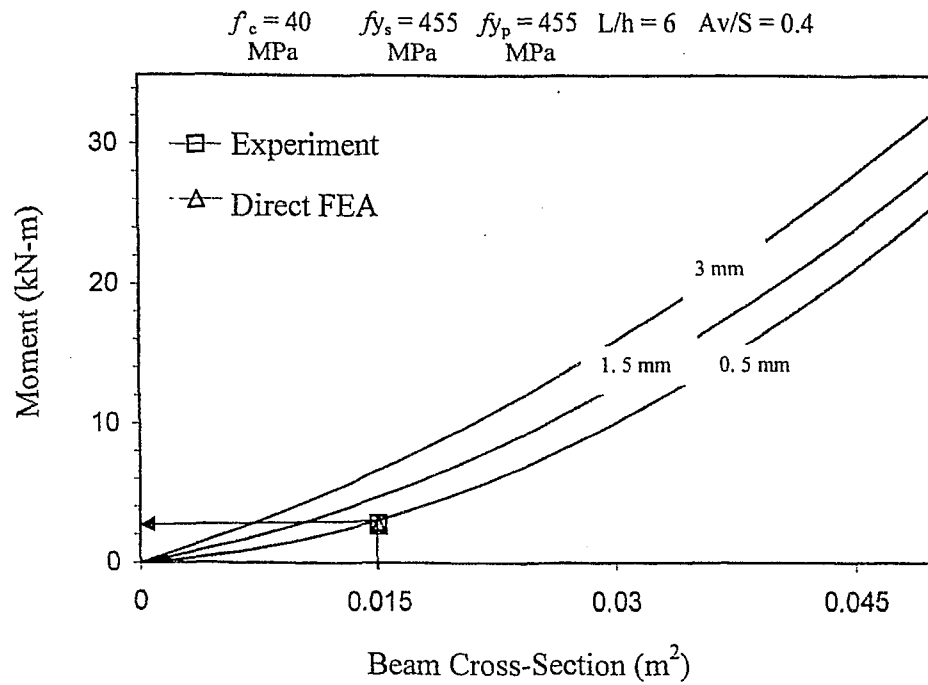


Fig. 5.12 Chart and F.E prediction of S<sub>1</sub>B<sub>100</sub>- 0.4 mm Beam

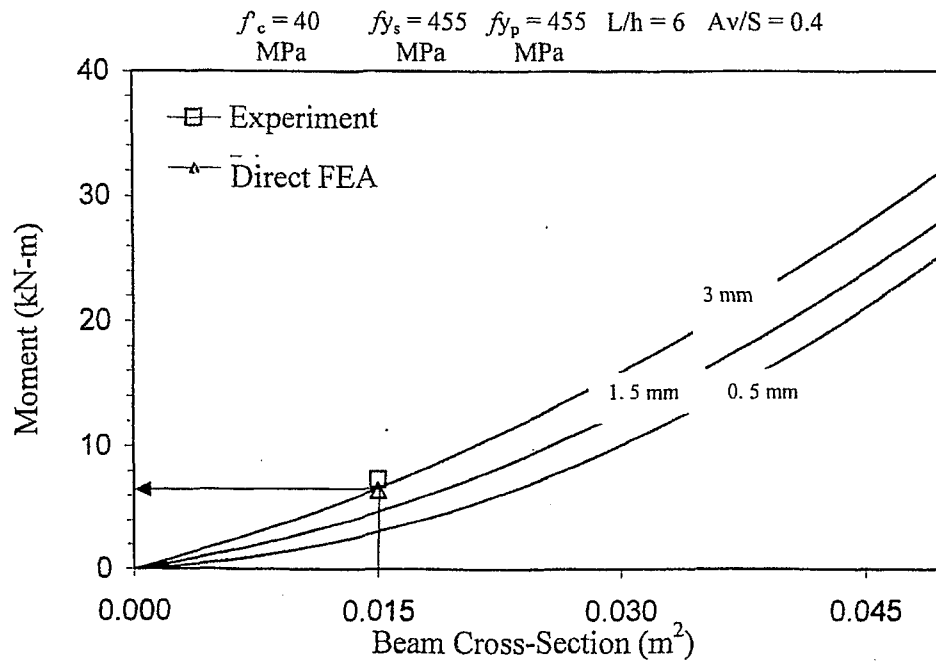


Fig. 5.13 Chart and F.E prediction of S<sub>1</sub>B<sub>100</sub>- 3 mm Beam

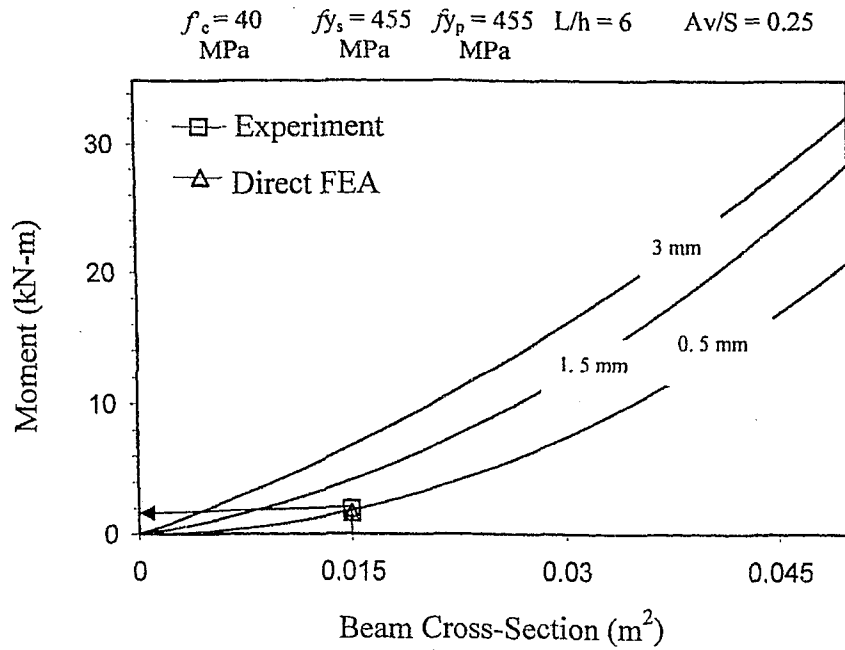


Fig. 5.14 Chart and F.E prediction of  $S_1B_{150}$  - 0.4 mm Beam

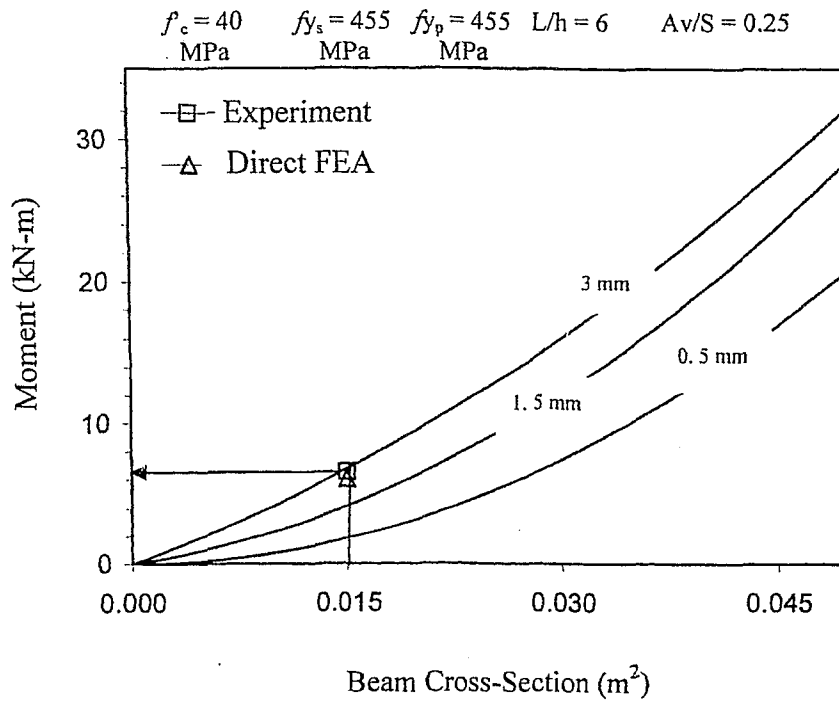


Fig. 5.15 Chart and F.E prediction of  $S_1B_{150}$  - 3 mm Beam

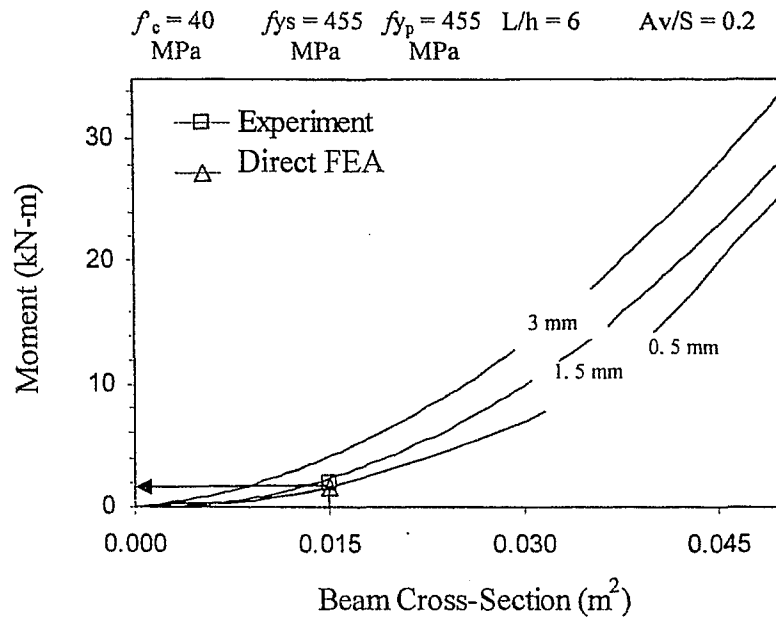


Fig. 5.16 Chart and F.E prediction of  $S_1B_{180}$  – 0.4 mm Beam

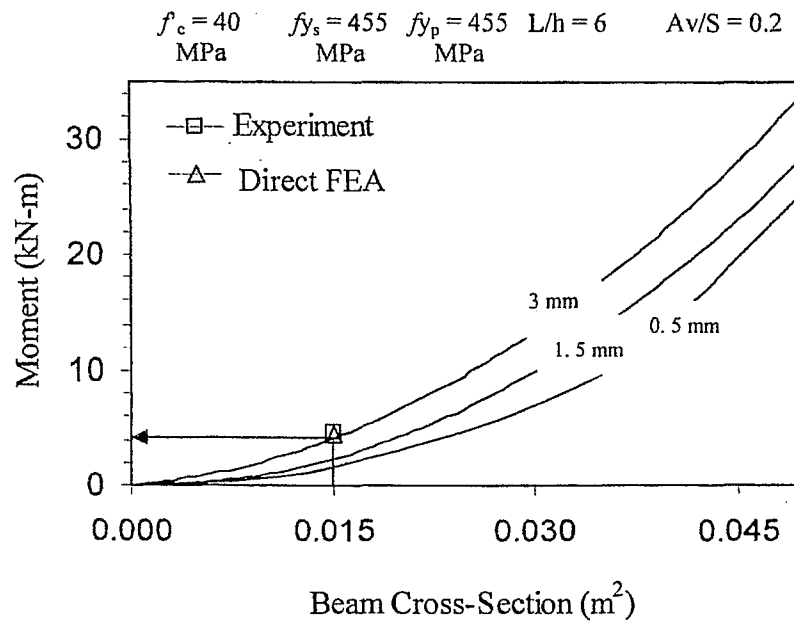


Fig. 5.17 Chart and F.E prediction of  $S_1B_{180}$  – 3 mm Beam

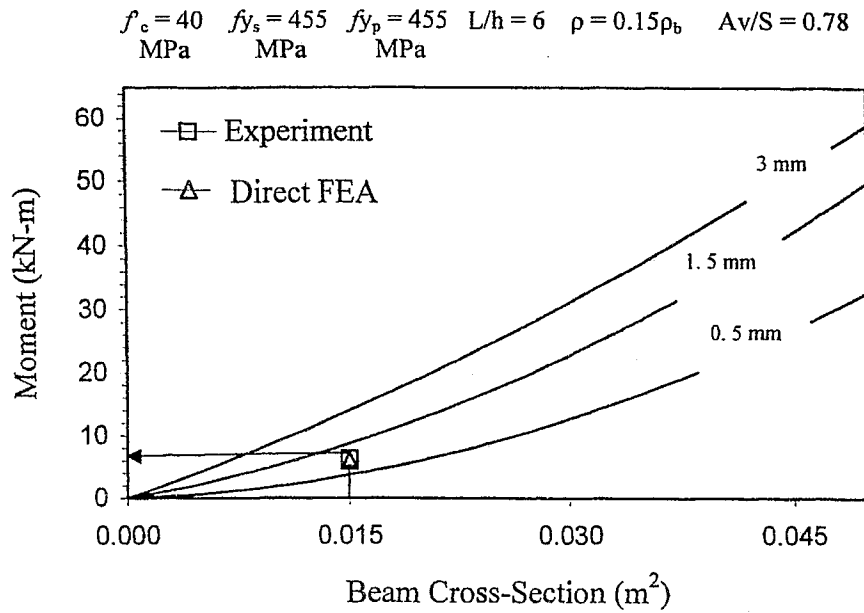


Fig. 5.18 Chart and F.E prediction of  $S_2B_{50} - 0.4$  mm Beam

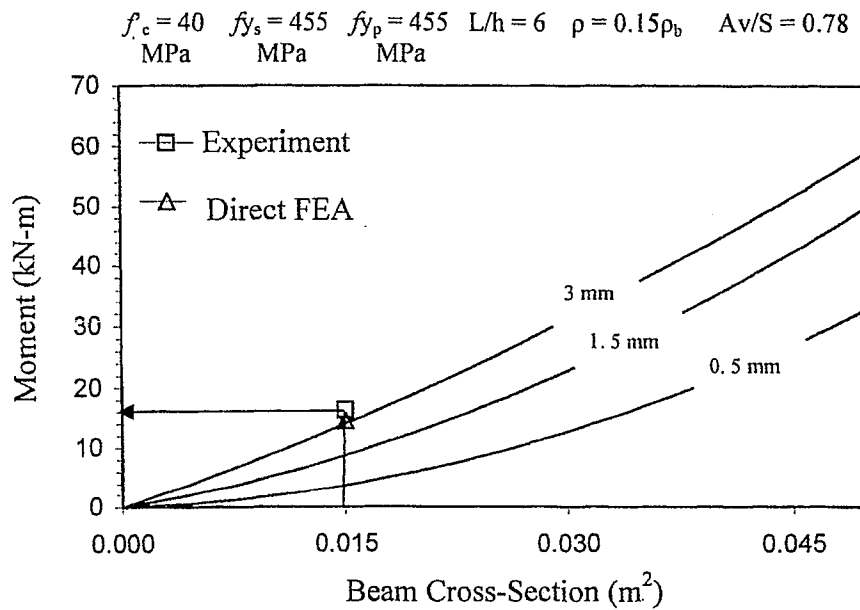


Fig. 5.19 Chart and F.E prediction of  $S_2B_{50} - 3$  mm Beam

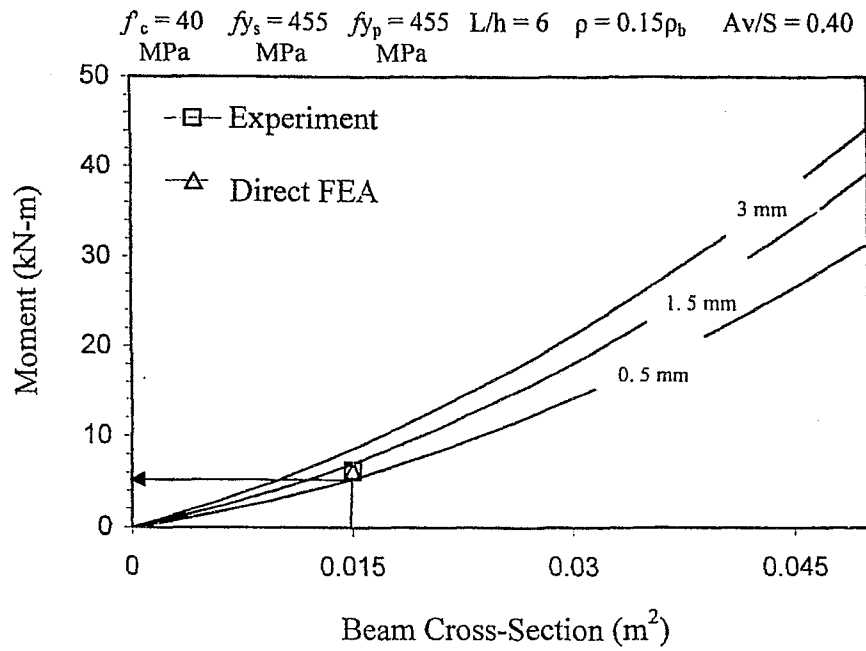


Fig. 5.20 Chart and F.E prediction of S<sub>2</sub>B<sub>100</sub> - 0.4 mm Beam

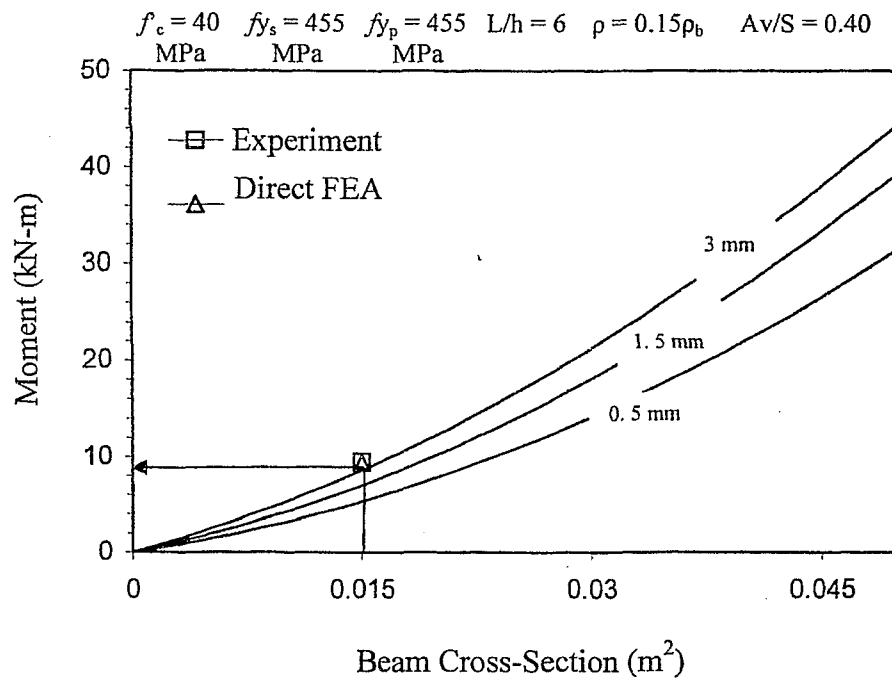


Fig. 5.21 Chart and F.E prediction of S<sub>2</sub>B<sub>100</sub> - 3 mm Beam



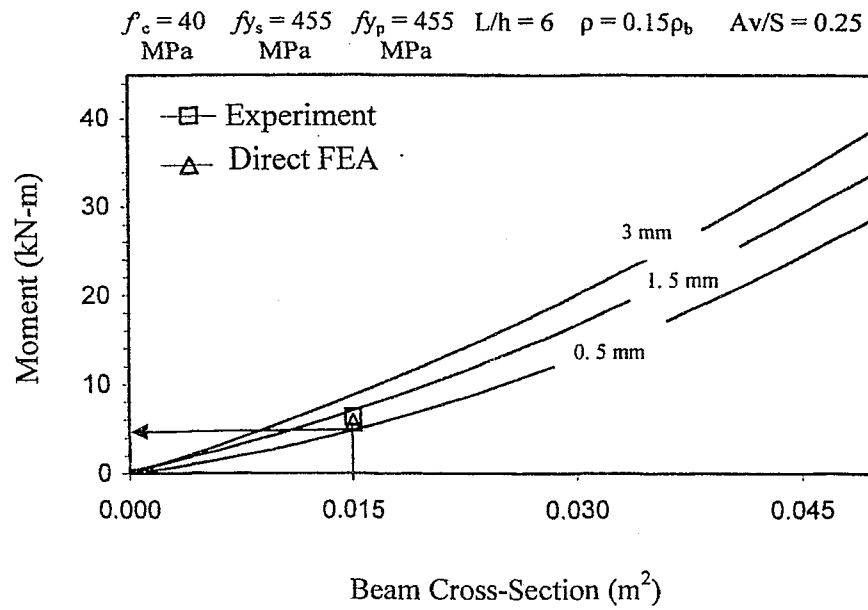


Fig. 5.22 Chart and F.E prediction of  $S_2B_{150} - 0.4$  mm Beam

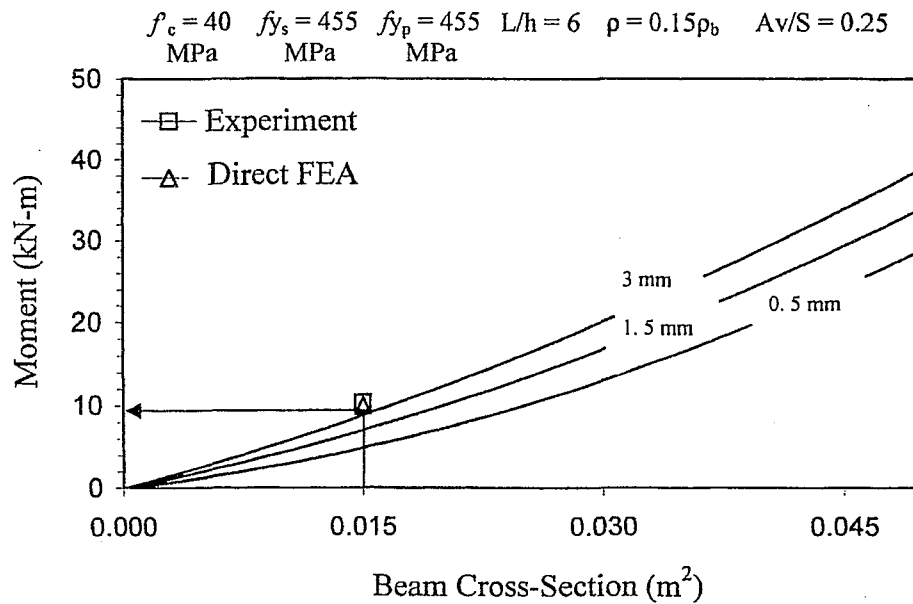


Fig. 5.23 Chart and F.E prediction of  $S_2B_{150} - 3$  mm Beam

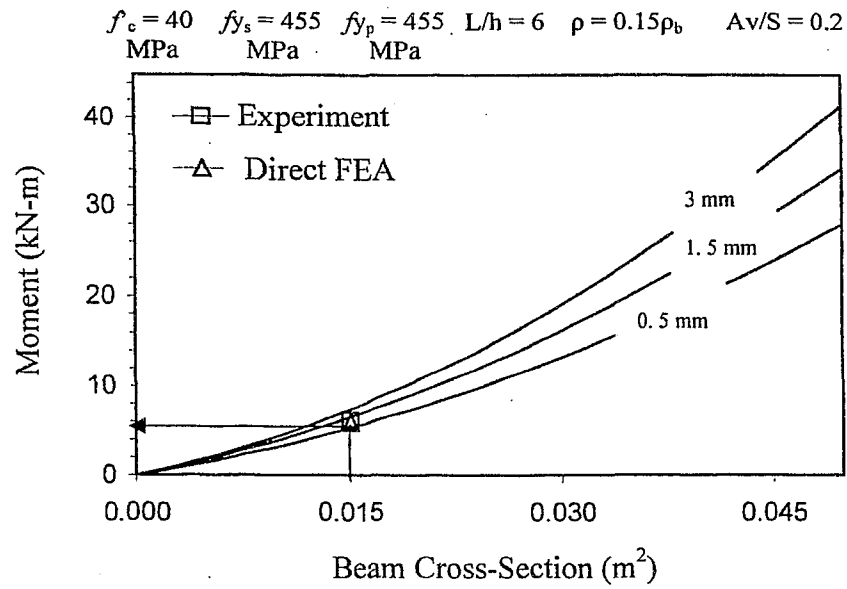


Fig. 5.24 Chart and F.E prediction of S<sub>2</sub>B<sub>180</sub> – 0.4 mm Beam

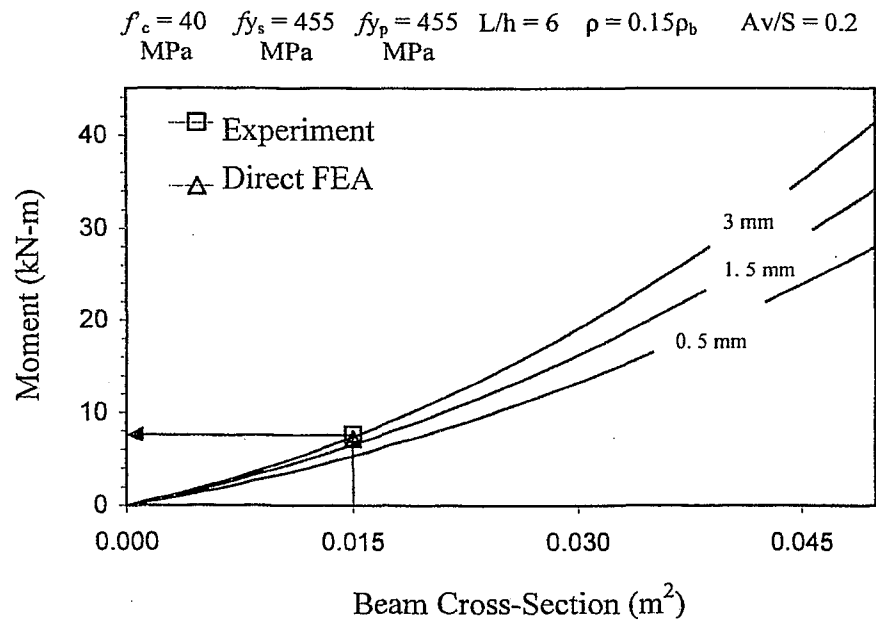


Fig. 5.25 Chart and F.E prediction of Beam S<sub>2</sub>B<sub>180</sub> – 3 mm Beam

Beam Designation	Moment Capacity						Euro Code 2	Comparative Study					
	Experiment	Direct FEA	Design Charts	CSA (1994)	ACI - 318	AUS- 3600		Chart/ FEA	Chart/ Exp.	CSA/ Exp.	ACI/ Exp.	AUS/ Exp.	EURO 2 /Exp.
	kN-m	kN-m	kN-m	kN-m	kN-m	kN-m		Ratio	Ratio	Ratio	Ratio	Ratio	Ratio
	(1)	(2)	(3)	(4)	(5)	(6)		(8)	(9)	(10)	(11)	(12)	(13)
S <sub>1</sub> B <sub>50</sub> - 0.4mm	2.64	2.54	2.50	2.13	2.12	2.12	2.13	0.98	0.95	0.81	0.80	0.80	0.81
S <sub>1</sub> B <sub>100</sub> - 0.4mm	2.80	2.64	2.60	2.13	2.12	2.12	2.13	0.98	0.93	0.76	0.76	0.76	0.76
S <sub>1</sub> B <sub>150</sub> - 0.4mm	1.93	1.60	1.55	2.13	2.12	2.12	2.13	0.97	0.80	1.10	1.10	1.10	1.10
S <sub>1</sub> B <sub>180</sub> - 0.4mm	1.97	1.66	1.75	2.13	2.12	2.12	2.13	1.05	0.89	1.08	1.08	1.08	1.08
S <sub>1</sub> B <sub>50</sub> - 3mm	10.2	-	9.75	14.76	14.48	14.70	14.57	-	0.96	1.45	1.42	1.44	1.43
S <sub>1</sub> B <sub>100</sub> - 3mm	7.33	-	6.50	14.76	14.48	14.70	14.57	-	0.89	2.01	1.98	2.01	1.99
S <sub>1</sub> B <sub>150</sub> - 3mm	6.55	-	6.25	14.76	14.48	14.55	14.57	-	0.95	2.25	2.21	2.22	2.22
S <sub>1</sub> B <sub>180</sub> - 3mm	4.61	-	4.60	14.76	14.48	14.55	14.57	-	1.00	3.20	3.14	3.16	3.16
S <sub>2</sub> B <sub>50</sub> - 0.4mm	6.33	6.06	* 6.25	4.67	4.48	4.53	3.96	1.03	0.99	0.74	0.71	0.72	0.63
S <sub>2</sub> B <sub>100</sub> - 0.4mm	6.27	6.18	* 6.00	4.67	4.48	4.53	3.96	0.97	0.96	0.74	0.71	0.72	0.63
S <sub>2</sub> B <sub>150</sub> - 0.4mm	6.33	5.73	* 5.75	4.67	4.48	4.53	3.96	1.00	0.91	0.74	0.71	0.72	0.63
S <sub>2</sub> B <sub>180</sub> - 0.4mm	6.13	5.88	* 5.50	4.67	4.48	4.53	3.96	0.94	0.90	0.76	0.73	0.74	0.65
S <sub>2</sub> B <sub>50</sub> - 3mm	16.34	-	* 14.50	17.20	17.02	17.47	16.32	-	0.89	1.05	1.04	1.07	1.00
S <sub>2</sub> B <sub>100</sub> - 3mm	9.53	-	* 9.25	17.20	17.02	17.94	16.32	-	0.97	1.80	1.79	1.88	1.71
S <sub>2</sub> B <sub>150</sub> - 3mm	10.27	-	* 9.25	17.20	17.02	17.44	16.32	-	0.90	1.67	1.66	1.70	1.59
S <sub>2</sub> B <sub>180</sub> - 3mm	7.67	-	* 7.25	17.20	17.02	17.92	16.32	-	0.95	2.24	2.22	2.34	2.13
Mean value	-	-	-	-	-	-	-	0.99	0.94	1.40	1.37	1.40	1.34
* Value calculated using linear interpolation between steel ratio "p" of 0.15 and 0.35 of balanced steel ratio "p <sub>b</sub> "													

Table 5.3 Comparative study with different methods of prediction

From Table 5.3, the ratio of chart prediction to direct finite element prediction is found in range between 0.94 and 1.03 with a mean value of 0.99 showing that the chart is as accurate as the finite element analysis. The ratio of chart prediction to experiments ranges between 0.80 and 1.00 with a mean value of 0.94 showing the accuracy of developed design charts.

Moreover, the code based design equations over predict the ultimate moment capacity of beams. From Table 5.3, the design procedure based on the Canadian Code over predicts the ultimate moment capacity for beams especially beams strengthened with thick plates. The Canadian codes prediction to experiment prediction is found to be in a range between 0.74 and 3.20 with a mean value of 1.40 showing that the predictions based on Canadian code over predict the ultimate moment capacity of the beams. The ACI code prediction to experiment prediction ranges between 0.71 and 3.14 with a mean value of 1.37 showing an over prediction when ACI code is used. The Australian code (AUS 3600, 1988) yields more or less the same mean value of 1.40, when compared with the experiments as shown in Table 5.3. Ratio of prediction based on European code (Euro-2) to experiment ranges between 0.71 to 3.16 with a mean value of 1.34.

Hence, it is clear that Code based design procedures are not suitable for the design of the proposed steel plated beams and proposed design charts are proved to be accurate in predicting the moment capacity of the proposed beams and can be used for design purposes.

### 5.7. Applicability of Design Charts for Beams with Different Strengthening Systems

These design charts can also be used to predict the flexural capacity of adhesively bonded steel plates provided that the failure of beams happen specifically in flexure either due to the crushing of concrete at the top or excessive yielding of steel plate. An attempt has been made to verify the performance of the proposed design charts in predicting the flexural capacity of adhesively bonded steel plated beams. For this purpose, experimental beams from Byung et al. (2003), Oehler (1992), Aprile et al. (2001), Hussain et al. (1995) and Ritchie et al. (1991) are selected. The detailed description of such experimental beams is presented in Table 5.4. All beams selected to compare the prediction based on design charts fails predominantly in flexure.

Two beams (S23 and S43S1) have been selected from the experiments done by Byung et al. (2003). Each beam had a cross-section area of 150 mm x 250 mm ( $0.038 \text{ m}^2$ ) with an effective length of 2.1 m. Two 16-mm diameter and two 13-mm diameter steel bars were provided as tensile longitudinal reinforcement at the bottom and top location respectively. External reinforcement in the form of 2-mm and 4-mm thick steel plates were attached using epoxy adhesive. 6-mm diameter steel bars uniformly spaced at 110 mm were provided for shear resistance. Details of material properties associated with the strength of concrete and steel are presented in Table 5.4.

From the experimental investigation done by Oehlers (1992), two beams (Beam 2/2/S and 2/4/S) have selected for prediction of moment capacity with the proposed design charts. The cross-section of beams was 130 mm x 175 mm ( $0.023 \text{ m}^2$ ) with length to

depth ratio of 8.4. These beams were reinforced for shear with 4-mm diameter of steel stirrups uniformly spaced at 75 mm and 45 mm respectively. 5-mm thick plate was attached on tension side of reinforced concrete beam. Longitudinal reinforcement was present in terms of a total steel area of  $402 \text{ mm}^2$  at the bottom and  $157 \text{ mm}^2$  at top of the beam. Material properties associated with concrete, rebars and steel plate are shown in Table 5.4.

One beam has been selected from the 14 reinforced concrete beams tested by Aprile et al. (2001). The beam had a cross-section dimension of 200 mm x 300 mm ( $0.06 \text{ m}^2$ ) with an effective length of 2.88 m. The beam was strengthened with 4-mm thick steel plate. The reinforcement ratio was fixed to be 0.56% of the balanced steel ratio. 6-mm diameter stirrups with a uniform spacing of 100 mm were provided as shear reinforcement. Details of material properties are presented in Table 5.4.

From the work done by Hussain et al. (1995), two beams (FBR2 and FBR3) are selected to test the predictions based on design charts. Each beam had a cross-section area of 150 mm x 150 mm ( $0.023 \text{ m}^2$ ) with an effective length of 1.2 m. 1-mm and 1.5-mm thick steel plate were attached to the concrete beams, using epoxy. A 4-mm diameter of steel bars was provided for shear resistance with a uniform spacing of 60 mm. Details of material properties are shown in Table 5.4.

One beam was selected from the experiments done by Riche in 1991. The beam had a cross-sectional area of 150 mm x 305 mm ( $0.464 \text{ m}^2$ ) with an effective length to depth

ratio of 9. Shear stirrups had a total area of  $99 \text{ mm}^2$  of steel uniformly spaced at 100 mm. The beam was singly reinforced with  $253 \text{ mm}^2$  of steel area provided at the bottom with 10 mm concrete cover. The steel plate used to enhance the strength was 2.6-mm thick. The details regarding the material properties are presented in Table 5.4.

References	Beam Specimen	Geometric data			Material Properties			Steel ratio % x pb	Av/S	Type of Failure (F or S)	Moment (Exp.) kN-m	Chart Prediction (kN-m)	Chart/ $M_{exp}$ ratio
		L/h ratio	b x h m	tp mm	$f'_c$ MPa	$f_{ys}$ MPa	$f_{yp}$ MPa						
(1)	(2)	(3)	(4)	(5)	(6)	(7)	(8)	(9)	(10)	(11)	(12)	(13)	(14)
Oh et al (2003)	S23	8.4	0.15 x 0.25	2	28.7	365	292	0.412	2.14	F	47.60	46.5	0.98
	S43S1	8.4	0.15 x 0.25	4	28.7	365	292	0.412	2.14	F	69.30	68.5	0.99
Oehlers (1992)	2/2/S	9	0.13 x 0.175	5	47	400	372	0.48	0.75	F	24.09	24	1.00
	2/4/S	9	0.13 x 0.175	5	47	400	372	0.48	1.25	F	25.00	25	1.00
Aprile et al. (2001)	-	9.5	0.20 x 0.30	4	30	460	360	0.33	0.5	F	62.00	68	1.10
Hussain et al.	FBR2	8	0.15 x 0.15	1	31	414	269	0.28	1.88	F	13.92	12.5	0.90
	FBR3	8	0.15 x 0.15	1.5	31	414	269	0.28	1.88	S/F	15.00	14	0.93
Ritchie et al. (1991)	O	9	0.15 x 0.305	2.5	43.5	414	200	0.17	0.97	F	42.70	40	0.94
Mean value													0.97
Where type of failure, F and S, correspond to flexure failure and shear failure respectively.													

Table 5.4 Predicted strength for epoxy bonded steel plated beams with design charts

Prediction of flexural capacity of such beams using proposed design charts superimposed by experimental values is illustrated in Figs. 5.26 to Fig. 5.33, and summarized in Table 5.4. The ratio of experimental to predicted values ranges between 0.90 and 1.10 with a mean value of 0.97, which shows a close agreement.

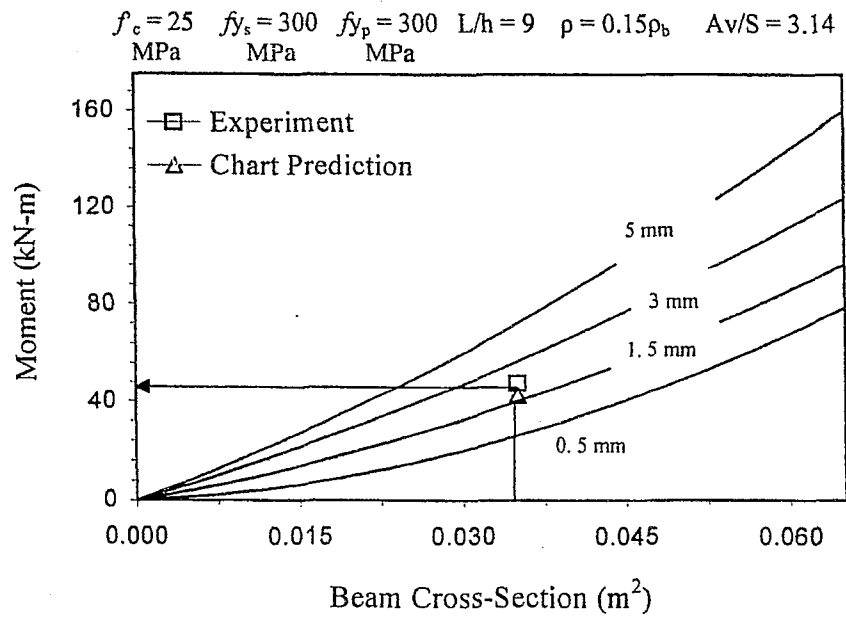


Fig. 5.26 Chart and experimental prediction for S23 beam (Byung et al. 2003)

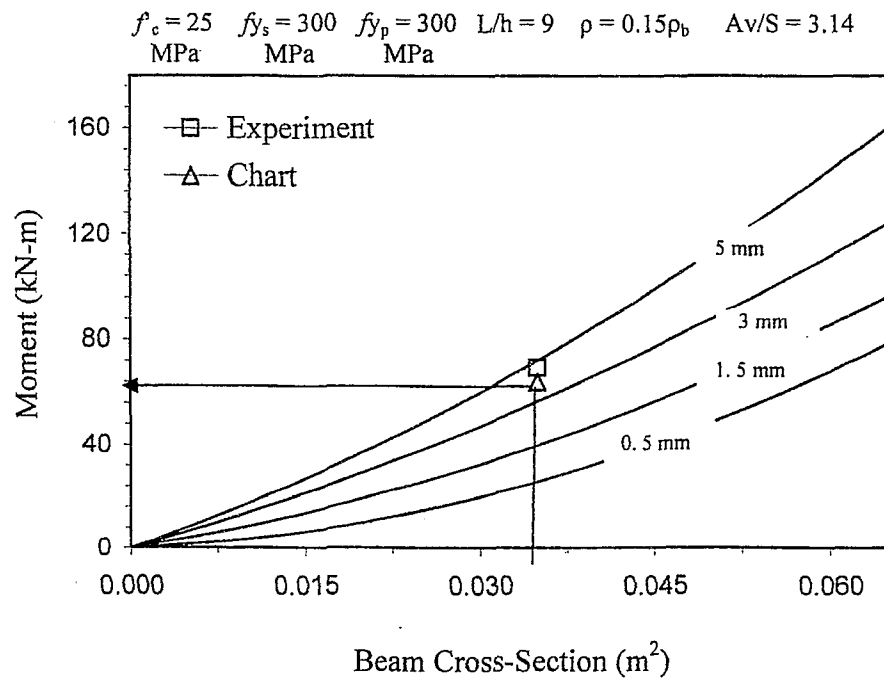


Fig. 5.27 Chart and experimental prediction for S43S1 beam (Byung et al. 2003)



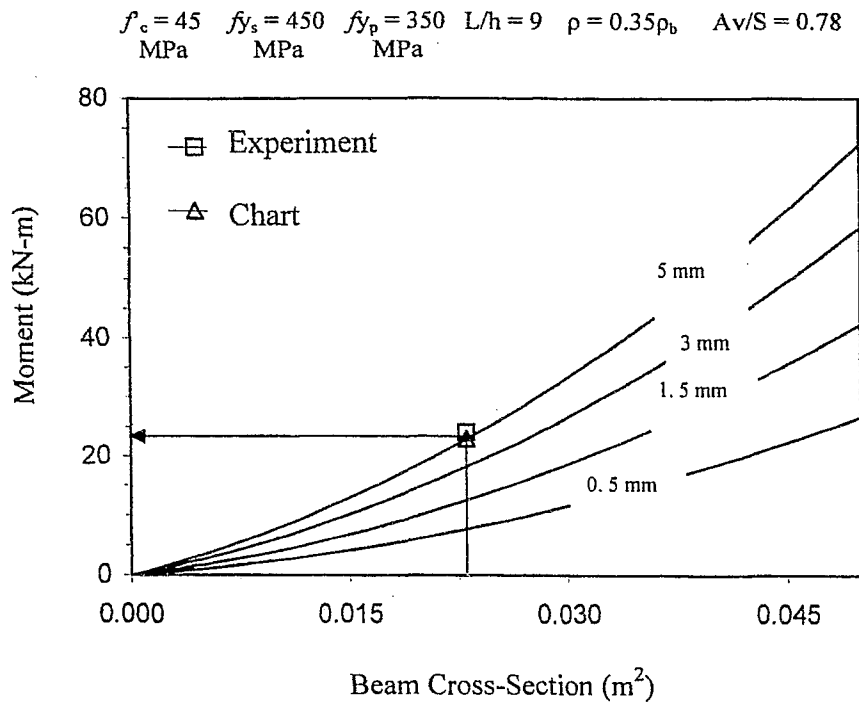


Fig. 5.28 Chart and experimental prediction for 2/2/S beam (Oehlers 1992)

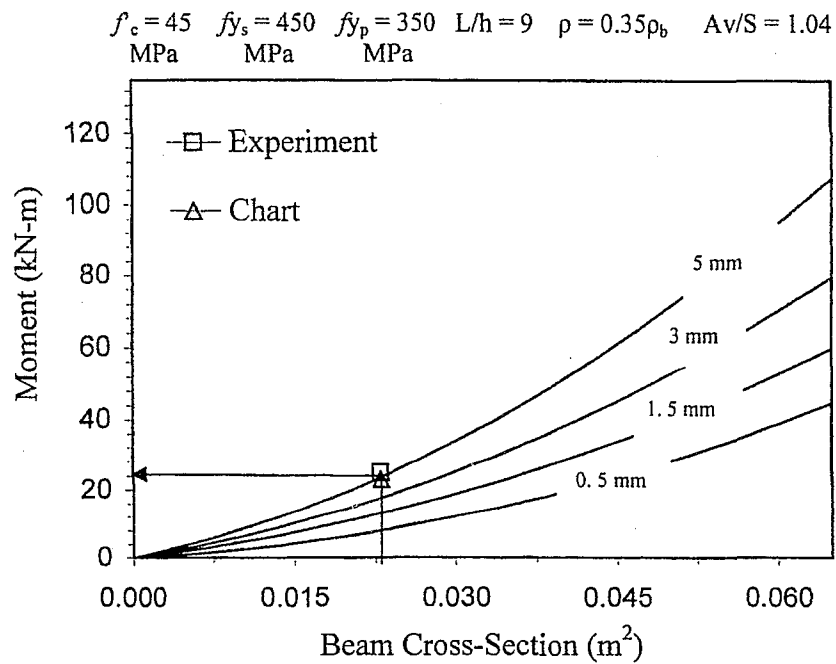


Fig. 5.29 Chart and experimental prediction for 2/4/S beam (Oehler 1992)

$$f'_c = 35 \text{ MPa} \quad f_{ys} = 450 \text{ MPa} \quad f_{yp} = 350 \text{ MPa} \quad L/h = 9 \quad \rho = 0.35\rho_b \quad A_v/S = 0.78$$

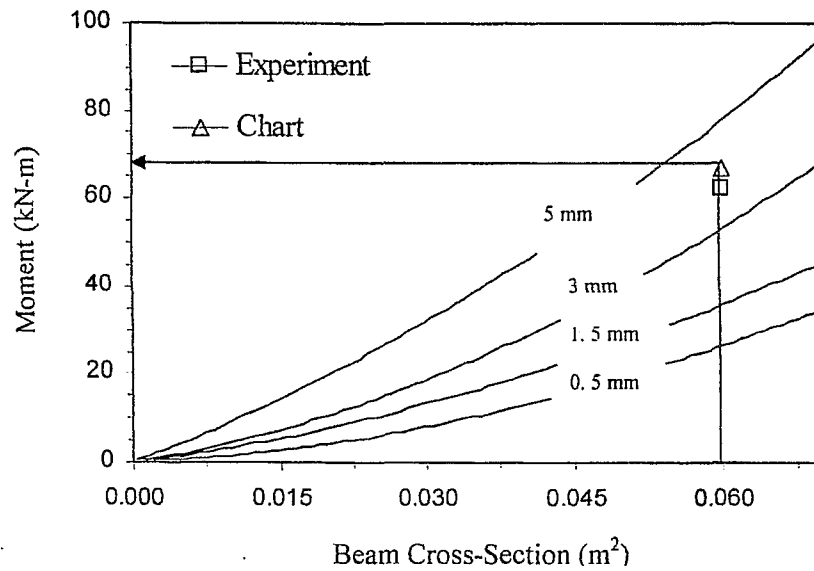


Fig. 5.30 Chart and experimental prediction for beam (Aprile et al. 2001)

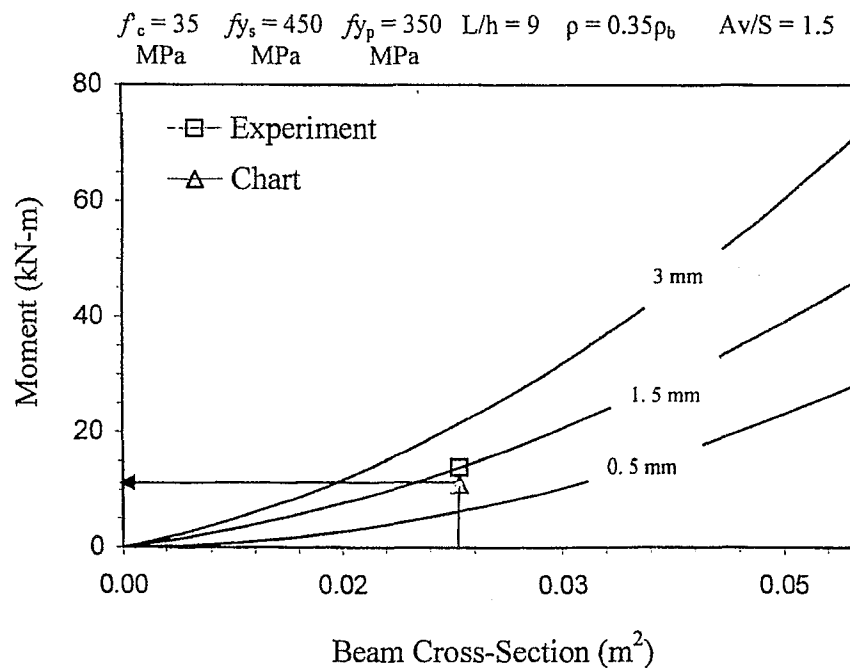


Fig. 5.31 Chart and experimental prediction for FBR2 beam (Hussain et al. 1995)

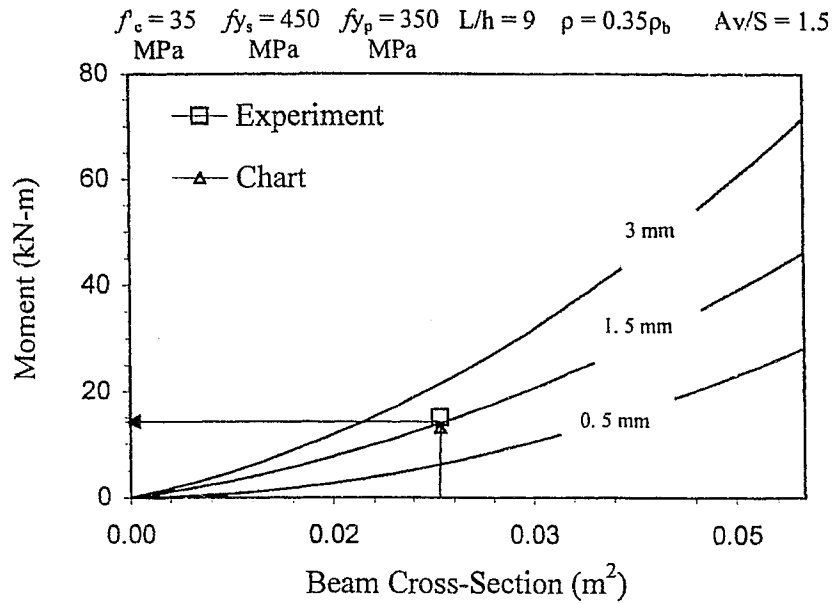


Fig. 5.32 Chart and experimental prediction for FBR3 beam (Hussain et al. 1995)

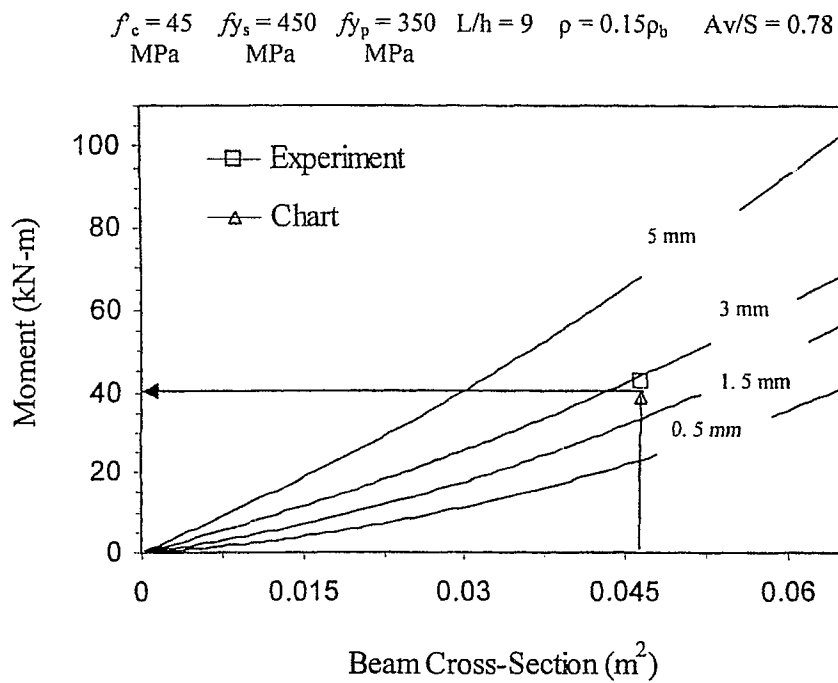


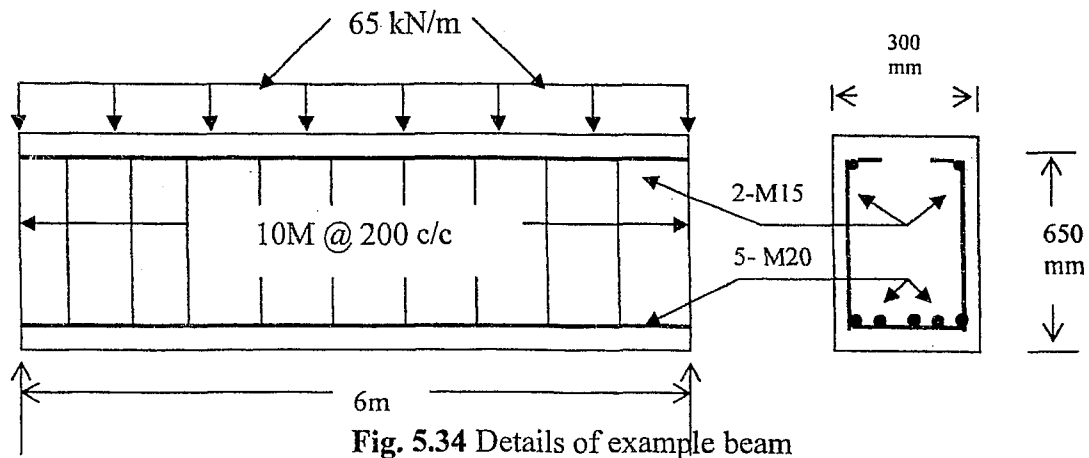
Fig. 5.33 Chart and experimental prediction for O beam (Ritchie et al. 1991)

All experimental beams summarized in Table 5.4, fails primarily in flexure and it is found that the moment capacity of such beams can be safely predicted using proposed design chart presented in Appendix C.

However, the proposed design charts should be used with caution and is not recommended for the design of all such beams. Engineers must rely on their experience and judgement before using the proposed design charts for the prediction of such composite beams. However, these design charts can be used in preliminary design to have an idea of the moment capacity before final design.

#### **5.8. Use of Proposed Design Charts – Design Example**

Let us consider, a simply supported existing deteriorated beam having a cross sectional area of 300 mm x 650 mm carrying a uniformly distributed load of 65 kN/m over its entire length of 6 m. Top bars consist of 2 - M15 steel bars while bottom bars consist of 5 - M20 bars (Fig. 5.34). A uniformly spaced 10M stirrups at 200 mm was provided to increase the shear resistance capacity of the beam. There is a loss of about 15% of the internal longitudinal reinforcement areas due to corrosion. This beam requires strengthening in order to take a load, which is 35% more than the existing load and the proposed mechanically bonded steel plate technique is chosen to retrofit beam. The compressive strength of concrete is found to be 38 MPa and yield strength of steel is 435 MPa.



**Solution:**

### Step 1: Calculation of Moment Capacity

The moment for which the beam was designed =  $M_{\max} = \frac{65 \times (6)^2}{8} = 292 \text{ kN-m}$

The balanced steel ratio =  $\rho_b = 0.026$  (CSA 1994)

Actual steel ratio of existing beam with respect to the cross-section area =  $\rho = 0.009$

Since  $\rho < \rho_b$  – beam was designed as an under reinforced beam

The resisting moment (before loss in internal steel) = 333 kN-m (CSA 1994)

The residual moment of resistance (after corrosion result in loss of steel area)

=  $M_{re} = 280 \text{ kN-m}$

Hence, this beam is critical even for existing load carrying capacity, which requires immediate strengthening either to resist the existing load or the load, specified in this example.

The moment for which the beam is to be strengthened =  $1.35 \times 292 = 394 \text{ kN-m}$ .

## Step 2: Selection of Appropriate Design Chart

In order to use design charts, the following parameter should be determined first.

- Existing beam should be checked for shear (in order to minimize the risk of brittle shear failure after strengthening) prior to obtaining ultimate moment capacity from proposed design chart.
- Ratio of existing length to total depth of the beam ( $L/h$ ),
- Cross-sectional area of reinforced concrete beam ( $b \times h$ ),
- Compressive strength of concrete ( $f'_c$ ),
- Yield strength of steel ( $f_{ys}$ ),
- Yield strength of steel plate to be provided for strengthening of existing member ( $f_{yp}$ ),
- Existing steel ratio ( $\rho$ ),
- Ratio of steel area of stirrups to spacing of stirrups.

For the given beam, these parameters are calculated as follows:

Compressive strength of concrete:  $f'_c = 38$  (MPa)

Yield strength of reinforcement:  $f_{ys} = 433$  (MPa)

Assumed yield strength of steel plate:  $f_{yp} = 350$  (MPa)

Length-to-depth ratio:  $L/h = 9.23$  (ratio)

Cross-sectional area:  $b \times h = 0.195$  ( $\text{m}^2$ )

Steel ratio of reinforced concrete beam w/o steel plate:  $\rho = 0.35\%$  (ratio)

Shear resistant factor:  $A_v/S = 0.5$  (ratio)

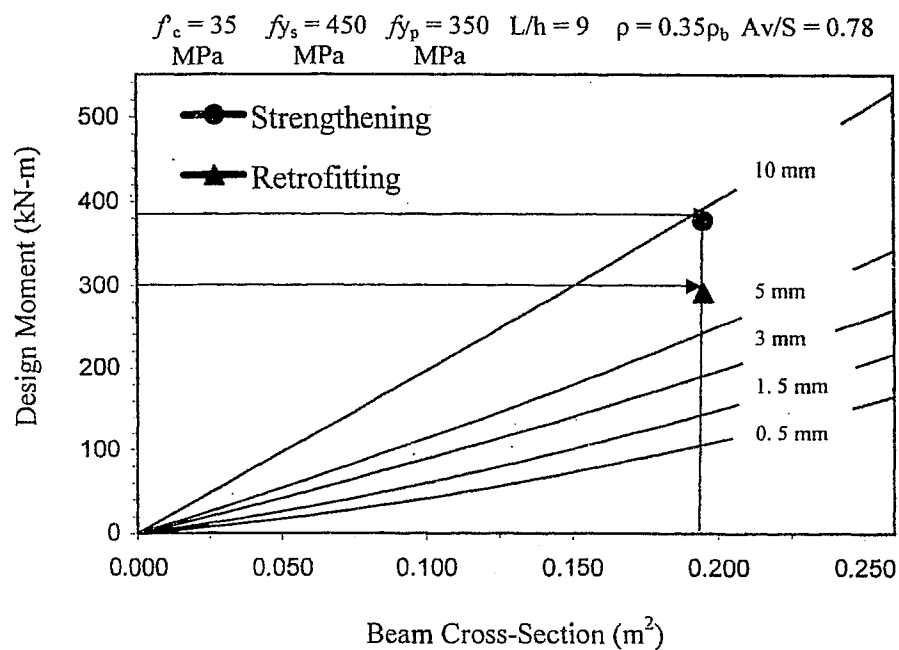


Fig. 5.35 Typical chart selected for design example

For strengthening purpose, the user can select a specific design chart for strengthening a typical example beam. Given the cross-section area ( $0.195 \text{ m}^2$ ) of the beam and the moment required after strengthening ( $394 \text{ kN-m}$ ), the required thickness of steel plate can be obtain at the intersection of both x and y-axis.

In the case of the existing beam, a 10-mm thick steel plate corresponding to a ultimate moment capacity of 400 kN-m has been chosen to resist an increased upcoming service load, which is 35% greater than the existing load. For retrofitting, a 8-mm thick steel plate can be selected as it yields an ultimate moment capacity of 300 kN-m, which is slightly greater than the moment for which beam was designed. A schematic representation of strengthened beam is shown in Fig. 5.35.

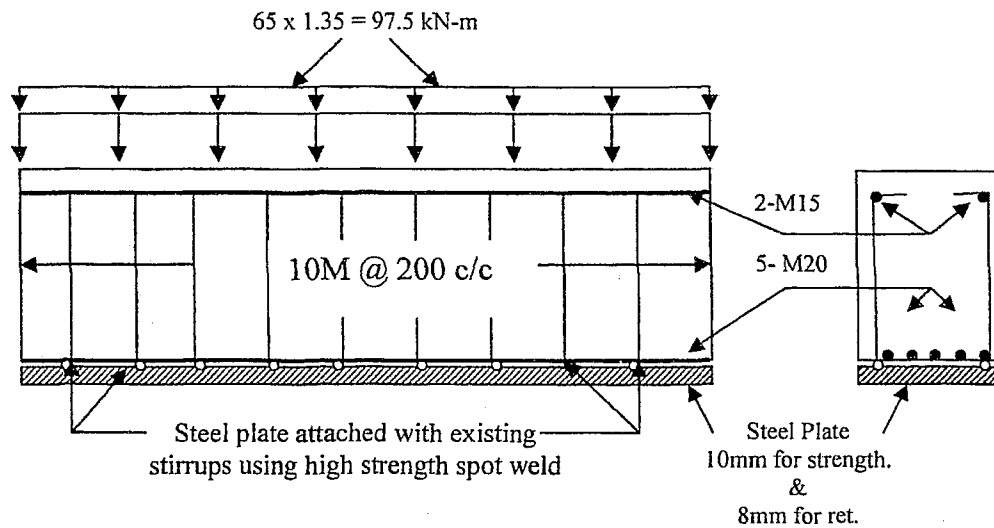


Fig. 5.36 Schematic of strengthened example beam



## Chapter 6      Conclusions and Recommendations

### 6.1.    Summary of Research Effort

An innovative technique of strengthening reinforced concrete members with mechanically bonded steel plate using welded connection has been presented in this research.

Based on the experimental investigation performed by other researchers, a finite element study was performed using the finite element software, *ABAQUS*. An attempt has been made to develop a finite element model that can simulate the behavior of experimented beams. Once the finite element model is developed and its performance is validated, it has been used to generate design charts to predict the ultimate moment capacity of strengthened beams.

The performance validation of these design charts has been presented by comparing their prediction to the results of a number of experimental investigations. Performance validation shows that these design charts can be helpful to predict the ultimate moment capacity of strengthened beams. Prevailing codes do not show good co-relation with the experimental results.

Another worth noted-advantage of these design charts is its utilization under different connection systems, such as adhesively bonded connection system provided that the mode of failure is ductile. These design charts proved to be a reasonable source of strength

prediction for other type of bonding systems. Practical implementation of such a system has also been emphasized in this study. Hence in this way the desired objectives of this research discussed earlier has been achieved.

## 6.2. Conclusions

The following conclusions were drawn from the present study:

- The proposed method of strengthening reinforced concrete beams using mechanically bonded steel plates has proved to be a cost effective and quick solution for enhancing the flexure capacity of deteriorated beams.
- Material properties associated with concrete ( $f'_c$ ), steel reinforcement ( $f_y$ ,  $f_p$ ), steel ratio ( $\rho$ ), stirrups spacing ( $S$ ), and geometric characteristics ( $b$ ,  $h$ ,  $L$ ) have a great influence on the strength of such systems.
- Finite-element analyses using developed finite element model to predict the behavior of such mechanical strengthened beams shows good correlation with the experimental results and FE model can be used to simulate the behavior of such system.
- Comparative studies show that the developed design charts obtained from comprehensive simulation of a large number of numerical beams, are as accurate as direct finite element analysis. Design charts can predict the flexural capacity of proposed steel plated beams with an accuracy of 97% compared with the experimental results.
- The proposed "Design Charts" proved to be a quick, efficient and cost effective solution for pre-designing and analyzing beams with mechanically bonded strengthening systems in practical applications.

### **6.3. Suggestion for Further Research**

Further research can be done in the following areas:

- The behavior of mechanically bonded beams should be analyzed by welding steel plate inside the stirrups at the bottom.
- Further experiment can be done to predict the ultimate flexural capacity of such novel form beams under cyclic and fatigue loading.
- As experiments have been done on a small scale to testify the mechanical strengthening procedures, the technique of welding steel plate to strengthen existing beams should be implemented in the field to analyze the behavior of strengthened beam under practical conditions.
- Feed back should be obtained from the construction industry to marketize this novel form strengthening technique.

## REFERENCES

- Abaqus users manual Volume I, version 6.4.1 (2004), Hibbitt, Karlsson & Sorensen, Inc., 1080 Main Street, Pawtucket, R.I. 02860-4847, USA, <http://www.abaqus.com>.
- Abaqus users manual Volume II, version 6.4.1 (2004), Hibbitt, Karlsson & Sorensen, Inc., 1080 Main Street, Pawtucket, R.I. 02860-4847, USA, <http://www.abaqus.com>.
- Abaqus users manual Volume III, version 6.4.1 (2004), Hibbitt, Karlsson & Sorensen, Inc., 1080 Main Street, Pawtucket, R.I. 02860-4847, USA, <http://www.abaqus.com>.
- ACI (2002), "*Building Code Requirements for Reinforced Concrete*", ACI Committee 318, ACI, Detroit, 111pp.
- Ali, M., Oehler, D.J., and Sung-Moo, P., (2001), "*Comparison of steel plating and FRP plating of reinforced concrete beams*", Composites Part A: Applied Science and Manufacturing, May, 32, pp. 1319-1328.
- Ali, M., and Oehlers, D.J., (2003), "*Strengthening of Reinforced Concrete Bridges by External Plates*", Technical Paper published in 62<sup>nd</sup> session at Kochi, Paper No. 476, pp 1-18.
- Ali, M., and Oehlers, D.J., (2003), "*Strengthening of reinforced concrete bridges by external plates*", Technical Paper, Volume 62-2/476, Indian Roads Congress.
- Aprile, A., Spacone, E., and Limkatanyu, S., (2001), "*Role of bond in RC beams strengthening with steel and FRP plates*", Journal of Structural Engineering, ASCE, 127(12), pp 1445-1452.
- Basker, K., Shanmugam, N.E., and Thevendran, V., (2002), "*Finite element analysis of steel-concrete composite plate girder*", Journal of Structural Engineering, September, pp. 1158-1168]

- Bonaci, J.F, and Maalej, M., (2000), "*Externally bonded FRP for service life extension of reinforced concrete infrastructures*", Journal of Infrastructure Systems, ASCE, 6(1), pp 41-51.
- Chajes, M., Finch, W.W., Januszka, T.F., and Thomson, T.A., (1996), "*Bond and force transfer of composite material plates bonded to concrete*", ACI Structural Journal, 93(2), pp 208-217.
- Chajes, M., Thomson, T., and Finch, W., (1994), "*Flexural strengthening of concrete using externally bonded composites materials*", Construction and Building Material, 8(3), pp 191-201.
- CSA, Canadian Standard Association (1994), "*Design of concrete structures (A23.3-94)*", CSA International, Rexdale, Ont. Canada.
- Famiyesin, O.O.R, Hossain, K.M.A., Chia, Y.H., and Slade P.A., (2001), "*Numerical and analytical predictions of the limit load of rectangular two way slabs*", Computers & Structures Journal, 79 (2001), pp. 43-52, Pergamon press, Elsevier Science Ltd.
- Famiyesin, O.O.R and Hossain, K.M.A, (1998a), "*Development of charts for partially clamped slabs by finite element predictions*", Journal of Structural Engineering, ASCE, Vol. 124, No. 11, November, pp. 1339-1349.
- Famiyesin, O.O.R., and Hossain, K.M.A., (1998b), "*Optimized Design Charts for fully restrained slabs by FE predictions*", , Journal of Structural Engineering, ASCE, Vol. 124, No. 5, May, pp. 560-569.
- Foley, C.H., and Buckhouse, E.R., (1999), "*Method of increasing the capacity and stiffness of reinforced concrete beams*", Practice Periodicals on Structural Design and Construction, February, pp 36-42.
- Garden, H.N., and Hollaway, L.C., (1998), "*An experimental study of the influence of the plate end anchorage of carbon fiber composites plates used to strengthened reinforced concrete beams*", Elsevier, Composite Structures, 42, pp. 175-188.

- Hamoush, S.A., and Ahmad, S.H., (1990), "*Debonding of steel plate-strengthened concrete beams*", Journal of Structural Engineering, ASCE, 116(2), pp 356-371.
- Hermite, L', R., and Bresson, J., (1967), "*Beton arms d'armatures colles*", RILEM colloque International, themr 2, Paris, September.
- Hossain, K.M.A., (1999), "*Strengthening of Beam with mechanically bonded thin steel plate*", Proc. 6<sup>th</sup> International conference on Structural failure, durability and retrofitting, ICSF, pp. 338-396.
- Hossain, K.M.A., (2001), "*Experimental Investigation on Beams with Mechanically Bonded Steel Plate as Tensile Reinforcement*" Research Report no. CE-SE-2001-2, University of Technology, Papua New Guinea, 120 pages.
- Hui-Shen, Teng, J.G., and Yang, J., (2001), "*Interfacial stresses in beams and slab bonded with thin plate*", Journal of Engineering Mechanics, ASCE, 127 (4), pp 399-406.
- Hussain, M., Alfarabi S., Basunbul I.A., Baluch, M.H., and Sulaimani, G.J., (1995), "*Flexure behavior of pre-cracked beams strengthened externally by steel plate*", ACI Structural Journal, 92(1), January-February, pp 15-22.
- ISIS Canada (1997), "*Innovator*", Newsletter of the Canadian Network of Centers of Excellence on Intelligent Sensing for Innovative Structures, April.
- Jim, J., (1999), "*Strengthening of building or bridge girders using mechanically bonded steel plate-Part-1*", B.Eng. Thesis, Dept. of Civil Engineering, University of Technology, Lae, Papua New Guinea, pp. 120pp.
- Jones, P., Swamy, R.N., and Charif, A., (1988), "*Plate Separation and anchorage of reinforced concrete beams strengthened by epoxy-bonded-steel plates*", The Structural Engineer, 66 (5), 85-94.

- Kabhari, V.M., Engineer, M.M., and Eckel, D.A., (1997), "*On durability of composites rehabilitation schemes for concrete: Use of peel test*" Journal of Material and Science, 32(1), pp 147-156.
- Kachlakev, D., and McCurry, D.D., (2000), "*Behavior of full-scale reinforced concrete beams retrofitted for shear and flexural with FRP laminates*", Composite Engineering Part B, Elsevier, 31,445-452.
- Karbhari, V.M., Chin, J.W., Hunston, D., Benmokrane, B., Juska, T., Morgan, R., Lesko, J.J., Sorathia, U., and Reynaud, D., (2003), "*Gap analysis for durability of fiber reinforced polymer composites in civil engineering structures*", Journal of composites for construction, ASCE, August, pp. 238-247.
- Kashif, S.A., Hossain, K. M.A., and Lachemi, M., (2004), "*Investigations on reinforced concrete beams with mechanically bonded steel plate*", 5th Structural Specialty Conference of the Canadian Society for Civil Engineering, ST-157, June 2- June 5, pp. ST-157-1- to-10, Saskatoon, Saskatchewan, Canada.
- Kountouris, G., (1990), "*Design charts for double skin composite elements, Dissertation*", University of Wales College of Cardiff, April.
- Kraker, A., Tichler, J.W., and Vrouwenvelder, A.C.W.M., (1982), "*Safety, reliability and service life of the structures*", Publication in Heron (Alexandria), Vol. 27, No.1, pp. 1-85.
- MacDonald, M.D., (1978), "*The flexural behavior of concrete beams with bonded external reinforcement*", Transport and Road research Laboratory supplementary report 415, Crowthorne, England.
- MacGregor, J.G., and Barlett, F.M., (2000), "*Reinforced Concrete: Mechanics and Design*", ISBN 0-13-101403-2000, Prentice Hall, Canada.
- Marco, A., and Nanni, A., (1997), "*Parametric study of beams with externally bonded FRP reinforcement*", ACI Structural Journal, Title No. 94-S45, September- October, pp. 493-501.

- Mays, G.C., and Smith, D.W., (1980), "*Slab of the future*", Concrete, pp-13-16, June.
- Mirza, S., and Lounis, Z., (2003), "*Durability design of concrete structures*", Journal of Civil Engineering, No. 238, January, pp. 1-34.
- Mukhopadhyaya, P., and Swamy, N., (2001), "*Interface shear stress: A new design criterion for plate debonding*", Journal of composite for construction, ASCE, 5(1), pp 35- 43.
- Narayan, N., Wright, H.D., Evans, H.R., and Francies, R.W., (1987), "*Double skin composite construction for submerged tube tunnels*", Steel Construction Today, 1, pp.187-189.
- Neale, K. W., (2001), "*Strengthening reinforced concrete structures with externally-bonded fiber reinforced polymers*", Design Manual No.4, September, ISIS Canada.
- Nethercot, D.A., and Ahmed, B., (1996), "*Numerical modeling of composite connections and composite frames*", Composite Construction in Steel and Concrete-III, Proc., Engineering Foundation Conf., ASCE, New York, pp 809-822.
- Nupiri, P., (2000), "*Strengthening of building or bridge girders using mechanically bonded steel plate- Part II*", B.Eng. Thesis, Dept. of Civil Engineering , University of Technology, Lae, Papua New Guinea, pp. 120pp.
- Oduyemi, T.O.W., and Wright, H.D, (1989), "*The behavior of double skin composite columns*", Report DS2, University of Wales College of Cardiff.
- Oduyemi, T.O.W., and Wright, H.D., (1990), "*The behavior of double skin composite beam-columns*", Report DS3, University of Wales College of Cardiff.
- Oehler, D.J., (1992), "*Reinforced concrete beams with plate glued to their soffits*", Journal of Structural Engineering, ASCE, 118(8), pp 2023-2029.
- Oehler, D.J., and Moran, J.P., (1990), "*Premature failure of externally plated reinforced concrete beams*", Journal of Structural Engineering, ASCE, 116(4), pp 978-995.



- Oehlers, D.J., Wright, H.D., and Burnet, M.J., (1994), "*Flexural strength of profiled beams*", Journal of Structural Engineering, ASCE, Vol. 120, No.2, February, 378-393.
- Oh, B.H., Cho, J.Y., and Park, D.G., (2003), "*Static and fatigue behavior of reinforced concrete strengthened with steel plate for flexure*", Journal of Structural Engineering, ACE, April, pp. 527-535.
- Ong, K.C.G., Mays, G.C., and Cusens, A.R., (1982), "*Flexural tests on steel-concrete open sandwiches*, Magazine of Concrete Research", Vol. 34, No. 120, 130-138, September.
- Ritche, P., Thomas, D., Lu, L., and Conelly, M., (1991), "*External reinforcement of concrete beams using fiber reinforced plastics.*" ACI Structural Journal, 88(4), pp. 490.
- Roberts, T.M., and Haji-Kazemi, H., (1989), "*Theoretical study of the behavior of reinforced concrete beams strengthened by externally bonded steel plates*", Proc. Institutions of Civil Engineers, Part 2, 87, 39-55.
- Sebastian, W.M., and McConnel, R.E., (2000), "*Nonlinear FE analysis of steel-concrete composite structures*", Journal of Structural Engineering, 126(6), pp 662-674.
- Solomon, S.K., Smith, D.W., and Cusens, A.R., (1976), "*Flexural tests on steel-concrete-steel sandwich*", Magazine of Concrete Research, Vol. 28, No. 94, 13-20, March.
- Tadeu, A.J.B., and Branco, F.J.G., (2000), "*Shear test of steel plates epoxy bonded to concrete under high temperature*", Journals of Material in Civil Engineering, ASCE, 12(1), pp. 70-80.
- Täljsten, B., (1996), "*Strengthening of beams by plate bonding*", Journal of Materials in Civil Engineering, November, pp. 206-21

- Thevendran, V., Chen, S., Shenmugam, N.E., and Liew, J.Y.R., (1999), "*Nonlinear analysis of steel-concrete composite curved in plan*", Finite Element Analytic Design, 32 (3), pp 125-139.
- Tureyen, A.K., and Robert, J.F., (2002), "*Shear test of FRP-reinforced concrete beams without stirrups*", ACI Structural Journal, Title No. 99-S44, July-August, pp. 427-434.
- Van Gemert, D.A., (1981), "*Repairing of concrete structures by externally bonded steel plates*", Proc. International Symposium on Plastics in Mat. and Struc. Engineering, Prague, Czechoslovakia, 519-526.
- Wright, H.D., Oduyemi, T.O.S, and Evans, H.R., (1991), "*The double skin composite elements*", Journal of Construction Steel Research, 19, pp. 111-132.
- Xanthakos, P.P., (1996), "*Bridge strengthening and rehabilitation*". Prentice-Hall, Eaglewood Cliffs, N.J.
- Yang, Z.J., Chen, J.F., and Proverbs, D., (2003), "*Finite element modeling of concrete cover separation failure in FRP plated RC beams*", Construction and Building Material, Elsevier, 17, pp 3-13.

## **Appendix – A**

(Input File)

# Beam S2B100-0.4mm

```

*Heading
  Analysis of S2b100-0.4mm
** Job name: S2B100 Model name: Model-1
*Preprint, echo=NO, model=NO, history=NO, contact=NO
**
** PARTS
**
*Part, name="Concrete Beam"
*End Part
*Part, name="Steel Plate"
*End Part
**
** ASSEMBLY
**
*Assembly, name=Assembly
**
*Instance, name="Concrete Beam-1", part="Concrete Beam"
*Node
  1,      100.,      0.,      0.
  2,      50.,      0.,      0.
  3,      0.,      0.,      0.
  4,      100.,     266.67,      0.
  5,      50.,     266.67,      0.
  6,      0.,     266.67,      0.
  7,      100.,     400.,      0.
  8,      50.,     400.,      0.
  9,      0.,     400.,      0.
 10,      100.,     533.33,      0.
 11,      50.,     533.33,      0.
 12,      0.,     533.33,      0.
 13,      100.,     800.,      0.
 14,      50.,     800.,      0.
 15,      0.,     800.,      0.
 16,      100.,      0.,     150.
 17,      50.,      0.,     150.
 18,      0.,      0.,     150.
 19,      100.,     266.67,     150.
 20,      50.,     266.67,     150.
 21,      0.,     266.67,     150.
 22,      100.,     400.,     150.
 23,      50.,     400.,     150.
 24,      0.,     400.,     150.
 25,      100.,     533.33,     150.
 26,      50.,     533.33,     150.
 27,      0.,     533.33,     150.
 28,      100.,     800.,     150.
 29,      50.,     800.,     150.
 30,      0.,     800.,     150.
*Element, type=C3D8R
  1, 16, 17, 20, 19, 1, 2, 5, 4
  2, 17, 18, 21, 20, 2, 3, 6, 5
  3, 19, 20, 23, 22, 4, 5, 8, 7
  4, 20, 21, 24, 23, 5, 6, 9, 8
  5, 22, 23, 26, 25, 7, 8, 11, 10

```

```

6, 23, 24, 27, 26, 8, 9, 12, 11
7, 25, 26, 29, 28, 10, 11, 14, 13
8, 26, 27, 30, 29, 11, 12, 15, 14
** Region: (Beam:Picked), (Material Orientation:Picked)
*Elset, elset=_PickedSet2, internal, generate
1, 8, 1
** Section: Beam
*Solid Section, elset=_PickedSet2, material=Concrete
1.,
*Rebar, Element=Continuum, Material=Rebar, Geometry=Isoparametric, Name=She
ar1
_PickedSet2, 19.635, 100, 0, 0.9, 2, 3
*Rebar, Element=Continuum, Material=Rebar, Geometry=Isoparametric, Name=She
ar2
_PickedSet2, 19.635, 100, 0, 0.1, 2, 3
*Rebar, Element=Continuum, Material=Rebar, Geometry=Isoparametric, Name=Bot
tomBars
_PickedSet2, 19.635, 100, 0, 0.067, 4, 2
*Rebar, Element=Continuum, Material=Rebar, Geometry=Isoparametric, Name=Top
Bars
_PickedSet2, 19.635, 100, 0, 0.933, 4, 2
*End Instance
**
*Instance, name="Steel Plate-1", part="Steel Plate"
*Node
1, 0., 0., 0.
2, 100., 0., 0.
3, 0., 200., 0.
4, 100., 200., 0.
5, 0., 400., 0.
6, 100., 400., 0.
7, 0., 600., 0.
8, 100., 600., 0.
9, 0., 800., 0.
10, 100., 800., 0.
11, 50., 0., 0.
12, 100., 100., 0.
13, 50., 200., 0.
14, 0., 100., 0.
15, 100., 300., 0.
16, 50., 400., 0.
17, 0., 300., 0.
18, 100., 500., 0.
19, 50., 600., 0.
20, 0., 500., 0.
21, 100., 700., 0.
22, 50., 800., 0.
23, 0., 700., 0.
*Element, type=S8R
1, 1, 2, 4, 3, 11, 12, 13, 14
2, 3, 4, 6, 5, 13, 15, 16, 17
3, 5, 6, 8, 7, 16, 18, 19, 20
4, 7, 8, 10, 9, 19, 21, 22, 23
** Region: (Plate:Picked), (Material Orientation:Picked)
*Elset, elset=_PickedSet2, internal, generate
1, 4, 1
** Section: Plate

```

```

*Shell Section, elset=_PickedSet2, material="Steel Plate"
0.4, 5
*End Instance
*Nset, nset=_PickedSet15, internal, instance="Concrete Beam-1",
generate
13, 15, 1
*Nset, nset=_PickedSet15, internal, instance="Steel Plate-1"
9, 10, 22
*Elset, elset=_PickedSet15, internal, instance="Concrete Beam-1"
7, 8
*Elset, elset=_PickedSet15, internal, instance="Steel Plate-1"
4,
*Nset, nset=_PickedSet16, internal, instance="Concrete Beam-1",
generate
1, 3, 1
*Nset, nset=_PickedSet16, internal, instance="Steel Plate-1"
1, 2, 11
*Elset, elset=_PickedSet16, internal, instance="Concrete Beam-1"
1, 2
*Elset, elset=_PickedSet16, internal, instance="Steel Plate-1"
1,
*Nset, nset=_PickedSet337, internal, instance="Steel Plate-1", generate
1, 23, 1
*Elset, elset=_PickedSet337, internal, instance="Steel Plate-1",
generate
1, 4, 1
*Nset, nset=_PickedSet401, internal, instance="Concrete Beam-1"
20, 26
*Nset, nset="Deflection Check", instance="Concrete Beam-1"
23,
*Nset, nset="Load Check", instance="Concrete Beam-1"
20, 26
*Nset, nset="Plate Stress", instance="Steel Plate-1"
1, 3, 5, 7, 9, 14, 17, 20, 23
*Elset, elset="Plate Stress", instance="Steel Plate-1", generate
1, 4, 1
*Elset, elset=_PickedSurf336_S2, internal, instance="Concrete Beam-1",
generate
1, 8, 1
*Surface, type=ELEMENT, name=_PickedSurf336, internal
_PickedSurf336_S2, S2
*Surface, type=NODE, name=_PickedSet337_CNS_, internal
_PickedSet337, 1.
** Constraint: Weld
*Tie, name=Weld, adjust=yes
_PickedSet337_CNS_, _PickedSurf336
*End Assembly
**
** MATERIALS
**
*Material, name=Concrete
*Concrete
11.325, 0.
17.931, 0.00064
24.5375, 0.00088
31.143, 0.00112
37.75, 0.00136

```

```

31.143, 0.002
24.5375, 0.0032
*Failure Ratios
1.15, 0.09765, 1.28, 0.3333
*Shear Retention
0.42, 0.003, 0., 0.
*Tension Stiffening
1., 0.
0., 0.001
*Elastic
27648., 0.15
*Material, name=Rebar
*Elastic
200000., 0.3
*Plastic
460., 0.
*Material, name="Steel Plate"
*Elastic
200000., 0.3
*Plastic
360., 0.
** BOUNDARY CONDITIONS
**
** Name: Pin Support Type: Symmetry/Antisymmetry/Encastre
*Boundary
_PickedSet16, PINNED
** Name: Roller Support Type: Symmetry/Antisymmetry/Encastre
*Boundary
_PickedSet15, YASYMM
** STEP: Applied Load
**
*Step, name="Applied Load", nlgeom=YES, inc=20
Application of Concentrated Load
*Static, riks
0.05, 1., 1e-05, 1., 1.,
**
** LOADS
**
** Name: Point Loads Type: Concentrated force
*Cload
_PickedSet401, 3, -23500.
**
** OUTPUT REQUESTS
**
*Restart, write, frequency=1
**
** FIELD OUTPUT: F-Output-1
**
*Output, field
*Node Output
CF, RF, U
*Element Output
S,
**
** HISTORY OUTPUT: Deflection
**
*Output, history

```

```
*Node Output, nset="Deflection Check"
U3,
**
** HISTORY OUTPUT: Load Check
**
*Node Output, nset="Load Check"
CF3,
**
** HISTORY OUTPUT: Plate Stress
**
*Element Output, elset="Plate Stress"
S22,
*El Print, freq=999999
CRACK,
COORD,
*Node Print, freq=999999
*End Step
```



## **Appendix – B**

**(Prediction of Moment Capacity Based on Codes)**

Series 1 Beams With 0.4mm Thick Steel Plate (Jim 1999)

**Geometrical Properties:**

Width,  $b_c = 100$  mm

Total depth,  $h_c = 150$  mm

Steel plate thickness,  $t_p = 0.4$  mm

Length of beam,  $L = 800$  mm

**Material Properties:**

Concrete compressive strength,  $f_c = 37.75$  MPa

Yield Strength of steel plate,  $f_{yp} = 360$  MPa

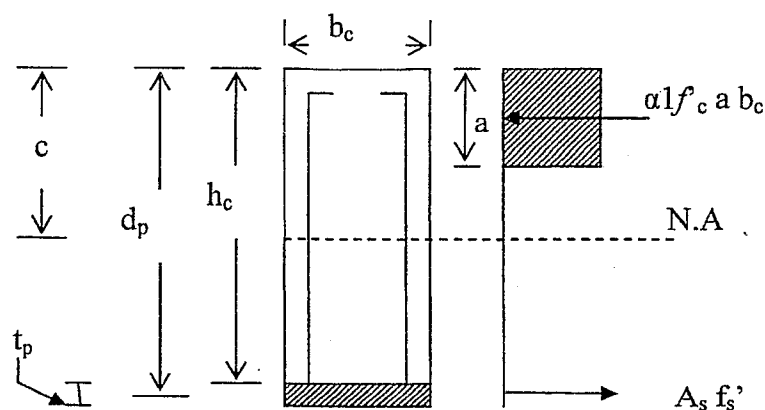


Fig. B. 1 Schematic of Series 1 Beams

### **Moment Capacity:**

Analysis is based on singly reinforced beam where  $C = T$  for equilibrium

Where  $C$  = Compressive force resisted by concrete &  $T$  = Tensile Force resisted by steel

$$\text{Depth of compressive stress, } a = \left( \frac{A_p \cdot f_y}{\alpha_1 \cdot f'_c \cdot b} \right)$$

Therefore;  $a = 4.81 \text{ mm}$

Where  $\alpha_1$  = Simplification factor of rectangular stress Block

$$\alpha_1 = 0.85 - 0.0015 f'_c = 0.793$$

$$\text{Area of Steel Plate, } A_p = b \times t_p = 100 \times 0.40 = 40 \text{ mm}^2$$

$$\text{Nominal Moment Capacity, } M_n = A_p \cdot f_y \left( d_p - \frac{a}{2} \right)$$

where  $h_p$  is depth of steel plate taken from extreme compression fiber of concrete to center of steel plate as shown in diagram.

$$M_n = 40 \times 360 \times (150.2 - 4.81/2) = 2.13 \text{ kN-m.}$$

Moment is constant for  $S_1B_{50}$ ,  $S_1B_{100}$ ,  $S_1B_{150}$  and  $S_1B_{180}$

### **Series 1 Beam with 3mm (Nupiri)**

Analysis of Series 1 Beams with 3mm thick plate (Nupiri 2000) is same except 3mm thick plate is used instead of 0.4mm.

$$M_n = 14.76 \text{ kN-m}$$

## CSA A.23.3 -1994

### Series 2 Beams With 0.4mm Thick Steel Plate (Jim 1999)

#### Geometrical Properties:

Width,  $b_c = 100 \text{ mm}$

Total depth,  $h_c = 150 \text{ mm}$

Steel plate thickness,  $t_p = 0.4 \text{ mm}$

Length of beam,  $L = 800 \text{ mm}$

Reinforcement = 2-5mm  $\Phi$  top bars & 2-5mm  $\Phi$  bottom bars

Distance from top compression face to centroid of compression bars = 10 mm

#### Material Properties:

Concrete compressive strength,  $f_c = 37.75 \text{ MPa}$

Tensile yield strength of steel bars,  $f_{ys} = 455 \text{ MPa}$

Yield Strength of steel plate,  $f_{yp} = 360 \text{ MPa}$

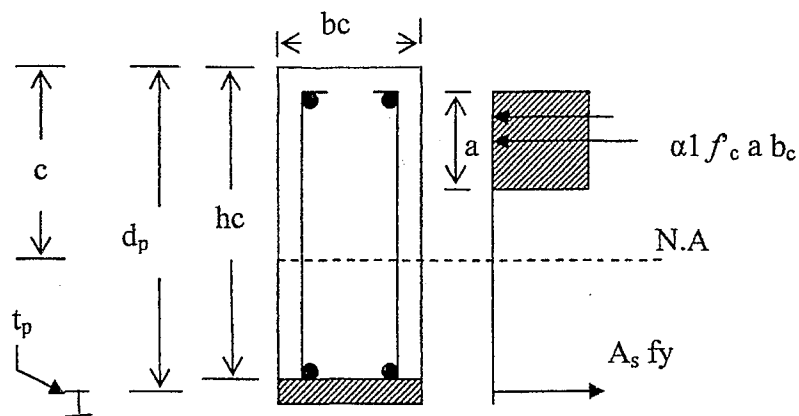


Fig. B. 2 Schematic of Series 2 Beams

For theoretical analysis series-2 beams is treated as doubly reinforced or T beams with plate perfectly bonded on the tension face as shown in Fig. B2.

Hence, recommended by the Canadian code of practice, the x-section is hypothetically divided into two beams. Free body diagram of couple forces acting on each beam at ultimate stages are shown in Fig. B3. Steel plate is lumped together with rebar for calculation.

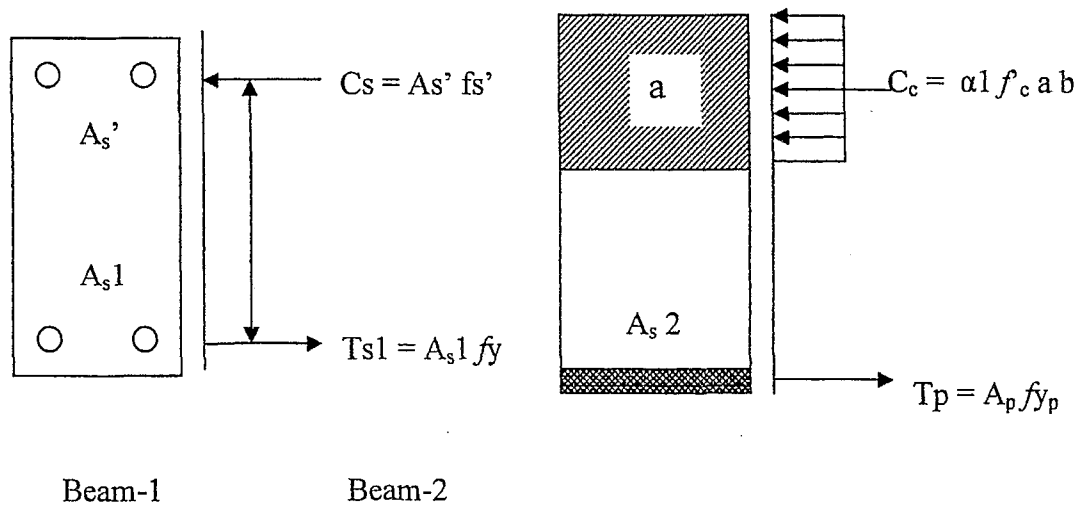


Fig. B. 3 Hypothetical division of doubly reinforced beam for analysis

Equation for calculating depth compressive stress block of Beam-2 can be obtain using concept of equilibrium and it is given by;

$$\text{Depth of Neutral Axis, } a = \left( \frac{(A_s - A_{s1}) f_y p}{\alpha 1 f'_c b} \right)$$

Where  $A_s$  = Total area of bottom steel (2-5mm  $\Phi$  bottom bars + 0.4mm steel plate)

$$A_s = 79.26 \text{ mm}^2, A_{s1} = 39.26 \text{ mm}^2 \text{ and } A_{s2} = A_s - A_{s1} = 40 \text{ mm}^2$$

$$\text{Depth of compressive stress block} = a = 6.079 \text{ mm}$$

Check whether compression steel yields or not!

$$\left(\frac{d'}{a}\right)_{lim} = \frac{1}{\beta_1} \left(1 - \frac{f_y}{700}\right)$$

$$\left(\frac{d'}{a}\right)_{lim} = 0.4$$

$$\left(\frac{d'}{a}\right) = 1.64 > 0.4 \text{ (Compression Steel does not yield)}$$

Solve for a:

$$(\alpha_1 \cdot f'_c \cdot b) a^2 + (0.0035 \cdot E_s \cdot A_s' - A_s \cdot f_y) a - (0.0035 \cdot E_s \cdot A_s' \cdot \beta_1 \cdot d') = 0$$

Where,  $E_s$  = Modulus of Elasticity of Steel = 200,000 MPa

$\beta_1$  = Simplification factor for stress block of concrete at ultimate

$$\beta_1 = 0.97 - 0.0025 f'_c \geq 0.67 = 0.875$$

$a = 7.54$  &  $a = -10.46$  (negative value should be ignored)

Check the ratio  $a/d < 0.5$  at ultimate (if compression steel yield)

$$\left(\frac{a}{d}\right) = 0.0538 < 0.5 \text{ (compression steel yield at ultimate)}$$

where  $d$  = Effective depth measured from extreme compressive fiber to centroid of rebar and steel plate

$$M_n = C_s \cdot (d_p - d') + C_c \cdot (d_p - a/2)$$

Where compressive force resisted by compression steel =  $C_s = E_s \cdot A_s' (\xi_s')$

$$\text{and } \xi_{s'} = \left(1 - \frac{\beta_1 d'}{a}\right) \xi_{cu}, \xi_{cu} = 0.0035$$

$$C_s = 6238.91 \text{ N or } 6.23 \text{ kN}$$

$$C_c = \alpha_1 f' c a b = 0.793 \times 37.75 \times 11.3198 \times 100 = 33,886.67 \text{ N or } 33.886 \text{ kN}$$

$$M_n = 6238.91 (150.02 - 10) + 33,886.67 (150.02 - 7.54/2) = 5.76 \text{ kN-mm.}$$

The nominal moment capacity ( $M_n$ ) is constant for all Series 2 (i.e. S<sub>2</sub>B<sub>50</sub>, S<sub>2</sub>B<sub>100</sub>, S<sub>2</sub>B<sub>150</sub> and S<sub>2</sub>B<sub>200</sub>) with 0.5mm thick plate beams except for those beams in which steel plate of 1mm thick was used (Nupiri 2000) but the methodology of getting nominal moment capacity is same.

#### **Series 2 Beam with 3mm (Nupiri)**

Analysis of Series 2 Beams with 3mm thick plate (Nupiri 2000) is same except 3mm thick plate is used instead of 0.5mm.

$$M_n = 17.20 \text{ kN-m}$$

## AUS 3600 -1994

### Series 1 Beams With 0.4mm Thick Steel Plate (Jim 1999)

#### Geometrical Properties:

Width,  $b_c = 100$  mm

Total depth,  $h_c = 150$  mm

Steel plate thickness,  $t_p = 0.4$  mm

Length of beam,  $L = 800$  mm

#### Material Properties:

Concrete compressive strength,  $f'_c = 37.75$  MPa

Yield Strength of steel plate,  $f_{sy} = 360$  MPa

#### Moment Capacity:

$$M_n = A_{st} f_{sy} d \left[ 1 - 0.6 \frac{A_{st} f_{sy}}{b d f'_c} \right] \quad (\text{AUS 3600 1994})$$

Where  $A_{st}$  = Area of steel plate

$$M_n = 2.12 \text{ kN-m}$$

Moment is constant for  $S_1B_{50}$ ,  $S_1B_{100}$ ,  $S_1B_{150}$  and  $S_1B_{180}$

#### S1B100 - 3mm

Analysis of Series 1 Beams with 3mm thick plate (Nupiri 2000) is same except 3mm thick plate is used instead of 0.4mm.

$$M_n = 14.48 \text{ kN-m}$$



## AUS 3600 -1994

### Series 2 Beams With 0.4mm Thick Steel Plate (Jim 1999)

#### Geometrical Properties:

Width,  $b_c = 100 \text{ mm}$

Total depth,  $h_c = 150 \text{ mm}$

Steel plate thickness,  $t_p = 0.4 \text{ mm}$

Length of beam,  $L = 800 \text{ mm}$

Reinforcement = 2-5mm  $\Phi$  top bars & 2-5mm  $\Phi$  bottom bars

Distance from top compression face to centroid of compression bars,  $d_{sc} = 10 \text{ mm}$

#### Material Properties:

Concrete compressive strength,  $f'_c = 37.75 \text{ MPa}$

Tensile yield strength of steel bars,  $f_{sy} = 455 \text{ MPa}$

Yield Strength of steel plate,  $f_{yp} = 360 \text{ MPa}$

#### Moment Capacity:

Check the moment capacity to determine if the compressive steel yielded or not:

$$k_u = \frac{1}{0.85\gamma} \cdot \frac{A_{st} - A_{sc}}{bd} \cdot \frac{f_{sy}}{f'_c} = 0.45 \quad (\text{AUS-3600, 1994})$$

$A_{st}$  = Total area of bottom steel (2-5mm  $\Phi$  bottom bars + 0.4mm steel plate) =  $80 \text{ mm}^2$

$A_{sc}$  = Area of 2-5mm  $\Phi$  bottom bars =  $39.26 \text{ mm}^2$

Strain in compression steel,  $\varepsilon_{sc} = \varepsilon_u \left( \frac{k_u d - d_{sc}}{k_u d} \right) = -0.0015 < 0.002$

(Com. Steel not yield)

Solve for  $k_u$ :

$$U1 = \frac{\varepsilon_u E_s A_{sc} - f_{sy} A_{st}}{0.85 f'_c \gamma b d} \text{ and } U2 = \frac{\varepsilon_u d_{sc} E_s A_{sc}}{0.85 f'_c \gamma b d^2}$$

Now using equation

$$k_u^2 + U1 k_u - U2 = 0 \quad \text{yield value of } k_u = 0.084$$

$$\text{Force in compressive steel} = C_s = E_s \varepsilon_u \left( \frac{k_u d - d_{sc}}{k_u d} \right) A_{sc} = 4502 \text{ N}$$

$$Mu = C_s (d - d_{sc}) + 0.85 f'_c b \gamma k_u d (d - 0.5 \gamma k_u d) = 4.53 \text{ kN-m}$$

### **Series 2 Beam with 3mm (Nupiri 2000)**

Analysis of Series 2 Beams with 3mm thick plate (Nupiri 2000) is same except 3mm thick plate is used instead of 3mm.

$$M_n = 17.44 \text{ kN-m}$$

## Euro Code -2

### Series 1 Beams With 0.4mm Thick Steel Plate (Jim 1999)

#### Geometrical Properties:

Width,  $b_c = 100 \text{ mm}$

Total depth,  $h_c = 150 \text{ mm}$

Steel plate thickness,  $t_p = 0.4 \text{ mm}$

Length of beam,  $L = 800 \text{ mm}$

#### Material Properties:

Concrete compressive strength,  $f_{ck} = 37.75 \text{ MPa}$

Yield Strength of steel plate,  $f_{yk} = 360 \text{ MPa}$

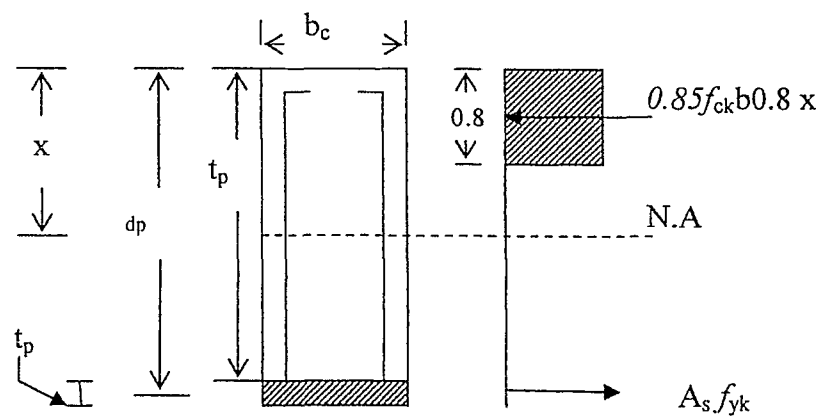


Fig. B. 4 Schematic of Series 1 Beams

### **Moment Capacity:**

Compressive force resisted by concrete,  $F_c = 0.85 \frac{f_{ck}}{\gamma_c} b 0.8x$  (Euro code-2)

Force Resisted by Steel plate,  $F_s = A_p \frac{f_{yk}}{\gamma_s}$  (Euro code-2)

where  $A_p$  = Area of steel plate  $x = 5.62$  (using equations for equilibrium)

$M_n = \{0.85 \cdot f_{ck} \cdot b \cdot (0.8x)\} (d - 0.4x) = 2.13 \text{ kN-m}$  (Euro code-2)

### **S1B100 - 3mm**

Analysis of Series 1 Beams with 3mm thick plate (Nupiri 2000) is same except 3mm thick plate is used instead of 0.4mm.

$M_n = 14.57 \text{ kN-m}$

**Euro Code -2**  
**Series 2 Beams With 0.4mm Thick Steel Plate (Jim 1999)**

**Geometrical Properties:**

Width,  $b_c = 100 \text{ mm}$

Total depth,  $h_c = 150 \text{ mm}$

Steel plate thickness,  $t_p = 0.4 \text{ mm}$

Length of beam,  $L = 800 \text{ mm}$

**Material Properties:**

Concrete compressive strength,  $f_{ck} = 37.75 \text{ MPa}$

Yield strength of steel plate,  $f_{yk} = 360 \text{ MPa}$

Yield strength of rebars,  $f_{yk} = 455 \text{ MPa}$

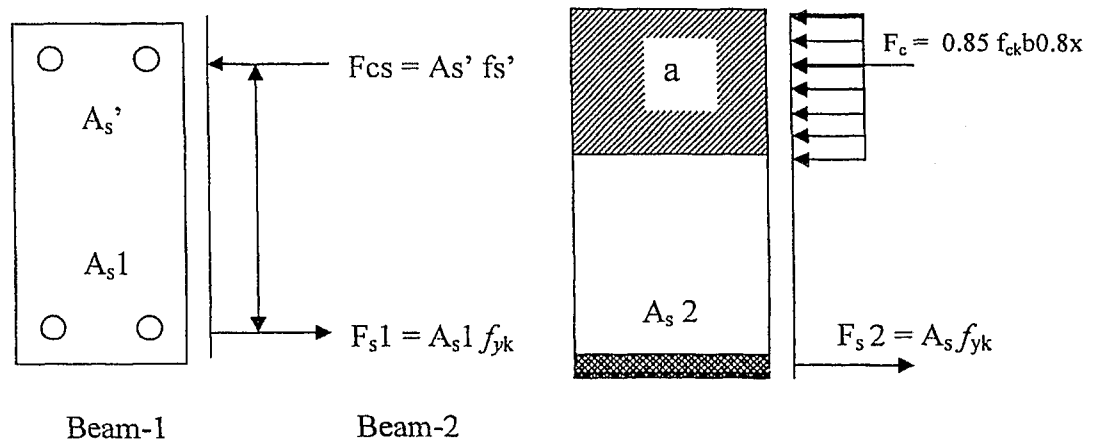


Fig. B. 5 Hypothetical sub-divisions of Series 2 beam

The x-section is hypothetically divided into two beams. Free body diagram of couple forces acting on each beam at ultimate stages are shown in Fig. B3. Steel plate is lumped together with rebar for calculation.

### **Moment Capacity:**

Rebar is lumped with steel plate

$$M_n = (0.85.f_{ck}.b.0.8x)(d - 0.4x) + (A_s' f_{yk})(d - d') \quad (\text{Euro code-2})$$

Depth of neutral axis is calculated using Beam 2 of Fig. B5, using equilibrium condition

$$x = 5.62 \text{ (} F_c = F_s \text{)}$$

Check whether compression steel yield

$$x/d = 0.0374 < 0.5 \text{ (compression steel yield)}$$

$$M_n = (0.85.f_{ck}.b.0.8x)(d - 0.4x) + (A_s' f_{yk})(d - d') = 3.96 \text{ kN-m}$$

### **Series 2 Beam with 3mm (Nupiri)**

Analysis of Series 2 Beams with 3mm thick plate (Nupiri 2000) is same except 3mm thick plate is used instead of 3mm.

$$M_n = 16.32 \text{ kN-m}$$

## ACI 318-2002

### Series 1 Beams With 0.4mm Thick Steel Plate (Jim 1999)

#### Geometrical Properties:

Width,  $b_c = 100$  mm

Total depth,  $h_c = 150$  mm

Steel plate thickness,  $t_p = 0.4$  mm

Length of beam,  $L = 800$  mm

#### Material Properties:

Concrete compressive strength,  $f'_c = 37.75$  MPa

Yield Strength of steel plate,  $f_{yp} = 360$  MPa

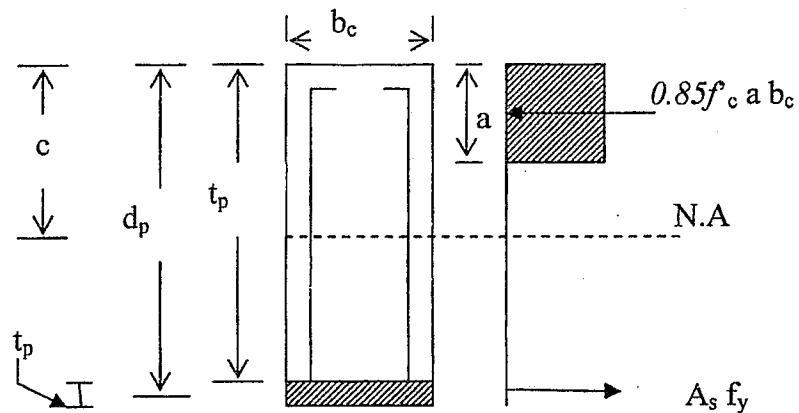


Fig. B. 6 Singly reinforced section

**Moment Capacity:**

Beam is analyzed as singly reinforced beam

$$\text{Depth of neutral axis, } a = \frac{Asf_y}{0.85f'_c b} = 4.48 \text{ mm}$$

$$\text{Nominal moment capacity, } M_n = Asf_y \left( d - \frac{a}{2} \right) = 2.12 \text{ kN-m}$$

**ACI 318-2002****Series 2 Beams With 0.4mm Thick Steel Plate (Jim 1999)****Geometrical Properties:**

$$\text{Width, } b_c = 100 \text{ mm}$$

$$\text{Total depth, } h_c = 150 \text{ mm}$$

$$\text{Steel plate thickness, } t_p = 0.4 \text{ mm}$$

$$\text{Length of beam, } L = 800 \text{ mm}$$

**Material Properties:**

$$\text{Concrete compressive strength, } f'_c = 37.75 \text{ MPa}$$

$$\text{Yield Strength of steel plate, } f_{ys} = 455 \text{ MPa}$$

$$\text{Yield Strength of steel plate, } f_{yp} = 360 \text{ MPa}$$

$$\text{Bottom steel ratio, } \rho = 0.022619$$

$$\text{Top steel ratio, } \rho' = 0.002618$$



### Moment Capacity:

Check whether compression steel yield or not:

For yielding of compression steel

$$(\rho - \rho') \geq 0.85 \cdot \beta_1 \cdot \frac{f'_c}{f_y} \cdot \frac{d'}{d} \left( \frac{600}{600 - f_y} \right) \quad (\text{ACI 318-2002})$$

Assumed that steel plate is lumped together with bottom rebars.

$$(\rho - \rho') = 0.02 \quad \text{and} \quad 0.85 \cdot \beta_1 \cdot \frac{f'_c}{f_y} \cdot \frac{d'}{d} \left( \frac{600}{600 - f_y} \right) = 0.0190$$

$$\text{Since } (\rho - \rho') > 0.85 \cdot \beta_1 \cdot \frac{f'_c}{f_y} \cdot \frac{d'}{d} \left( \frac{600}{600 - f_y} \right) \quad (\text{compression steel yielded})$$

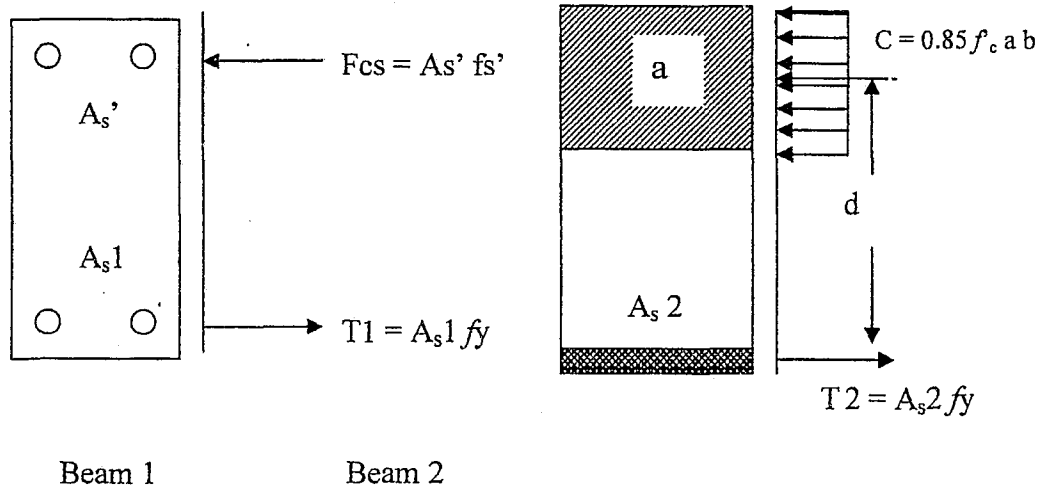


Fig. B. 7 Couple forces acting on beams at ultimate stages

Recommended by ACI code, the x-section is hypothetically divided into two beams. Free body diagram of couple forces acting on each beam at ultimate stages are shown in Fig. B6. Steel plate is lumped together with rebar for calculation. Using equation of equilibrium for Beam 2 to calculate the depth of neutral axis:

$$a = \frac{A_s 2 f_y}{0.85 f'_c b} = 5.67 \text{ mm}$$

$$M_n = 0.85 f'_c ab \left( d - \frac{a}{2} \right) + A_s' f_y (d - d') = 4.48 \text{ kN-m}$$

### **Series 2 Beam with 3mm (Nupiri)**

Analysis of Series 2 Beams with 3mm thick plate (Nupiri 2000) is same except 3mm thick plate is used instead of 3mm.

$$M_n = 17.44 \text{ kN-m}$$

**Appendix - C**  
**(Proposed Design Charts)**

